AD-A162 686

CHEMICAL
RESEARCH &
DEVELOPMENT
CENTER

UNCLASSIFIED
SECURITY CLASSIFICATION OF THIS PAGE

REPORT DOCUMENTATION PAGE

1a. REPORT SECURITY CLASSIFICATION UNCLASSIFIED	1b. RESTRICTIVE MARKINGS AD-A162686
2a. SECURITY CLASSIFICATION AUTHORITY	3. DISTRIBUTION/AVAILABILITY OF REPORT Approved for public release; distribution is unlimited.
2b. DECLASSIFICATION/DOWNGRADING SCHEDULE	
4. PERFORMING ORGANIZATION REPORT NUMBER(S) CRDC-CR-86004	5. MONITORING ORGANIZATION REPORT NUMBER(S)
6a. NAME OF PERFORMING ORGANIZATION Virginia Polytechnic Institute & State University, Dept of Engr Science & Mechanics 6b. OFFICE SYMBOL (If applicable)	7a. NAME OF MONITORING ORGANIZATION
6c. ADDRESS (City, State, and ZIP Code) Blacksburg, VA 24061	7b. ADDRESS (City, State, and ZIP Code)
8a. NAME OF FUNDING/SPONSORING ORGANIZATION CRDC 8b. OFFICE SYMBOL (If applicable) SMCCR-RSP-A	9. PROCUREMENT INSTRUMENT IDENTIFICATION NUMBER DAAK11-83-K-0011
8c. ADDRESS (City, State, and ZIP Code) Aberdeen Proving Ground, MD 21010-5423	10. SOURCE OF FUNDING NUMBERS PROGRAM ELEMENT NO. / PROJECT NO. / TASK NO. / WORK UNIT ACCESSION NO.

11. TITLE (Include Security Classification)
Viscous Fluid Motion in a Spinning and Nutating Cylinder

12. PERSONAL AUTHOR(S)
Herbert, Thorwald

13a. TYPE OF REPORT	13b. TIME COVERED	14. DATE OF REPORT (Year, Month, Day)	15. PAGE COUNT
Contractor	FROM 83 Aug TO 85 Apr	1985 November	117

16. SUPPLEMENTARY NOTATION
COR: Miles C. Miller, SMCCR-RSP-A; (301) 671-2186/2158

17. COSATI CODES		
FIELD	GROUP	SUB-GROUP
01	01	
20	04	

18. SUBJECT TERMS (Continue on reverse if necessary and identify by block number)
Projectile Stability
Liquid Payloads
Aeroballistics

19. ABSTRACT (Continue on reverse if necessary and identify by block number)
Spin-stabilized projectiles with liquid payloads can experience a severe flight instability characterized by a rapid yaw-angle growth and a simultaneous loss in spin rate. Laboratory experiments and field tests have shown that this instability originates from the internal fluid motion in the range of high viscosity. After evaluation of the experimental data and analysis of the equations for the fluid motion in a spinning and nutating cylinder, we have developed a simple model of this flow. Disregarding the finite length of the cylinder, this model provides the flow field and the viscous contribution to the liquid moments in analytical form. At low Reynolds number, the flow field agrees well with computational results for the center section of a cylinder of aspect ratio 4.3. The roll moment caused by this flow largely agrees with experimental data for a wide range of reynolds numbers. Estimates of the temperature variation indicate that discrepancies at very low Reynolds numbers may originate from associated changes of the viscosity during the experiments. The flow in an infinitely long cylinder has been utilized as a basic flow
(continued on reverse)

20. DISTRIBUTION/AVAILABILITY OF ABSTRACT	21. ABSTRACT SECURITY CLASSIFICATION
☒ UNCLASSIFIED/UNLIMITED ☐ SAME AS RPT. ☐ DTIC USERS	UNCLASSIFIED

22a. NAME OF RESPONSIBLE INDIVIDUAL	22b. TELEPHONE (Include Area Code)	22c. OFFICE SYMBOL
TIMOTHY E. HAMPTON	(301) 671-2914	SMCCR-SPD-R

DD FORM 1473, 84 MAR 83 APR edition may be used until exhausted. All other editions are obsolete.

SECURITY CLASSIFICATION OF THIS PAGE
UNCLASSIFIED

19. Abstract (Continued)

subject to axially periodic cellular disturbances. Both, the inviscid and the viscous situations have been studied. Parametric excitation of cellular motions has been found at low Reynolds numbers. A small experiment has been designed to visualize this cellular motion in a finite-length cylinder.

PREFACE

The work described in this report was authorized under Contract No. DAAK11-83-K-0011. This work was started in August 1983 and completed in April 1985.

The use of trade names or manufacturers' names in this report does not constitute endorsement of any commercial products. This report may not be cited for purposes of advertisement.

This report has been approved for release to the public.

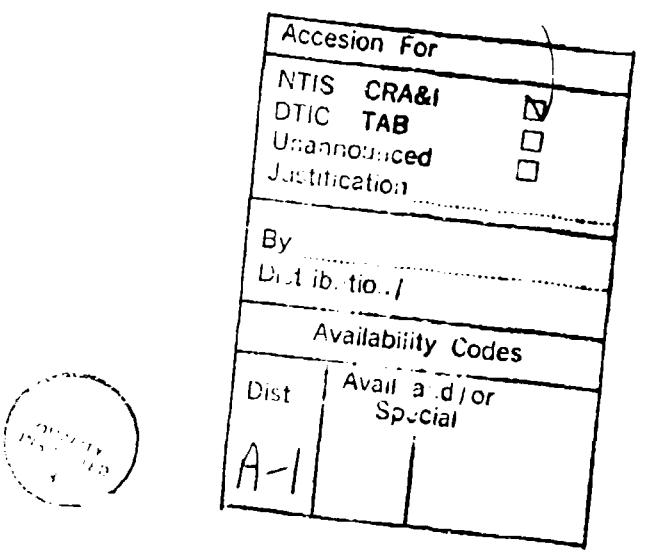

Blank

TABLE OF CONTENTS

Blank

VISCOUS FLUID MOTION IN A SPINNING AND NUTATING CYLINDER

1. Accomplishments

The working period for this contract was originally 83/08/02 - 85/02/02, but has been extended until 85/04/30 in order to provide for completing the experimental setup for flow visualization. During this working period, the following personnel has been partly supported under contract DAAK11-83-K-0011:

Thorwald Herbert, Professor, Principal Investigator
J. Wallace Grant, Assistant Professor
Relja Zivojnovic, Graduate Student (M. S. level)
German Santos , Graduate Student (Ph.D. level)
Charlotte R. Hawley, Research Specialist

David Pierpond, Undergraduate Student, has been involved in the experimental work at no cost. His senior project is close to completion. Parts of the theoretical work have been supported by the Army Research Office under Contract DAAG29-82-K-0129.

1.1. Presentations

New research findings have been reported at the following conferences:

(1) "The Flow of Highly Viscous Fluid in a Spinning and Nutating Cylinder," 1983 Scientific Conference on Chemical Defense Research, November 14-18, 1983, Aberdeen Proving Ground, Maryland.

(2) "Highly Viscous Fluid Flow in a Spinning and Nutating Cylinder," Second Army Conference on Applied Mathematics and Computing, May 22-25, 1984, Troy, New York.

(3) "Instability of the Viscous Flow in a Spinning and Nutating Cylinder," ARO Workshop on Liquid-Filled Shells, September 20-21, 1984, Aberdeen Proving Ground, Maryland.

(4) "Instability of the Viscous Flow in a Spinning and Nutating Cylinder," 1984 Scientific Conference on Chemical Defense Research, November 13-16, 1984, Aberdeen Proving Ground, Maryland.

(5) An abstract of a paper entitled "On the Fluid Motion in Liquid-Filled Shells," has been submitted for presentation at the 1985 Scientific Conference on Chemical Defense Research, November 19-22, 1985, Aberdeen Proving Ground, Maryland.

1.2. Publications

A selection of results has been published in the following papers:

(1) "The Flow of Highly Viscous Fluid in a Spinning and Nutating Cylinder," Proc. 1983 Scientific Conference on Chemical Defense Research, Aberdeen Proving Ground, Maryland, (Eds. R. L. Dimmick, Jr. & M. Rausa), Report CRDC-SP-84014, (1984).

(2) "Highly Viscous Fluid Flow in a Spinning and Nutating Cylinder," Trans. Second Army Conference on Applied Mathematics and Computing, Troy, New York, ARO Report 85-1 (1985).

(3) "On the Viscous Roll Moment in a Spinning and Nutating Cylinder," Proc. 1984 Scientific Conference on Chemical Defense Research, Aberdeen Proving Ground, Maryland, to be published.

(4) "Viscous Fluid Motion in a Spinning and Nutating Cylinder," submitted for publication in *Journal of Fluid Mechanics*.

Copies of the papers (1), (2) and of the manuscripts (3) and (4) are attached as Appendices A.1 - A.4.

2. Technical Discussion

2.1. Introduction

It is well-known that spin-stabilized shells carrying liquid payloads can suffer dynamical instability. For cylindrical cavities and low viscosity of the liquid, the instability due to basically inviscid inertial waves can be predicted by the Stewartson-Wedemeyer theory (Stewartson 1959; Wedemeyer 1966). This theory rests on the boundary-layer approach and is, therefore, restricted to the range of sufficiently large Reynolds numbers. The instability of certain shells like the XM761 (D'Amico 1977; 1978), however, escapes such a prediction and is also distinguished in character owing to the rapid loss in spin rate. Experiments with a full-scale liquid-filled cylinder (Miller 1982) and subsequent field tests (D'Amico & Miller 1979) establish that this new flight instability is most pronounced for liquid fills of very high viscosity.

We have conducted an analysis of this problem in order to support the ongoing experiments and to independently obtain insight into the anatomy of the flow phenomena. The initial steps of this analysis are reported elsewhere (Herbert 1982): evaluation of the experimental

data base, dimensional analysis, scaling aspects, governing equations, and discussion of various simplifying assumptions. Two observations in this earlier work led to the approach discussed in the following. First, if the despin (negative roll) moments (Miller 1982) and void observations (Miller 1981) are correlated with the Reynolds number Re, at least three regions can be distinguished. At low Re, the despin moment increases proportional to Re, and the void in an incompletely filled cylinder is parallel to the spin axis. This suggests a simple fluid motion that is essentially independent of the axial coordinate, except in the neighborhood of the end walls. In a middle range of Re, the despin moment assumes a maximum, and a wavy distortion of the void seems to indicate a cellular structure of the fluid motion. This cellular motion can, in principle, originate from hydrodynamic instability of the basic flow with respect to axially periodic disturbances. At still higher Reynolds numbers, the despin moment decreases with increasing Re in a manner not clearly defined by the few available data points. The void observations indicate, however, that the motion ultimately becomes turbulent.

The second observation is the appearance of the nutation rate and angle as a small parameter in the equations for the deviation from solid-body rotation. The forcing term due to nutation can be considered small enough for linearization of the equations in the situations of practical interest.

Consequently, our research focused on three topics. First, theoretical analysis of "simple" fluid motions at low Reynolds number that satisfy the linearized equations for the deviation from rigid body rotation. Second, analysis of inviscid and viscous inertial modes and their relevance for the occurrence of a maximum despin moment at moderate Reynolds numbers. Third, the design of a small-scale, low-cost experiment for visualization of the interior fluid motion. The results of these efforts are discussed in sections 2.2, 2.3 and 2.4, respectively.

2.2. The Deviation from Solid Body Rotation

A formal analysis of the equations† for the deviation of the velocity field from solid body rotation suggests that (1) the equations can be linearized without introducing major errors, (2) at low Reynolds numbers Re^*, the velocity field is independent of the axial direction over a considerable part of the relatively long ($\gamma = 4.3$) cylinder, and (3) the flow is in the axial direction and turns at the ends. Application of these conceptual assumptions turned out very

† Detailed equations are given in Appendix A.4

* We use the notation introduced in Appendix A.4.

fruitful. A detailed description of the results and comparison with computational and experimental data is given in the paper "Viscous Fluid Motion in a Spinning and Nutating Cylinder" (Appendix A.4), submitted for publication in the Journal of Fluid Mechanics. A sample program with the relevant subroutines for reproducing the theoretical results is given in Appendix B. Here, we report only the main conclusions.

The model of a two-dimensional unidirectional flow in a finite segment of an infinite cylinder yields the solution of the linearized equations in analytical form. The disregard of the end walls has some obvious consequences: the turning flow near the ends and the associated contributions of pressure and shear stresses to the moments cannot be obtained from this model. Nevertheless, we gather understanding as well as quantitative information. The velocity field of the core flow agrees well with computational results (Vaughn et al. 1985) for low Reynolds numbers. The analytical result is an evident example for the formation of boundary layers. The core flow can be utilized as a basic flow in studies of hydrodynamic instability with respect to cellular motions. The parametric excitation of such cells by the azimuthally periodic deviation has been discussed by Herbert (1984). The core flow also represents the lowest-order approximation to the solution of the nonlinear equations and can be extended by higher-order terms.

The roll moment agrees well with measured and computed values, and can also be found at Reynolds numbers too large for successful numerical simulations. The roll moment originates from Coriolis forces. While the direct calculation of the yaw moment suffers from neglecting the pressure contribution, the yaw moment can be found from the roll moment using the relations given by Murphy (1984, 1985). The pitch moment remains an open issue. The average rate of change of temperature is found to be proportional to roll moment and spin rate. This estimate needs further verification once more detailed data become available.

The simple form and scaling relations of our results provide guidance for sorting and evaluating the experimental data base. The results also suggest various improvements in the experimental procedures. First, the changes in temperature and viscosity should be carefully monitored. With the effective viscosity known, a closer agreement between theory and observation is to be expected. Second, the yet neglected variation of the roll moment with the spin rate is considered relevant and in fact provides the roll moment in some range of Reynolds numbers. Instead of recording the roll moment as a function of Re by using numerous viscosities at fixed spin rate, very similar data can be generated by varying the spin rate for a few

fluids. For directing the research efforts within this project, it has been most revealing that the characteristic variation of roll moment versus Reynolds number, in particular the sharp maximum at $Re \approx 19$ is a property of the unidirectional model flow. This result contradicted the earlier working hypothesis which attributed the occurrence of this maximum to hydrodynamic instability and the onset of cellular motions.

2.3. Cellular Structure of the Motion

Although not as relevant to the moments as earlier thought, the cellular motion at surprisingly low Reynolds numbers is in itself an interesting physical phenomenon. In our analysis, we superpose to the steady basic flow $\mathbf{v}_a = (0, r, v_z)$, p_a disturbances $\dot{\mathbf{v}} = (u, v, w)$, p sufficiently small for linearization. Substitution into the governing equations and neglect of products between disturbances and terms of order $0(\epsilon^2)$ provide the following stability equations:

$$\left[\frac{\partial u}{\partial t} + \frac{\partial u}{\partial \phi} - 2\left(1 + \tau_z\right)v + \frac{\partial p}{\partial r}\right] - \frac{1}{Re}\left[D''u - \frac{u}{r^2} - \frac{2}{r^2}\frac{\partial v}{\partial \phi}\right]$$

$$+ \left[v_z\frac{\partial u}{\partial z} + 2\tau_\phi w\right] = 0$$

$$\left[\frac{\partial v}{\partial t} + \frac{\partial v}{\partial \phi} + 2\left(1 + \tau_z\right)u + \frac{1}{r}\frac{\partial p}{\partial \phi}\right] - \frac{1}{Re}\left[D''v - \frac{v}{r^2} + \frac{2}{r^2}\frac{\partial u}{\partial \phi}\right]$$

$$+ \left[v_z\frac{\partial v}{\partial z} - 2\tau_r w\right] = 0$$

$$\left[\frac{\partial w}{\partial t} + \frac{\partial w}{\partial \phi} + \frac{\partial p}{\partial z}\right] - \frac{1}{Re}\left[D''w\right] + \left[\left(\frac{\partial v_z}{\partial r} - 2\tau_\phi\right)u\right.$$

$$\left. + \left(\frac{1}{r}\frac{\partial v_z}{\partial \phi} + 2\tau_r\right)v + v_z\frac{\partial w}{\partial z}\right] = 0$$

$$\frac{1}{r}\frac{\partial}{\partial r}(ru) + \frac{1}{r}\frac{\partial v}{\partial \phi} + \frac{\partial w}{\partial z} = 0$$

Three groups of terms have been separated by square brackets in these equations. The first group, if set to zero, represents the equations for inviscid inertial modes $\sim \exp(im\phi + i\alpha z + \sigma t)$, where m is the (integer) azimuthal wavenumber, α the axial

wavenumber, and $\sigma = \sigma_r + i\sigma_i$ provides the amplification rate σ_r and frequency σ_i. Usually, an equation for the pressure is used for obtaining the analytical solution (Stewartson 1959). We have derived an alternative system in terms of u, v and applied a spectral collocation method to be used for more general cases in order to check the numerical results against the exact values.

The programs are designed to provide results for arbitrary values of the azimuthal and axial wavenumber. A typical spectrum for $m = 1$, $\alpha = 1$ is shown in figure 1. In the complex s-plane, $s = \sigma + im$, stable ($s_r < 0$) eigenvalues are located to the left of the vertical s_i-axis, while eigenvalues in the right half-plane indicate instability. In the inviscid case, the eigenvalues are located on the s_i-axis ($s_r = 0$) and are neutral. The eigenfunctions associated with the eigenvalue of maximum frequency are shown in figure 2. Note that only the no-penetration condition for the radial velocity component is satisfied, while v and w slip at the cylinder walls.

The second group of terms in the stability equations is multiplied by $1/Re$ and represents the viscous correction to the inertial modes. By eliminating w and p, a system of ordinary differential equations for u and v has been derived. Due to the higher order of this system, all boundary conditions can be satisfied. Programs have been developed for calculating spectra of (complex) eigenvalues, for tracing single eigenvalues as a function of Re, α, and for obtaining the eigenfunctions. At high Re, the results follow the trends predicted by asymptotic theories. Our analysis, however, also covers the range of low Reynolds numbers, where the inertial modes suffer rapid decay ($s_r < 0$).

Spectra of eigenvalues for viscous inertial modes at $m = 1$, $\alpha = 1$ in an infinite cylinder are shown in figure 3 for $Re = 1000$ and in figure 4 for $Re = 100$. All eigenvalues move to the left as Re decreases, indicating stabilization of the modes. The eigenfunctions for the least stable mode at $Re = 100$ are shown in figure 5. Note that all velocity components vanish at the cylinder wall.

The most interesting aspect of the stability equations is the third group of terms. The coefficients in this group, v_z, τ_r, and τ_ϕ, are of order $O(\epsilon)$ and periodic in ϕ. The periodicity in ϕ leads to a coupling of the mode equations for m and $m \pm 1$, and may cause primary resonance between inertial modes. In view of viscous damping, this resonance is likely to occur as ϵ exceeds a critical value that decreases as Re increases.

The analysis of this parametrical instability has been prepared by solving the full set of stability equations with the coupling terms between modes artificially set to zero. A spectrum of eigenvalues in the σ-plane for $m = 0$, $\alpha = 1$ and $Re = 100$ is shown in figure 6. This spectrum consists of the superposition of the spectra for $m = 0, \pm 1$ of the viscous equations. As the coupling terms are taken into account, the spectrum drastically changes, as shown in figure 7. Most remarkable is the appearance of a small number of eigenvalues in the unstable right half-plane. These eigenvalues are either real or appear as complex conjugate pairs. This reflects the fact that the physical solution must be real. Instability at lower values of the axial wavenumber α can be found at low Reynolds number. Figure 8 shows an example of instability at $Re = 20$. A single pair of complex conjugate eigenvalues appears in the unstable domain; the amplification rate decreases with the Reynolds number.

The analysis of the parametric instability of the azimuthally periodic flow is rather costly in terms of computer time. Within the framework of this contract, we were not able to complete a systematic parameter study that could provide a lower limit or critical Reynolds number for the onset of cellular motion; neither were experimental data available for a comparison of eigenfunctions. It has been shown, however, that cellular motions can appear at low Reynolds numbers as a result of resonant coupling beetween inertial modes.

2.4. Flow Visualization

Although theoretical (Herbert, Appendix A.4) and computational (Vaughn et al. 1985) work provides some insight into the interior fluid motion, the nature of the phenomena remains largely in the dark. This is especially true for the range of medium and high Reynolds numbers where finite-amplitude cellular motions and, ultimately, turbulence are expected to occur. This range is barely within the scope of computational methods nor can it be fully explored with the theoretical means of sections 2.2, 2.3.

Previous experiments (Miller 1981) using a partially filled full-scale cylinder revealed some axial nonuniformity of the flow at higher Re without showing details of the flow field. Later attempts to use flow tracers (Miller & Oberkampf, personal communication) had little success due to the high spin rates (accelerations) combined with minute density differences between working fluid and tracer particles. Even carefully centrifuged and selected particles failed to follow the liquid path, probably due to changes of temperature during the run.

Attempts to employ laser-induced fluorescence (Miller 1984) were partly successful after changing the time scale, i.e. to lower spinrate, nutation rate, and viscosity at fixed values of the dimensionless parameters. These efforts have been discontinued, however, due to continuing lighting problems.

Evaluation of the experimental attempts to visualize the fluid flow clearly reveals the extreme full-scale conditions as evil. Conclusive experiments can be conducted by exploiting the principals of dynamical similarity and appropriate scaling laws. These aspects have been discussed in earlier work (Herbert 1982) and extended by the analysis in Appendix A.4.

Between the three reference quantities, radius a, spinrate ω, and density ρ for length, time, and mass, respectively, the density of different fluids offers little variability. However, length and time scale can be easily changed. For dynamical similarity, the following dimensionless quantities must be fixed:

$\lambda = c/a$	aspect ratio
θ	nutation angle
$\tau = \Omega/\omega$	frequency
$Re = \rho\omega a^2/\mu$	Reynolds number

The nutation angle must remain the same in a scaled setup. Radius a and half-length c of the cylinder must be scaled by the same factor in order to keep the aspect ratio fixed. A second factor can be applied to both spinrate ω and nutation rate Ω, in order to preserve the frequency. Keeping Re fixed requires changing the kinematic viscosity $\nu = \mu/\rho$ by the same factor as ωa^2. Since the desired tendency is toward smaller radii and spinrates, we require less viscous fluids than those used in the full-scale experiments. Such fluids are easy to find.

It is obvious that the main thrust of an experiment may require specific optimum conditions. Flow visualization requires low velocities, i.e. low values of ωa. Measurements of moments require optimum values of $\omega^2 a^5$. Minimizing the rate of change of temperature requires a minimum of $\omega^3 a^2$. A good setup for flow visualization, therefore, may produce moments in a hardly measurable range.

The goal of our efforts was to show that a low-cost device ($\simeq$\$500) can be designed for flow visualization. Details had to be kept simple. Accuracy and convenience had to compromise. The results of these efforts are shown in figures 9 and 10.

A one-inch inner diameter cylinder of aspect ratio $\lambda = 4.3$ is used. The cylinder is cut from a pyrex glass tube with the inner diameter accurate within 1/5000 inch, but with varying wall thickness that affects the optical quality. The cylinder is filled with mixtures of water and glycerin. The mixing ratio is used to vary viscosity. On top, the cylinder is closed with a screwed-in plastic plug. A center hole allows access to the interior, especially for removing air bubbles. The hole can be closed using a toothpick.

The cylinder is glued to a drive plug and axis machined from a single piece of aluminum. The one-sided support allows easy (optical) access to the cylinder and permits using cylinders of different length. One-sided support is affordable due to the moments being approximately five orders of magnitude smaller than in the full-scale experiments. The axis is twice supported by ball bearings. The cylinder and shaft are driven via timing belts over exchangeable sets of pulleys. The most expensive piece of the spin arrangement is a ≤ 24V d.c. motor with sufficient torque in the range of 500 - 5000 rpm. Motor and cylinder support are mounted to an aluminum frame that can be inclined to the vertical axis by 5, 10, 15 and 20° using different support holes and struts.

The horizontal support plate is machined to leave the center position free for access and is screwed to a commercial record player (Garrard model 775). The plate can be offset in order to align the center of mass of the cylinder with the nutation axis. The record player provides nutation rates of 33, 45, and 78 rpm. The hollow axis is only utilized to provide power to the spin motor. A 10-contact slip ring of high quality has been kindly donated by Poly-Scientific, Blacksburg, VA, but has been saved for more sophisticated experiments. A nail with a smooth top and a brush fixed to the turntable proved sufficient for transmitting a single voltage.

The remaining components of the experiment are: a Heathkit regulated power supply for the spin motor, a strobelight for controlled pulsed lighting, and suitable flow tracers.

As flow tracers we use Afflair 100 Silver Pearl, kindly donated by EM Chemicals, Hawthorne, NY. The material consists of very fine and shiny plastic platelets commercially used for cosmetic purposes. Although of specific weight different from that of the fluid, the low accelerations in the scale model permit practically buoyant behavior of the platelets over considerable time. The strobelight (General Radio Strobotac) with adjustable frequency is used for lighting as well as for measuring the spin rate of the cylinder.

At the slow time scale of the experiment, the fluid motion can be visually inspected while running the apparatus. At high viscosities, the apparatus can also be suddenly stopped, with the

flow tracers "frozen" in the resting fluid. The platelets align with surfaces of constant shear. Therefore, by manually rotating the cylinder forth and back, the three-dimensional structure of the field can be inspected. This crude observation is very helpful in developing the visualization technique. A detailed account of the technique (appropriate particle density, pitfalls such as the history of particle distribution and alignment) will be given by Pierpont (1985).

A typical view of the "frozen" pattern is shown in figure 11. Note, however, that the stereoscopic view by eye reveals the spatial distribution of the particles which is here projected into a single plane. The photograph also shows some undesirable reflections from the cylindrical surfaces. Visualization of the frozen pattern can be essentially improved by using a light sheet parallel to the spin axis. Sheet lighting also enables photographic recording of the flow structure while the apparatus is in operation.

A continuous light sheet is produced by a Spectra Physics model 120 (15 mW) helium-neon laser and a cylinder lens. In order to avoid the need for accurately firing the camera (35 mm Pentax with 50 mm lens) at a certain time, a cylindrical card board screen with a vertical slot and a 90° offset opening is fixed to the circumference of the turntable. The shutter is manually opened and closed after the laser sheet of light flashed through the slot. Some photographs taken with the apparatus in motion are shown in the figures. The figures show the pattern in the x,z-plane (the plane spanned by spin axis and nutation axis) as seen at $\phi = 0°$ in the y-direction. The series of figures 12,13,14 is for different nutation rates of 33, 45, 78 rpm, respectively at otherwise fixed parameters. The figures reveal the changing pattern and formation of cells at a Reynolds number $Re \approx 40$. At slightly higher Re, additional cells appear as shown in figure 15. At the high value of $Re \approx 8000$, the flow is highly unsteady and irregular (turbulent) with a superposed large-scale cellular motion. This cellular motion accumulates the platelets in streaks around the cylinder wall, as shown in figure 16. Number and position of the streaks depends sensitively on the parameters, see figure 17. The distortion of the bright line near the axis is very similar to the distortion of the void in Miller's (1981) photographs at low viscosity.

Specification of accurate Reynolds numbers suffers from some uncertainty in monitoring and measuring the wide range of viscosities for the hygroscopic water-glycerin mixtures exposed to uncontrolled thermal conditions. Falling-sphere viscometry is the easy way out, but requires a whole variety of spheres, different in diameter and specific gravity. To within this uncertainty, however, the figures clearly reveal the cellular structure of the flow and the changes of

the structure as Reynolds number and rate increase. Perhaps the most striking result of this visual study of the flow structure is the manifold of pattern at higher Reynolds numbers. A systematic analysis of these patterns cannot be conducted within the ongoing senior project. Neither can a coarse sampling of pattern in the y,z-plane be completed before submission of this report. However, the feasibility of flow visualization with simple means by proper sealing has been clearly demonstrated. A manifold of cellular motions in the laminar range has been observed as well as turbulent flow at high Reynolds numbers.

Some improvements are suggested from experience with the present experiment:

(1) More accurate measurements of viscosity and spinrate in order to reproduce experimental conditions.

(2) Redesign of the spin drive plug: a steel axis should be fixed to the bearings with an easy-to-detach cylinder bottom plug snug-fit to the axis.

(3) Refined laser-light sheet (thinner, plane can be rotated) and more sophisticated shutter release for the camera (controlled by timing pulse at proper turntable position).

(4) Higher precision of the cylinder for improved optical quality.

(5) Replacement of the record player by a turntable with continuously variable rate of rotation and heavier duty bearings.

Various of these improvements can be achieved with minor efforts and expenses, but not within the time frame of this contract. Moreover, we are confident that using photochromic dye exposed to a pulsed laser beam would allow visualization and - with some effort - quantitative analysis of velocity profiles.

ACKNOWLEDGMENT

The open cooperation and sharing of data with Miles C. Miller (CRDC) and Harold R. Vaughn (Sandia Laboratories) are greatly appreciated. Ri-Hua Li deserves credit for his assistance in developing the analytical solution.

REFERENCES

D'Amico, W. P. 1977 "Field Tests of the XM761: First Diagnostic Test," Ballistic Research Laboratory, Memorandum Report 1325.

D'Amico, W. P. 1978 "Field Tests of the XM761: Second Diagnostic Test," Ballistic Research Laboratory, Memorandum Report ARBRL-MR-02806.

D'Amico, W. P. & Miller, M. C. 1979 "Flight Instability Produced by a Rapidly Spinning, Highly Viscous Liquid," *J. of Spacecraft and Rockets*, Vol. 16, pp. 62-64.

Herbert, Th. 1982 "Fluid Motion in a Rotating and Nutating Cylinder - Part I," Report prepared under the Scientific Services Program. Appeared as Report CRDC-CR-84087 (1984).

Herbert, Th. 1984 "Highly Viscous Fluid Flow in a Spinning and Nutating Cylinder," Proc. of the Second Army Conference on Applied Mathematics and Computing, Troy, NY.

Miller, M. C. 1981 "Void Characteristics of a Liquid Filled Cylinder Undergoing Spinning and Coning Motion," *J. of Spacecraft and Rockets*, Vol. 18, pp. 286-288.

Miller, M. C. 1982 "Flight Instabilities of Spinning Projectiles Having Nonrigid Payloads," *J. of Guidance, Control, and Dynamics*, Vol. 5, pp. 151-157.

Miller, M. C. 1984 "Visualization Studies of Viscous Liquid Flow in a Spinning and Coning Cylinder," Proc. 1984 Scientific Conference on Chemical Defense Research, Nov. 13-16, 1984, Aberdeen Proving Ground, Maryland.

Murphy, C. M. 1984 "A Relationship between Liquid Roll Moment and Liquid Side Moment," Ballistic Research Laboratory Memorandum Report ARBRL-MR-03347.

Murphy, C. M. 1985 "A Relation between Liquid Roll Moment and Liquid Side Moment," *J. of Guidance, Control, and Dynamics*, Vol. 8, pp. 287-288.

Pierpont, D. 1985 "Design of an Experiment for Visualization of the Flow in a Spinning and Nutating Cylinder," Senior Project Report, VPI & SU.

Stewartson, K. 1959 "On the Stability of a Spinning Top Containing Liquid," *J. of Fluid Mech.*, Vol. 5, Part 4, pp. 577-592.

Vaughn, H. R., Oberkampf, W. L. & Wolfe, W. P. 1985 "Fluid Motion Inside a Spinning Nutating Cylinder," *J. of Fluid Mech.*, Vol. 150, pp. 121-138.

Wedemeyer, E. H. 1966 "Viscous Corrections to Stewartson's Stability Criterion," Ballistic Research Laboratory, Report 1325.

Figures

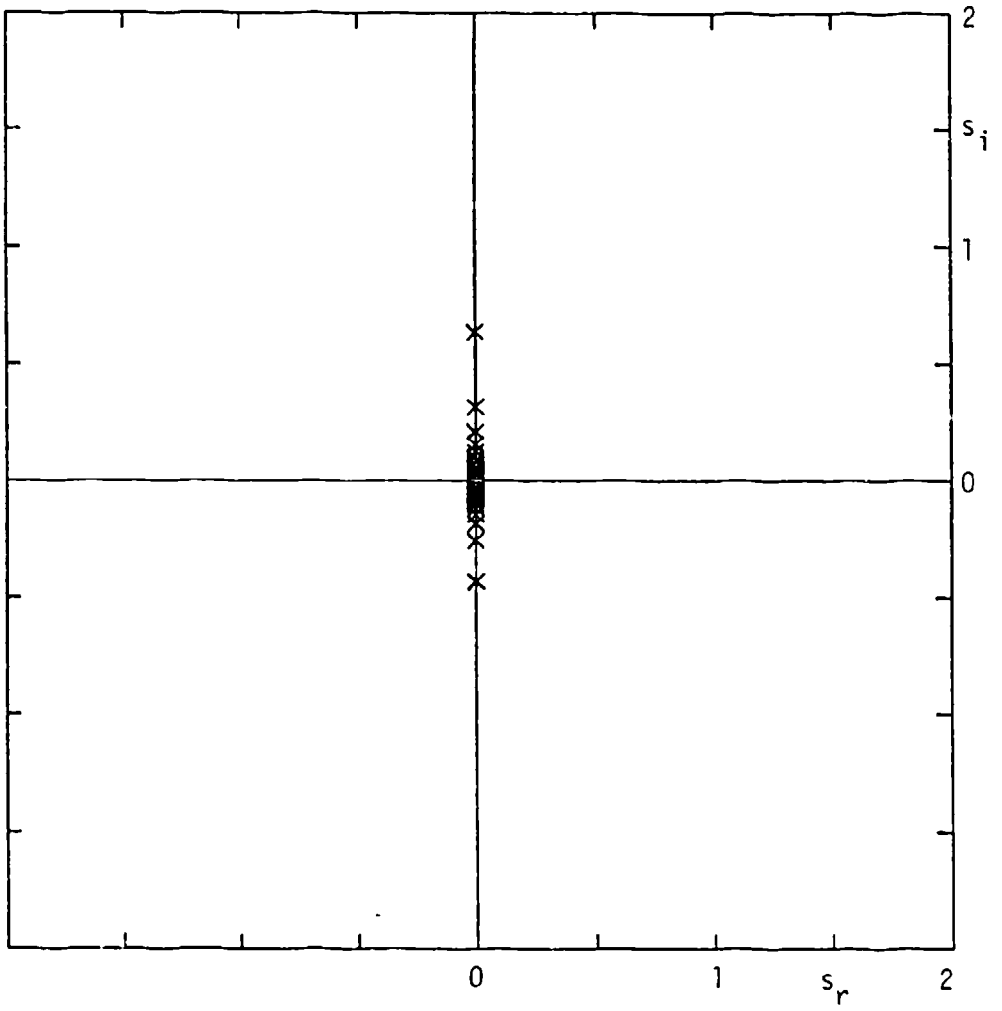

MOD-1 (INVISCID) M 1
TETA 20.00 ALFA 1.0000
TAU 0.16670
OZ 0.15665 JJ 24

Figure 1.

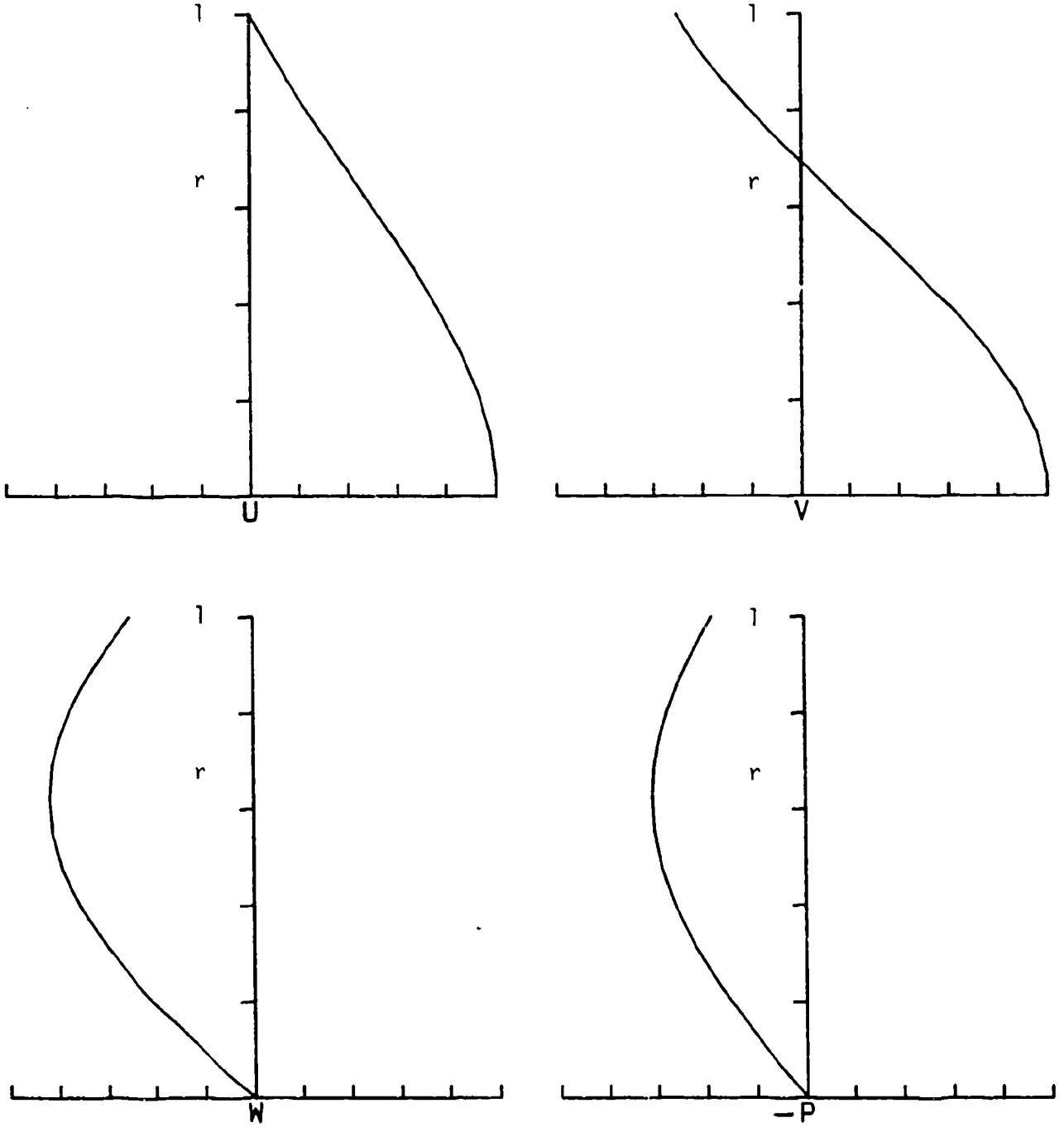

MOD-2 (INVISCID)
TETA 20.00
TAU 0.16670
OZ 0.15665
JJ 18

M 1
ALFA 1.0000
SS 0.000000
0.637582

Figure 2.

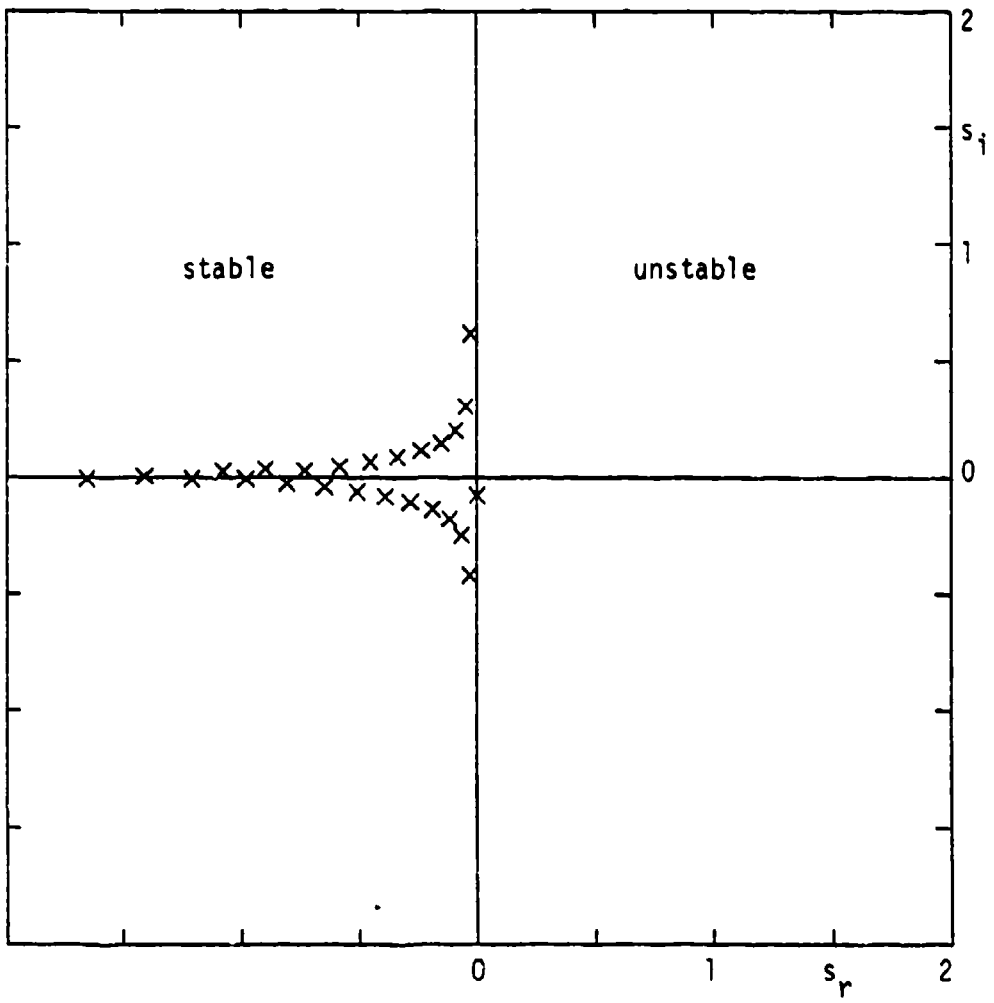

MOD-4

RE 1000.00
TETA 20.00
TAU 0.16670
OZ 0.15665

M 1
ALFA 1.0000

JJ 18

Figure 3.

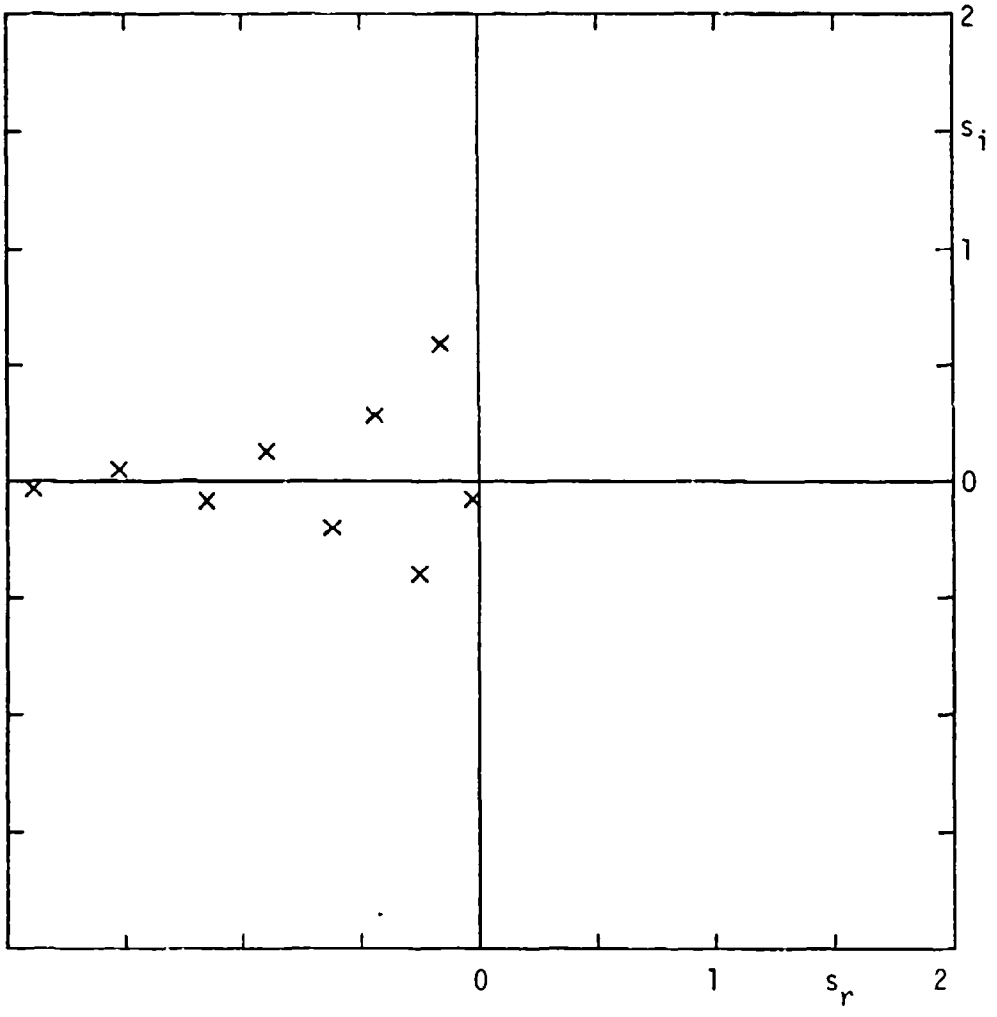

MOD-4

RE 100.00
TETA 20.00
TAU 0.16870
OZ 0.15665

M 1
ALFA 1.0000

JJ 18

Figure 4.

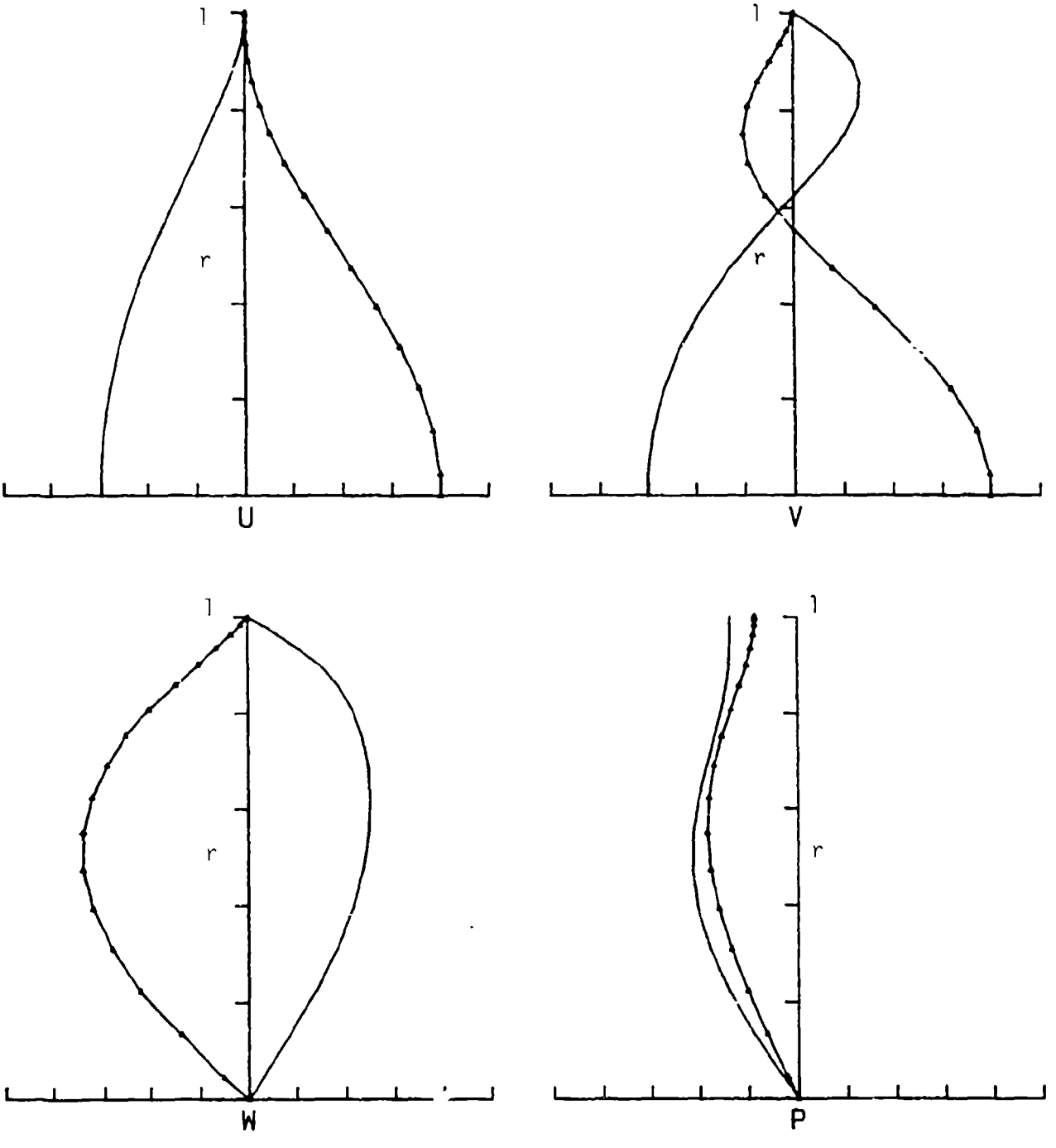

MOD-5

RE	100.00
TETA	20.00
TAU	0.16670
OZ	0.15665
JJ	18

M	1
ALFA	1.0000
SS	-0.157474
	0.590158

Figure 5.

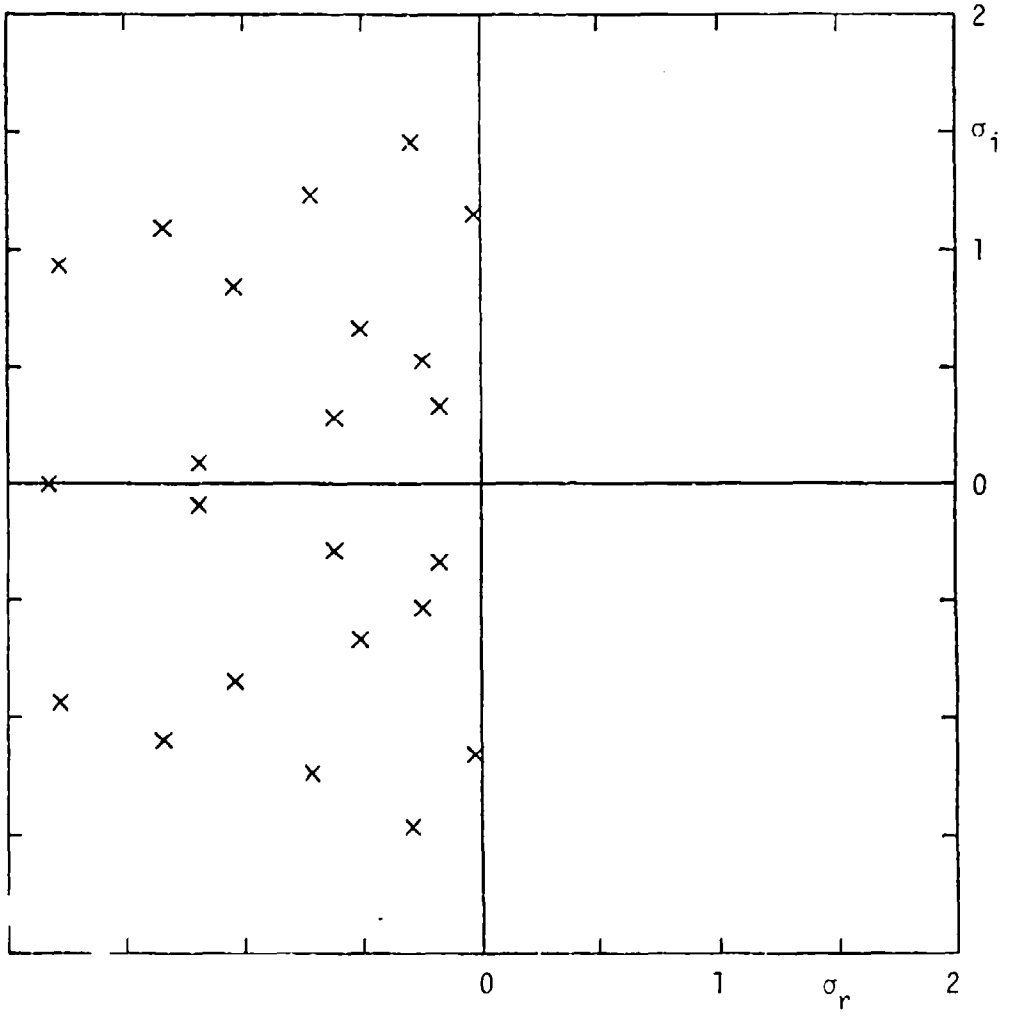

RES--1

RE	100.00	ALFA	1.0000
TETA	20.00		
TAU	0.16670	MX	3
ØZ	0.15665	JJ	10
EPS	0.05701		

Figure 6.

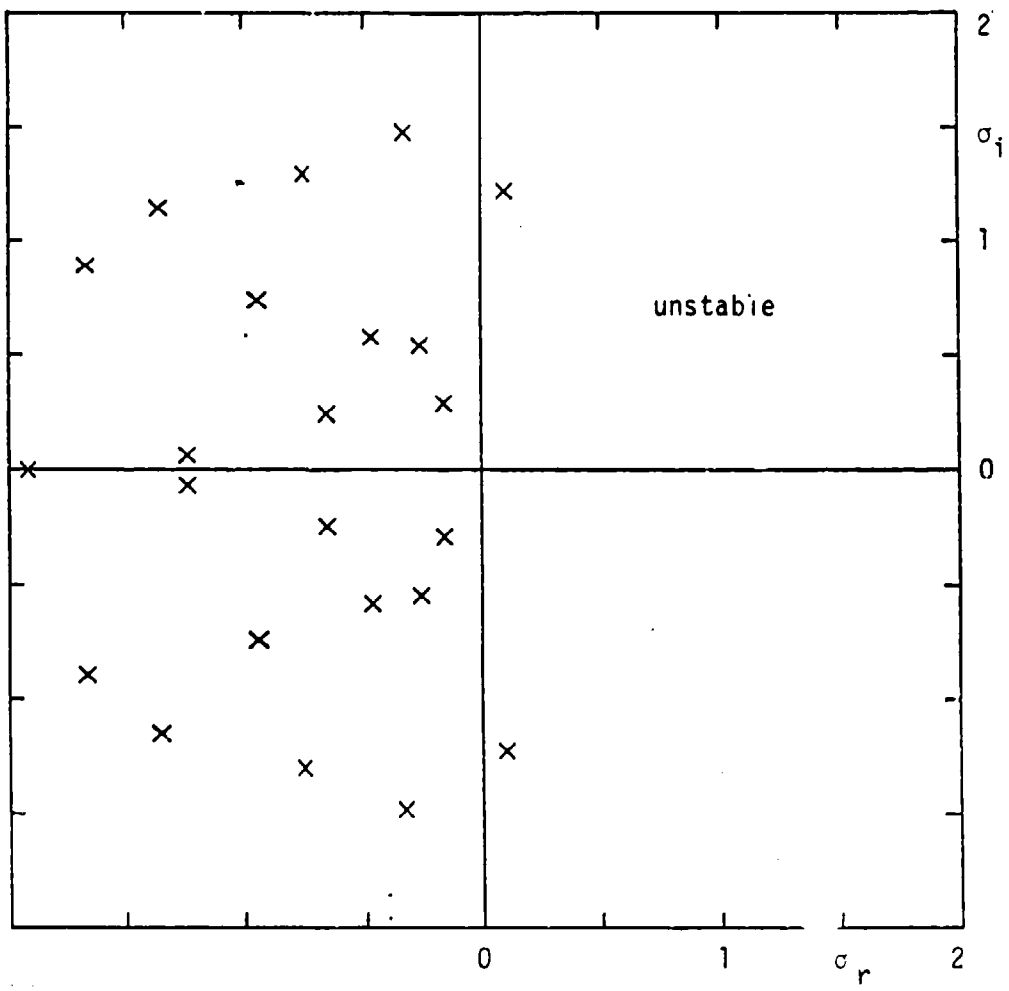

CEL-1

RE	100.00	ALFA	1.0000
TETA	20.00		
TAU	0.16670	MX	3
ØZ	0.15665	JJ	10
EPS	0.05701		

Figure 7.

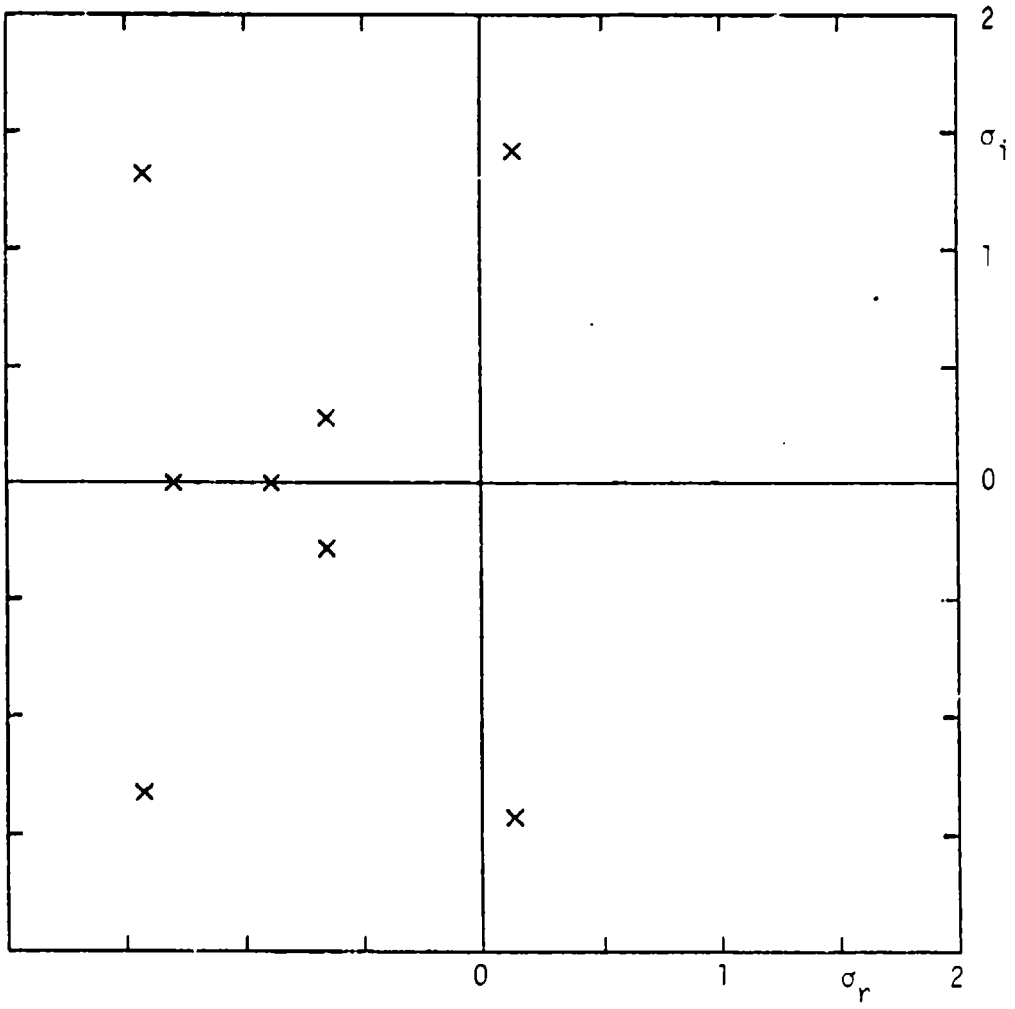

CEL-1

RE 20.00
TETA 20.00
TAU 0.16670
OZ 0.15665
EPS 0.05701

ALFA 0.3000

MX 3
JJ 10

Figure 8.

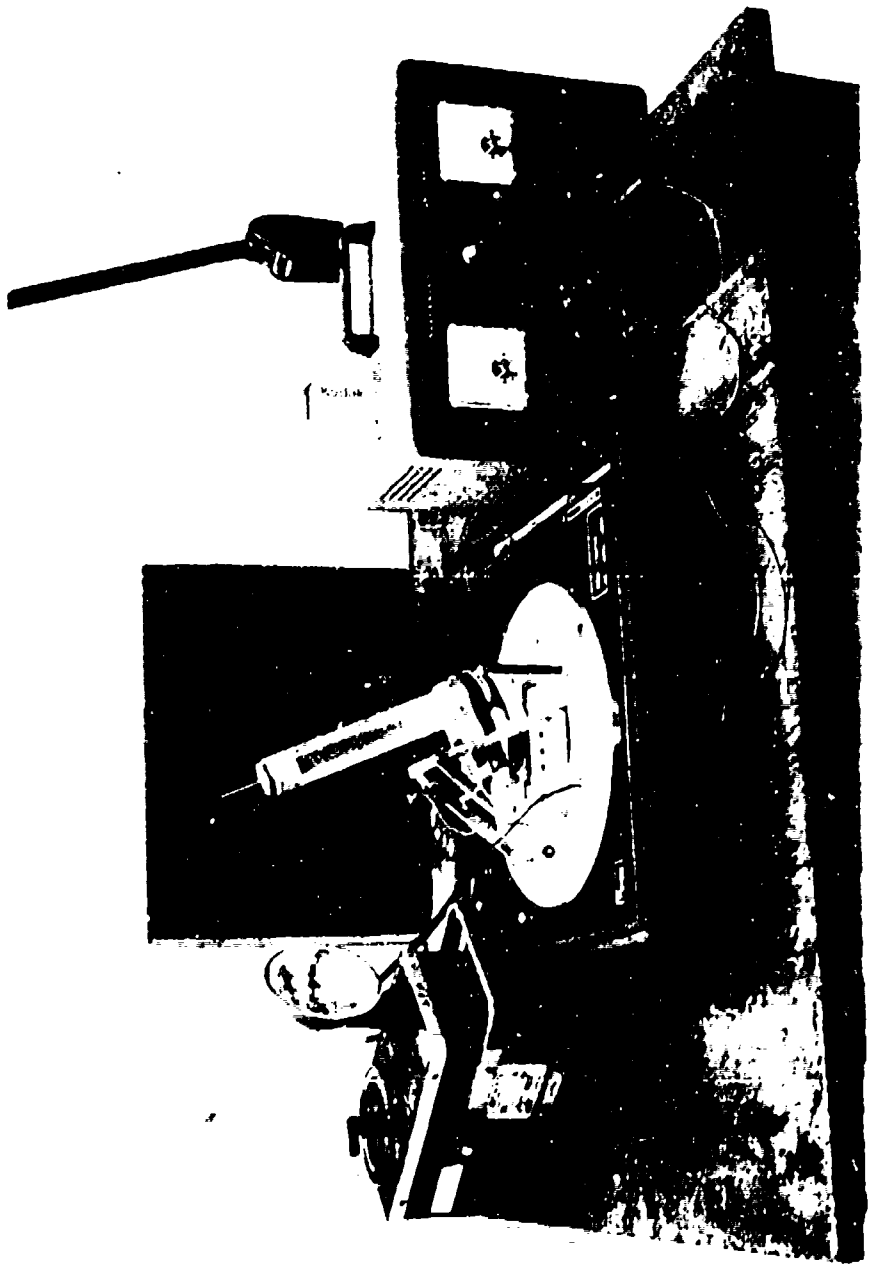

Figure 9.

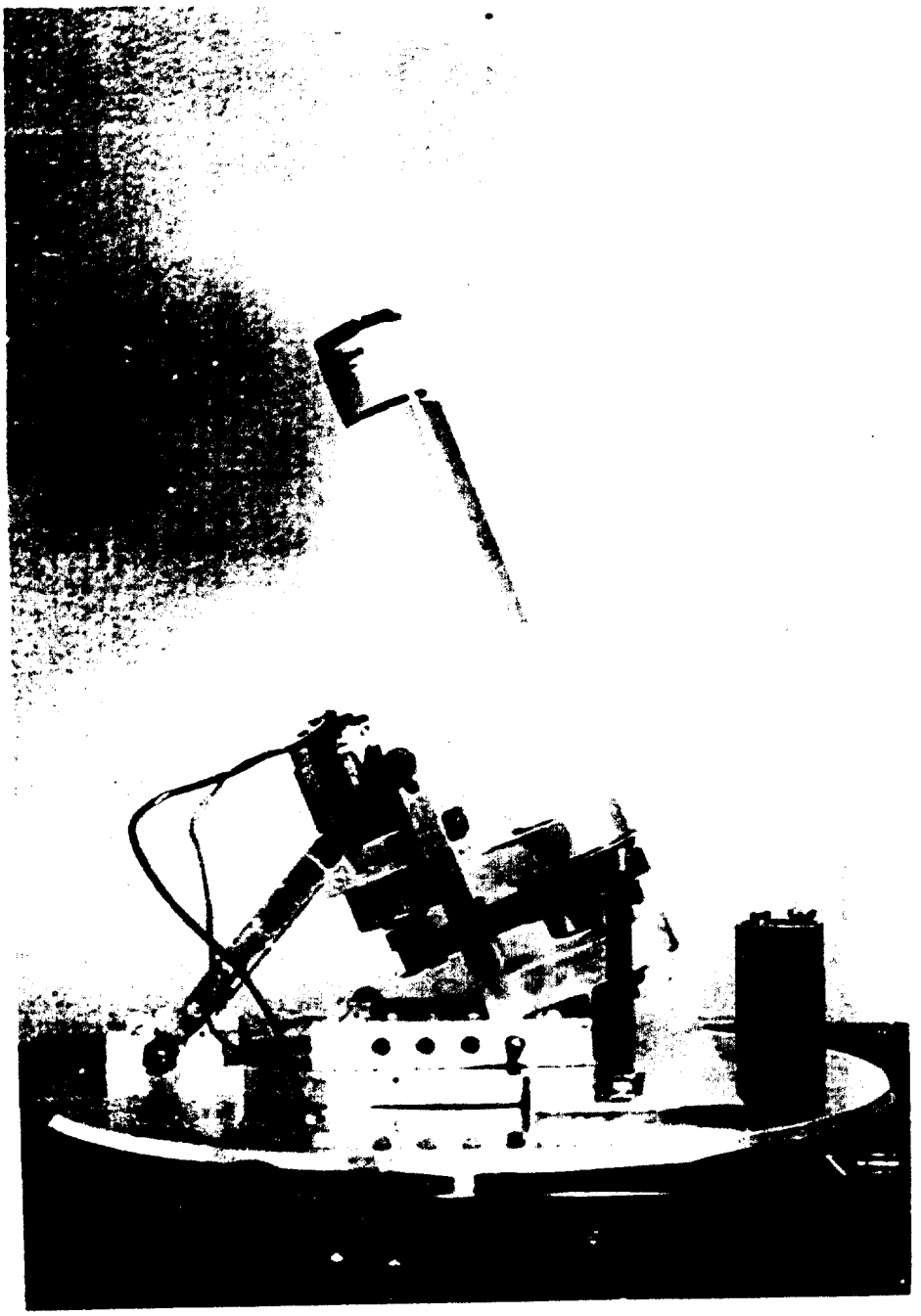

Figure 10.

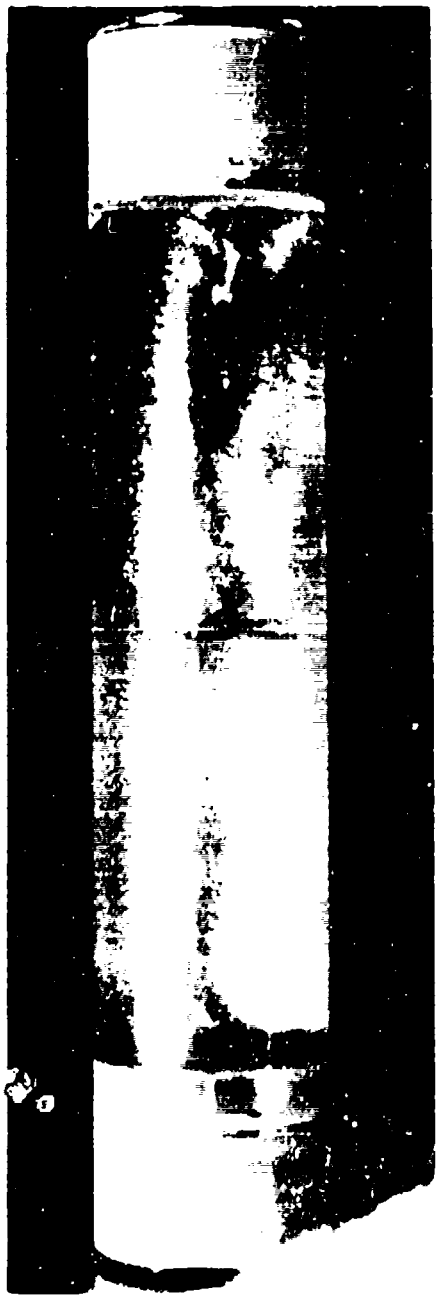

80% Glycerin

$T = 21\,^{\circ}C$

$\nu \approx 66$ cSt

$\theta \approx 20^{\circ}$

$\omega \approx 500$ rpm

$\Omega = 45$ rpm

$Re \approx 130$

Figure 11

94% Glycerin

$T = 26\,^{\circ}C$

$\nu \approx 235$ cSt

$\theta \approx 20^{\circ}$

$\omega \approx 600$ rpm

$\Omega = 33$ rpm

$Re \approx 40$

Figure 12

94% Glycerin

$T = 26\,^{\circ}C$

$\nu \approx 235$ cSt

$\theta \approx 20^{\circ}$

$\omega \approx 600$ rpm

$\Omega = 45$ rpm

$Re \approx 40$

Figure 13

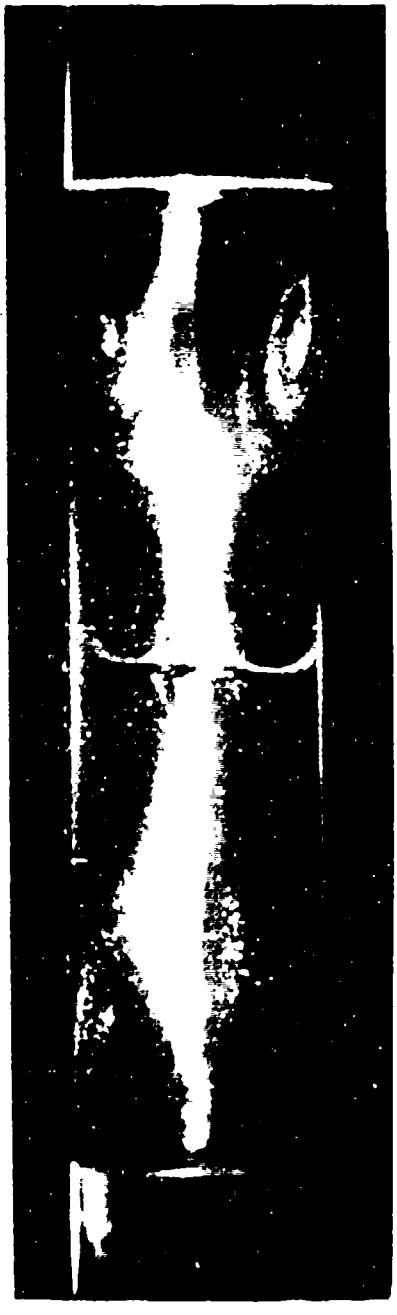

94% Glycerin

$T = 26\,^{\circ}\mathrm{C}$

$\nu \approx 235$ cSt

$\theta \approx 20^{\circ}$

$\omega \approx 600$ rpm

$\Omega = 78$ rpm

$Re \approx 40$

Figure 11

94% Glycerin

$T = 26\,^{\circ}C$

$\nu \approx 235$ cSt

$\theta \approx 20^{\circ}$

$\omega \approx 750$ rpm

$\Omega = 33$ rpm

$Re \approx 50$

Figure 15

100% Water

$T = 26\,^{\circ}C$

$\nu \approx 0.95$ cSt

$\theta \approx 20^{\circ}$

$\omega \approx 450$ rpm

$\Omega = 45$ rpm

$Re \approx 8000$

low particle density

Figure 16

100% Water

$T = 26\,^{\circ}C$

$\nu \approx 0.95$ cSt

$\theta \approx 20^{\circ}$

$\omega \approx 450$ rpm

$\Omega = 78$ rpm

$Re \approx 8000$

high particle density

Figure 17

Appendix A.1

Blank

CRDC-SP-84014

PROCEEDINGS OF THE 1983 SCIENTIFIC CONFERENCE ON CHEMICAL DEFENSE RESEARCH

by Richard L. Dimmick, Jr.
Michael Rausa

RESEARCH DIRECTORATE

October 1984

US Army Armament, Munitions & Chemical Command
Aberdeen Proving Ground, Maryland 21010-5423

APPENDIX A

E.

THE FLOW OF HIGHLY VISCOUS FLUID IN A SPINNING AND NUTATING CYLINDER

Thorwald Herbert
Department of Engineering Science and Mechanics
Virginia Polytechnic Institute and State University
Blacksburg, Virginia 24061

Abstract

Evaluation of the sparse experimental data and analysis of the equations for the fluid motion in a spinning and nutating cylinder suggest a theoretical analysis in three steps: (1) analysis of the viscous flow in an infinitely long cylinder, (2) hydrodynamic stability analysis of this basic flow, and (3) study of the end effects. A status report is given on the first of these tasks. The purely axial basic flow is governed by ordinary differential equations. Analytical and numerical solutions show the different character of this flow at low and high Reynolds numbers. The resulting moments are consistent with experimental data.

Introduction

Spin-stabilized projectiles with liquid payloads can experience a severe flight instability that is characterized by a rap yaw angle growth and a simultaneous loss in spin rate. Experiments with a full-scale liquid-filled cylinder (Miller 1982) have shown that this instability originates from the internal motion of fluids in the range of high viscosities. We have initiated a theoretical analysis of this problem in order to support the ongoing experiments and to obtain independently insight into the flow phenomena. The initial steps of our approach are reported elsewhere (Herbert 1982): evaluation of the experimental data base, dimensional analysis, scaling aspects, governing equations, and discussion of various simplifying assumptions. Two observations in this earlier work led to the results presented here. First, if the despin moment data and void observations (Miller 1981) are correlated with the Reynolds number, at least three regions can be distinguished. At low Reynolds numbers Re, the despin moment increases proportional to Re, and the void in an incompletely filled cylinder is parallel to the spin axis. In a middle range, a maximum of the despin moment exists that seems to be associated with the onset of a void distortion due to a cellular motion of the

fluid. At higher Reynolds numbers, the despin moment decreases in a manner that is not clearly defined by the few available data points. The void observations indicate, however, that the motion ultimately is turbulent. In the theoretical approach, the initial increase in the despin moment is attributed to a simple basic flow that can be studied disregarding the end effects. The occurrence of a cellular motion at higher Reynolds numbers and the reduced despin moment can, in principle, be associated with a hydrodynamic instability of the basic flow. Accounting for the end effects should provide the final polish of the results. The second observation was the appearance of a parameter in the equations for the deviation from solid body rotation that can be considered small enough for linearization in the situations of practical and experimental interest.

In the following, we describe the development of a simple system of equations for the basic flow and discuss asymptotic solutions and numerical results. A comparison is made with computer simulations of the flow (Vaughn 1983) and with experimental data (Miller 1982).

The Basic Flow

We consider the motion of a fluid of density ρ and viscosity μ in a cylinder of radius a and length 2c. The cylinder rotates with the spin rate ω about its axis, the z-axis. The z-axis is inclined by the nutation angle θ with respect to the inertial Z-axis and the Z,z-plane rotates with the nutation rate Ω about the Z-axis. The two rotation axes intersect in the center of mass of the cylinder. In contrast to the experimental procedures (Miller 1982), we consider $\omega>0$, $\Omega>0$, and $\theta>0$ as constant. We describe the motion by the Navier-Stokes equations, written in the aeroballistic or nutating coordinate system x,y,z, where x is normal to z in the Z,z-plane:

$$\rho\left[\frac{D\underset{\sim}{V}_n}{Dt} + 2\underset{\sim}{\Omega} \times \underset{\sim}{V}_n + \underset{\sim}{\Omega} \times (\underset{\sim}{\Omega} \times \underset{\sim}{r})\right] = -\nabla p_n + \mu\nabla^2\underset{\sim}{V}_n$$

$$\nabla\cdot\underset{\sim}{V}_n = 0. \qquad (1)$$

$\underset{\sim}{V}_n$ is the velocity measured in the nutating system, p_n the pressure, and $\underset{\sim}{r}$ the position vector. The body force due to gravity is neglected. Equations (1) are subject to the no-slip and no-penetration conditions at the cylinder walls.

In the next step, we split the velocity and pressure fields according to

$$\underset{\sim}{V}_n = \underset{\sim}{V}_s + \underset{\sim}{V}_d, \quad p_n = p_s + p_d \qquad (2)$$

where $\underset{\sim}{V}_s, p_s$ describe the state of pure solid body rotation, whereas $\underset{\sim}{V}_d, p_d$ describe the deviation from solid body rotation. It is obvious that $\underset{\sim}{V}_d \equiv 0$, $p_d \equiv 0$ if either one of the following conditions is satisfied: $\omega=0$, $\Omega=0$, $\theta=0$ or $\mu\to\infty$ (solid fill).

The equations for $\underset{\sim}{V}_d$ are written in terms of non-dimensional quantities, using a, ω, and ρ for scaling length, time and mass. Note that this choice is

ambiguous (Herbert 1982) and excludes the case of no spin. The problem then depends on four non-dimensional parameters:

$\lambda = c/a$	aspect ratio
$\sigma = \sin\theta$	
$\tau = \Omega/\omega$	frequency
$Re = \rho\omega a^2/\mu$	Reynolds number.

The aspect ratio is only contained in the boundary conditions.

Finally, cylindrical coordinates r,ϕ,z are introduced. The equations for the (non-dimensional) components v_r, v_ϕ, v_z of the velocity deviation and the pressure deviation p' are given as equations (4.22) by Herbert (1982). The most remarkable fact about these equations is the appearance of a force term $2\tau\sigma r\cos\phi$ in the z-momentum equation. If this term vanishes, the equations support only a trivial solution. It is obvious, therefore, that the deviation velocity is of order $O(\tau\sigma)$. At close analysis, $\tau\sigma = (\Omega/\omega)\sin\theta$ turns out to be a rather small parameter. Even a conservative estimate with $\Omega<500$ rpm, $\omega>3000$ rpm and $\theta<20^0$ provides values $\tau\sigma<0.057$. It seems well justified, then, to linearize the equations in $\tau\sigma$. It is also worth noting that this linearization imposes no restriction on the Reynolds number Re.

The resulting system of linear equations is still quite difficult to solve, mainly owing to the boundary conditions. Use of the boundary layer approximation would simplify the task, but seems inappropriate in the interesting range of Reynolds numbers. The equations suggest, however, that a solution can be found when the boundary conditions at the end walls of the cylinder are relaxed. As a first step, therefore, a steady flow (basic flow) is sought disregarding the end walls, i.e. for an infinitely long cylinder. Despite other initial thoughts, the force term in the z-momentum equation causes a deviation velocity that is purely axial,

$$\underset{\sim}{V}_d = (0,\ 0,\ \omega a v_z),\ p_d = 0. \tag{3}$$

It is also consistent with the equations to assume a solution in the form

$$v_z = 2\tau\sigma[f(r)\cos\phi + g(r)\sin\phi] \tag{4}$$

where

$$f'' + \frac{1}{r}f' - \frac{1}{r^2}f - Re\ g = -Re\ r \tag{5a}$$

$$g'' + \frac{1}{r}g' - \frac{1}{r^2}g + Re\ f = 0 \tag{5b}$$

$$f,g \begin{cases} = 0 & \text{at } r = 1 \\ \text{finite} & \text{at } r = 0. \end{cases} \tag{5c}$$

The prime denotes d/dr. These equations seem to call for an analytical solution, but our attempts were not yet successful. For low Reynolds numbers, it is obvious that

$$f = O(Re), \quad g = O(Re^2) \tag{6}$$

and in more detail

$$f = \frac{Re}{8}(r - r^3) + O(Re^3) \tag{7a}$$

$$g = \frac{Re^2}{192}(2r - 3r^3 + r^5) + O(Re^4). \tag{7b}$$

A series including higher order terms in Re has been constructed but converges only for Re<12. Another interesting limit can be easily obtained for Re→∞:

$$\left.\begin{matrix} f \to 0 \\ g \to r \end{matrix}\right\} \text{ as } Re \to \infty. \tag{8}$$

Owing to the loss of the highest derivatives, this solution cannot satisfy the boundary conditions and is valid only outside the thin boundary layers near the cylinder sidewall.

Without any detailed knowledge of the solution in the medium range of Re, it can be seen that the basic flow exhibits characteristically different behavior at low and high Reynolds numbers. At low Re, the component f in the plane ϕ=0 (Z,z-plane) is dominating. At high Re, f is negligible (except in the boundary layer), and the component g in the plane $\phi=90^0$ is dominating.

In the medium range of Re, we have applied a spectral collocation method for numerical solution. This method is especially capable of resolving the steep gradients in the boundary layers at large Re. Figure 1 shows the numerical results in the form of contour lines of equal axial velocity. The flow to the right or above the (thicker) zero-velocity line is toward the reader. The shift of the velocity maximum from ϕ=0 at Re=0.01 to $\phi=90^0$ at R=1000, and the pronounced boundary layer formation in the latter case is clearly visible.

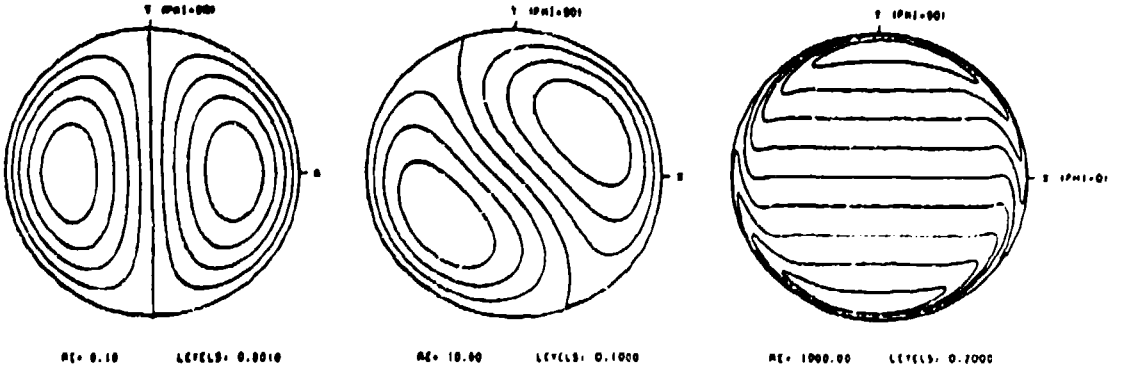

Figure 1. Contour lines of equal axial velocity, $v_z/(2\pi\sigma)$ = const., for Re=0.01, 10 and 1000. The difference between levels is 0.001, 0.1 and 0.2, respectively.

For supporting the relevance of our solution, Figure 2 shows the comparison with computational results for the velocity distributions in the center cross-section (z=0) of the cylinder. The data were kindly provided by Dr. Vaughn, Sandia National Laboratories. The agreement for Re=14.9 is considered representative for the range of lower Reynolds numbers. At the higher Re=45.7, a minor but systematic deviation between our solution and the Sandia results exists that seems to be due to a superposed cellular motion. This cellular motion is not yet incorporated into in our analysis and will be subject to further study. The axial flow considered here will provide the basic flow for an analysis of the hydrodynamic stability. It is encouraging, though, that our simple theory yields results in essential agreement with the computational solution of the full Navier-Stokes equations for a finite-length cylinder. The computational effort for solving the ordinary differential equations (5) is rather small, typically 25 msec (IBM 3081) per solution.

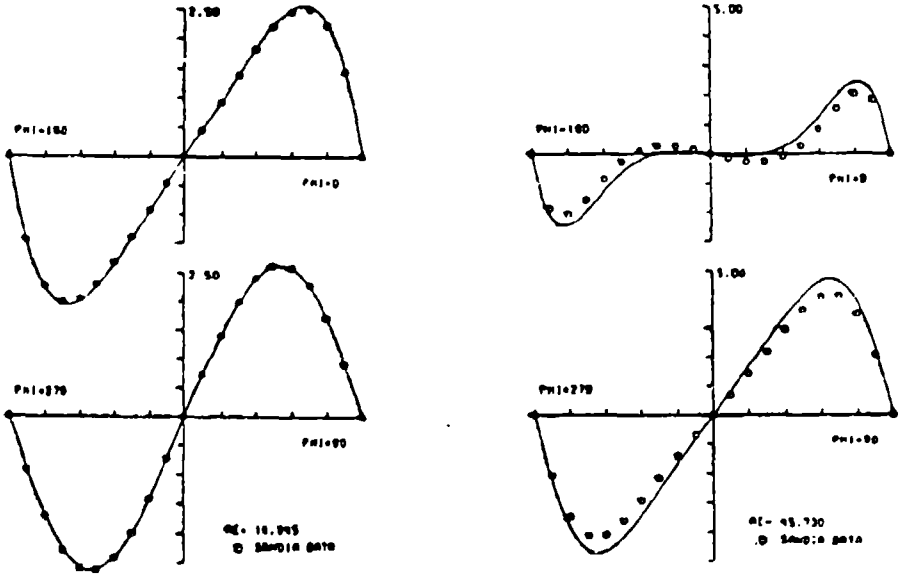

Figure 2. Radial distribution of the axial velocity (in fps) at z=0 for Re=14.9 and Re=45.7. The symbols show the solution to the full Navier-Stokes equations (Vaughn, personal communication).

Moments

In order to compare with the experimental data for the despin moments, we have analyzed the moments that arise from the deviation velocity $\underset{\sim}{V}_d$, disregarding the contribution of pure solid body rotation. Conservation of angular momentum for the fixed cylindrical control volume R (surface S) requires

$$\underset{\sim}{M} = \frac{\partial}{\partial t}\iiint_R (\underset{\sim}{r} \times \underset{\sim}{V}_d)\rho dR + \iiint_R [\underset{\sim}{r} \times (2\underset{\sim}{\Omega} \times \underset{\sim}{V}_d)]\rho dR$$
$$+ \iint_S [\underset{\sim}{r} \times (\underset{\sim}{V}_s + \underset{\sim}{V}_d)]\rho(\underset{\sim}{V}_d \cdot \underset{\sim}{n})dS - \sum (\underset{\sim}{r} \times \underset{\sim}{F}_d) \qquad (9)$$

where $\underset{\sim}{M}$ is the resultant torque on the system. The first term on the right-hand side vanishes for steady $\underset{\sim}{V}_d$. The second term originates from Coriolis forces in the nutating system. The third term describes the net rate of angular momentum flux through the control surface with the outer normal $\underset{\sim}{n}$. The contribution from $\underset{\sim}{r} \times \underset{\sim}{V}_d$ vanishes since $\underset{\sim}{V}_d$ has only an axial component. The last term gives the moments due to the shear forces at the cylindrical surface. There is no pressure contribution since $p_d = 0$.

Substitution of $\underset{\sim}{V}_d$ and v_z provides the following expressions for the components of $\underset{\sim}{M}$:

$$M_x = m_\ell (2\Omega a \sin\theta)(\omega a) \left\{ \frac{g'(1)}{Re} - \int_0^1 r^2 f dr \right\} \tag{10a}$$

$$M_y = m_\ell (2\Omega a \sin\theta)(\omega a) \left\{ -\frac{f'(1)}{Re} - \int_0^1 r^2 g dr \right\} \tag{10b}$$

$$M_z = m_\ell (2\Omega a \sin\theta)^2 \left\{ \int_0^1 r^2 f dr \right\} \tag{10c}$$

where m_ℓ is the liquid mass in the cylinder. The derivatives g', f' in M_x, M_y originate from the shear forces at the cylinder, whereas the integrals provide the rate of angular momentum flux. The despin moment M_z is due to Coriolis forces. Note, however, that the interpretation of M_z will be different if the flux through the cylinder end walls is prohibited.

Using the differential equations (5a,b) and integration by parts, the integrals in (10a,b,c) can be expressed as

$$\int_0^1 r^2 f dr = -\frac{g'(1)}{Re}, \quad \int_0^1 r^2 g dr = \frac{f'(1)}{Re} + \frac{1}{4}. \tag{11}$$

The moments can therefore be written as

$$M_y = m_\ell (2\Omega a \sin\theta)(\omega a)\, \hat{M}_y, \quad \hat{M}_y = -\frac{1}{4} - \frac{2}{Re} f'(1) \tag{12a}$$

$$M_z = m_\ell (2\Omega a \sin\theta)^2\, \hat{M}_z, \quad \hat{M}_z = -\frac{1}{Re} g'(1) \tag{12b}$$

$$M_x = -\frac{\omega}{\Omega \sin\theta} M_z. \tag{12c}$$

Since $f'(1) < 0$, $g'(1) < 0$ for all finite $Re \neq 0$, the moment M_z about the spin axis is always positive, whereas $M_x < 0$. For small Reynolds number, the series solution (7) provides

$$\hat{M}_y = \frac{1}{4} - \frac{Re^2}{768}, \quad \hat{M}_z = \frac{Re}{96} \tag{13}$$

which allows a quick estimate of the moments for Re < 10, say. The linear increase of M_z with Re is consistent with the experimental data.

The values of $\hat{M}_y$ and $\hat{M}_z$ from numerical solutions are given in Figure 3. It is interesting to note that $\hat{M}_z$ has a pronounced maximum at Re=19. $\hat{M}_y$ varies between 1/4 and -1/4 with a sign change at Re=31. A comparison with experimental data for M_z (Miller 1982) is given in Figure 4 on a doubly logarithmic scale. The data are reduced to $\hat{M}_z$ using the initial spin rate ω=4000 rpm. For Re < 10, the experimental points agree with the simple law $\hat{M}_z$ = Re/96. The systematic deviation for higher Reynolds numbers Re < 200 seems to be due to the occurrence of a cellular motion that is likely to reduce the moment M_z. The two data points for Re > 10^3 indicate turbulent flow.

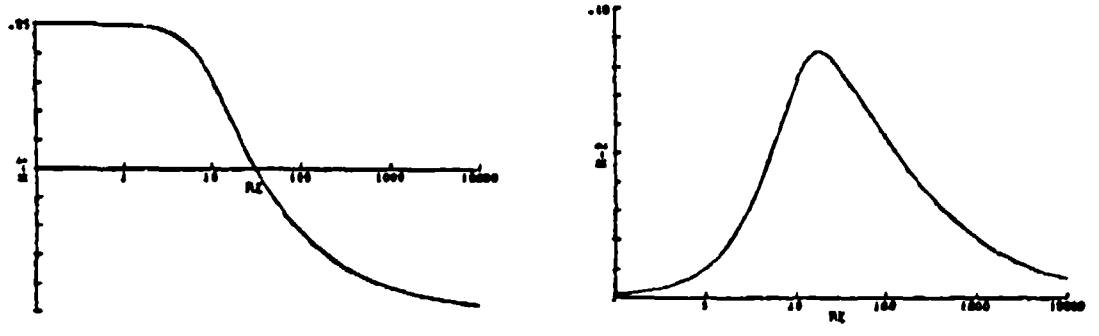

Figure 3. The nondimensional coefficients $\hat{M}_y$ and $\hat{M}_z$ in the moments (12a,b) versus the Reynolds number Re.

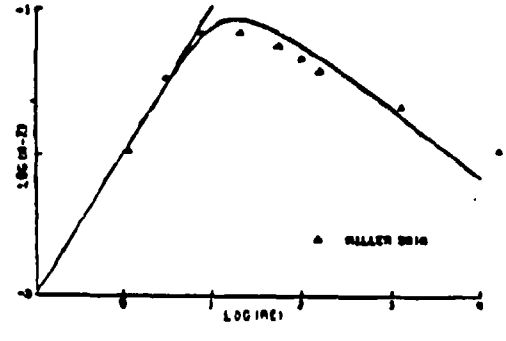

Figure 4. Comparison of the theoretical values of $\hat{M}_z$ with the experimental data of Miller (1982). The straight line shows the asymptotic law $\hat{M}_z$ = Re/96.

Conclusions

The theory developed here is a first but virtually essential step toward understanding and predicting the gross features of the fluid motion in a spinning and nutating cylinder. The axial basic flow allows for an analysis of the hydrodynamic instability with respect to a cellular motion and provides the basis for refinements of the theory.

Acknowledgment

The open cooperation and sharing of data with Miles C. Miller (CRDC) and Harold R. Vaughn (Sandia Laboratories) are greatly appreciated. This work is supported by the Army Research Office under Contract DAAG29-82-K-0129 and by the Army AMCCOM under Contract DAAK11-83-K-0011.

References

Herbert, Th. 1982 "Fluid Motion in a Rotating and Nutating Cylinder - Part I," Report prepared under the Scientific Services Program.

Miller, M. C. 1981 "Void Characteristics of a Liquid Filled Cylinder Undergoing Spinning and Coning Motion," Journal of Spacecraft and Rockets 18, 286-288.

Miller, M. C. 1982 "Flight Instabilities of Spinning Projectiles Having Nonrigid Payloads," Journal of Guidance, Control, and Dynamics 5, 151-157.

Vaughn, H. R. 1983 "Numerical Solution to the Navier-Stokes Equations for Spinning and Nutating Fluid Payloads," Proceedings of this Conference.

Appendix A.2

ARO Report 85-1

TRANSACTIONS OF THE SECOND ARMY

CONFERENCE ON APPLIED MATHEMATICS AND COMPUTING

Sponsored by

The Army Mathematics Steering Committee

on behalf of

THE CHIEF OF RESEARCH, DEVELOPMENT

AND ACQUISITION

APPENDIX A

HIGHLY VISCOUS FLUID FLOW IN A SPINNING AND NUTATING CYLINDER

Thorwald Herbert
Department of Engineering Science and Mechanics
Virginia Polytechnic Institute and State University
Blacksburg, Virginia 24061

ABSTRACT. Spin-stabilized projectiles with liquid payloads can experience a severe flight instability characterized by a rapid yaw angle growth and a simultaneous loss in spin rate. Laboratory experiments and field tests have shown that this instability originates from the internal fluid motion in the range of high viscosity. Evaluation of the experimental data and analysis of the equations for the fluid motion in a spinning and nutating cylinder suggest a theoretical approach in three major steps: (1) analysis of the steady viscous flow in an infinitely long cylinder, (2) hydrodynamic stability analysis of this basic flow, and (3) analysis of the end effects. The basic flow has been found in analytical form. At low Reynolds number, this flow agrees well with computational results for the center section of a cylinder of aspect ratio 4.3. The despin moment caused by this flow largely agrees with experimental data for a wide range of Reynolds numbers. Current work aims at the stability of this flow.

1. INTRODUCTION. It is well-known that spin-stabilized shells carrying liquid payloads can suffer dynamical instability. For cylindrical cavities and low viscosity of the liquid, the instability due to basically inviscid inertial waves can be predicted by the Stewartson-Wedemeyer theory [1,2]. This theory rests on the boundary-layer approach and is, therefore, restricted to the range of sufficiently large Reynolds numbers. The instability of certain shells like the XM 761 [3,4], however, escaped such a prediction and is also distinguished in character owing to the rapid loss in spin rate. Experiments with a full-scale liquid cylinder [5] and subsequent field tests [6] established that this new flight instability is most pronounced for liquid-fills of very high viscosity.

We conduct a theoretical analysis of this problem in order to support the ongoing experiments and to independently obtain insight into the anatomy of the flow phenomena. The initial steps of this analysis are reported elsewhere [7]: evaluation of the experimental data base, dimensional analysis, scaling aspects, governing equations, and discussion of various simplifying assumptions. Two observations in this earlier work led to the building-block approach discussed in the following. First, if the despin (negative roll) moments [5] and void observations [8] are correlated with the Reynolds number Re, at least three regions can be distinguished. At low Re, the despin moment increases proportional to Re, and the void in an incompletely filled cylinder is parallel to the spin axis. This suggests a simple fluid motion that is essentially independent of the axial coordinate, except in the neighborhood of the end walls. In a middle range of Re, the despin moment assumes a maximum, and a wavy distortion of the void seems to indicate a cellular structure of the fluid motion. This cellular motion can, in principle, originate from hydrodynamic instability of the basic flow with respect to axially periodic disturbances. At still higher Reynolds numbers, the despin moment decreases with increasing Re in a manner not clearly defined by the few available data

points. The void observations indicate, however, that the motion ultimately becomes turbulent.

The second observation was the appearance of the nutation rate and angle as a small parameter in the equations for the deviation from solid-body rotation. The forcing term due to nutation can be considered small enough for linearization of the equations in the situations of practical and theoretical interest.

In the following, we describe the development of a simple system of equations for the basic flow. Analytical solutions are given for the flow field and for the liquid moments. A comparison is made with computer simulations of the flow [9] and with experimental data [5]. The properties of inertial modes at low Reynolds numbers and the possibility of instability due to primary resonance is discussed.

2. GOVERNING EQUATIONS. We consider the motion of a fluid of density ρ and viscosity μ in a cylinder of radius a and length 2c that rotates with the spin rate ω about its axis of symmetry, the z-axis. We consider the motion with respect to the nutating coordinate system x,y,z. This system is obtained from the inertial system X,Y,Z by a rotation with the nutation angle θ about the axis Y=y. Therefore, x is in tne Z,z-plane, and this plane rotates about the Z-axis with the nutation rate Ω. The two axes of rotation intersect in the center of mass of the cylinder, as shown in Fig. 1. In contrast to the experimental procedures [5], we consider $\omega>0$, Ω, and $0\le\theta\le\pi/2$ as constant. The fluid motion is governed by the Navier-Stokes equations written in the nutating coordinate system:

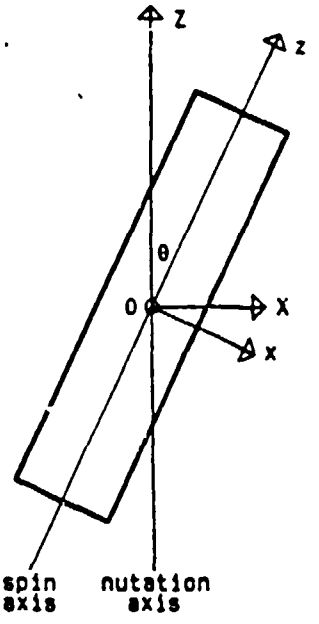

Figure 1. Definition sketch.

$$\rho\left[\frac{D\underset{\sim}{V}_n}{Dt} + 2\underset{\sim}{\Omega} \times \underset{\sim}{V}_n + \underset{\sim}{\Omega} \times (\underset{\sim}{\Omega} \times \underset{\sim}{r})\right] = -\nabla P_n + \mu\nabla^2\underset{\sim}{V}_n \qquad (1)$$

$$\nabla\cdot\underset{\sim}{V}_n = 0.$$

$\underset{\sim}{V}_n$ is the velocity measured in the nutating frame, P_n the pressure, and $\underset{\sim}{r}$ the position vector. The body force due to gravity has been disregarded. Equations (1) are subject to the no-slip and no-penetration conditions at the cylinder walls.

It is convenient [7] to split the velocity and pressure fields according to

$$\underset{\sim}{V}_n = \underset{\sim}{V}_s + \underset{\sim}{V}_d, \quad P_n = P_s + P_d$$

where $\underset{\sim}{V}_s, P_s$ describe the state of pure solid body rotation, whereas $\underset{\sim}{V}_d, P_d$ represent the deviation from solid body rotation. The advantage of this isolated view on the deviation is obvious: $\underset{\sim}{V}_d$ and the reduced pressure P_d are responsible for the observed flight instability. A glance at the equations shows that $V_d \equiv 0$ and $P_d \equiv 0$ if either one of the following conditions is satisfied: $\omega=0$, $\Omega=0$, $\theta=0$ or $\mu \to \infty$ (solid fill).

The equations for $\underset{\sim}{V}_d$, P_d are then written in terms of nondimensional quantities $\underset{\sim}{v}_d$, p_d. We use a, ω, and ρ for scaling length, time, and mass. Note that this choice is ambiguous [7] and excludes the case $\omega=0$ (which lacks practical interest). The problem then depends on four nondimensional parameters:

$\lambda = c/a$	aspect ratio
$\sigma = \sin\theta$	
$\tau = \Omega/\omega$	frequency
$Re = \rho\omega a^2/\mu$	Reynolds number.

The aspect ratio enters the solution only through the boundary conditions. The boundary conditions on $\underset{\sim}{v}_d$ are homogeneous.

In cylindrical coordinates r,ϕ,z, the equations for the nondimensional deviation velocity $\underset{\sim}{v}_d = (v_r, v_\phi, v_z)$ and pressure p_d take the form

$$\frac{1}{r}\frac{\partial}{\partial r}(rv_r) + \frac{1}{r}\frac{\partial v_\phi}{\partial \phi} + \frac{\partial v_z}{\partial z} = 0 \tag{2a}$$

$$D'v_r - \frac{v_\phi^2}{r} - 2(1+\tau_z)\,v_\phi + 2\tau_\phi v_z = -\frac{\partial p_d}{\partial r} + \frac{1}{Re}\left[D''v_r - \frac{v_r}{r^2} - \frac{2}{r^2}\frac{\partial v_\phi}{\partial \phi}\right] \tag{2b}$$

$$D'v_\phi + \frac{v_r v_\phi}{r} + 2(1+\tau_z)\,v_r - 2\tau_r v_z = -\frac{1}{r}\frac{\partial p_d}{\partial \phi} + \frac{1}{Re}\left[D''v_\phi - \frac{v_\phi}{r^2} + \frac{2}{r^2}\frac{\partial v_r}{\partial \phi}\right] \tag{2c}$$

$$D'v_z + 2\tau_r v_\phi - 2\tau_\phi v_r = -\frac{\partial p_d}{\partial z} - 2r\tau_r + \frac{1}{Re}D''v_z \tag{2d}$$

where

$$D' = \frac{\partial}{\partial t} + \frac{\partial}{\partial \phi} + v_r\frac{\partial}{\partial r} + \frac{v_\phi}{r}\frac{\partial}{\partial \phi} + v_z\frac{\partial}{\partial z}$$

$$D'' = \frac{\partial^2}{\partial r^2} + \frac{1}{r}\frac{\partial}{\partial r} + \frac{1}{r^2}\frac{\partial^2}{\partial \phi^2} + \frac{\partial^2}{\partial z^2}$$

and

$$\tau_r = -\varepsilon\cos\phi,\ \tau_\phi = \varepsilon\sin\phi,\ \tau_z = \tau\cos\theta,\ \varepsilon = \tau\sin\theta \qquad (3)$$

The primary effect of nutation is contained in the ϕ-periodic force term $-2r\tau_r = 2\varepsilon r\cos\phi$ in the z-momentum equation (2d). If this term vanishes throughout, $\varepsilon=0$, equations (2) support a trivial solution $\underset{\sim}{v}_d=0$, $p_d=0$. For sufficiently small $\varepsilon\neq 0$, it is obvious that the deviation velocity is of order $O(\varepsilon)$. In the situations of practical interest, $\varepsilon = (\Omega/\omega)\sin\theta$ turns out to be a rather small parameter. Even a conservative estimate with $\Omega \leq 500$ rpm, $\omega \geq 3000$ rpm, and $\theta \leq 20^\circ$ provides values of $\varepsilon \leq 0.057$. Consequently, it seems well justified to linearize the equations in ε. This linearization imposes no restriction on the Reynolds number.

3. THE BASIC FLOW. The system of equations after linearization is still quite difficult to solve. Any serious attempt to satisfy all boundary conditions leads directly to a purely computational approach. Use of the boundary-layer approximation would simplify the task but seems inappropriate in the interesting range of low Reynolds numbers. Recalling that the flow in a relatively long cylinder (aspect ratio $\lambda=4.3$) at low Re exhibits little axial variation over much of the cylinder length [7], we have relaxed the boundary conditions at the end walls. As a first step, we seek for a steady flow in an infinitely long cylinder.

At closer analysis, the z-independent force term in eq. (2d) can only be balanced by a purely axial deviation velocity. It is consistent with the linearized equations to assume a solution in the form

$$\underset{\sim}{v}_d = (0,\ 0,\ v_z),\ p_d = 0 \qquad (4)$$

and moreover,

$$v_z = v_z(r,\phi) = 2\varepsilon[f(r)\cos\phi + g(r)\sin\phi] \qquad (5)$$

Substituting (4),(5) into the linearized equations provides

$$f'' + \frac{1}{r}f' - \frac{1}{r^2}f - \mathrm{Re}\,g = -\mathrm{Re}\,r \qquad (6a)$$

$$g'' + \frac{1}{r}g' - \frac{1}{r^2}g + \mathrm{Re}\,f = 0 \qquad (6b)$$

$$f=0,\ g=0 \quad \text{at} \quad r=1 \qquad (6c)$$

$$f,\ g \quad \text{finite} \quad \text{at} \quad r=0 \qquad (6d)$$

The primes denote d/dr. For Re→0, the solution of these equations can be found in the form of series

$$f = \frac{\mathrm{Re}}{8}(r - r^3) - \frac{\mathrm{Re}^3}{9216}(7r - 12r^3 + 6r^5 - r^7) + O(\mathrm{Re}^5) \qquad (7a)$$

$$g = \frac{Re^2}{192}\,(2r - 3r^3 + r^5) + O(Re^4). \qquad (7b)$$

With higher terms included, these series converge for $Re \le 12$. In the limit $Re \to \infty$, one obtains

$$f \to 0, \quad g \to r \quad \text{as} \quad Re \to \infty. \qquad (8)$$

Owing to the loss of the highest derivatives, however, this solution cannot satisfy the boundary conditions (6c) and is valid only outside the thin boundary layers near the wall at r=1. Even without any knowledge of the solution in the intermediate range, the different character of the basic flow at low and high Reynolds numbers is evident. At low Re, the component f in the z,x-plane $\phi=0$ is dominating. At high Re, f is negligible in the core of the cylinder while g in the z,y-plane $\phi=90^0$ is dominating.

In earlier work [10], we have applied a spectral collocation method for numerical solution of eqs. (6). Here, we derive an analytical solution by introducing the complex function F=g+if. Eqs. (6) can then be written in the form

$$r^2F'' + rF' - (1 + iRe\ r^2)F = - iRe\ r^3 \qquad (9a)$$

$$F = 0 \quad \text{at} \quad r = 1 \qquad (9b)$$

$$F \text{ finite} \quad \text{at} \quad r = 0 \qquad (9c)$$

A particular solution of the inhomogeneous equation (9a) is $F_0=r$, whereas the homogeneous part of (9a) is the equation for the modified Bessel functions $I_1(qr)$ and $K_1(qr)$ of the complex argument qr with $q = \sqrt{Re/2}\,(1 + i)r$. For (9c), $K_1(qr)$ cannot contribute to the solution. Finally, (9b) provides

$$F(r) = g + if = r - I_1(qr)/I_1(q). \qquad (10)$$

Expressing the solution in terms of Kelvin functions of real argument is of little advantage for the numerical evaluation. The solution is valid for arbitrary Re but may be unstable as Re exceeds some critical value. It is straightforward to derive the approximations (7) from the ascending series for I_1 (and to explain the convergence problem for larger Re). The asymptotic expansion for large arguments provides

$$F \to r - \sqrt{r}\ e^{q(r-1)}. \qquad (11)$$

This expression agrees to within 1% with (8) provided that $r \le 1 - \delta$. The boundary layer thickness δ can be obtained from the transcendental equation

$$\delta = \sqrt{2/Re}\,[4.605 - \tfrac{3}{2}\,\ln\,(1 - \delta)], \qquad (12)$$

e.g., $\delta=0.223$ for Re=1000. The characteristic changes in the flow structure with increasing Re, in particular the shift of the velocity maximum from $\phi=0$ at Re=2 to $\phi\approx90^0$ at Re=200 are shown in Fig. 2.

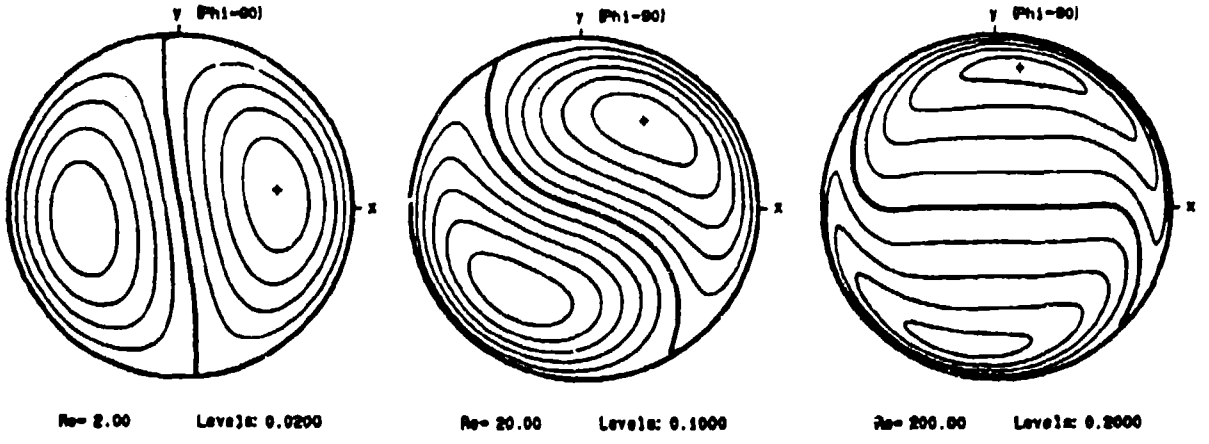

Figure 2. Contour lines of equal axial velocity, $v_z/(2\epsilon)$ = const., for Re=2, 20, and 200. The difference between levels is 0.02, 0.1, and 0.2, respectively. The + marks the velocity maximum.

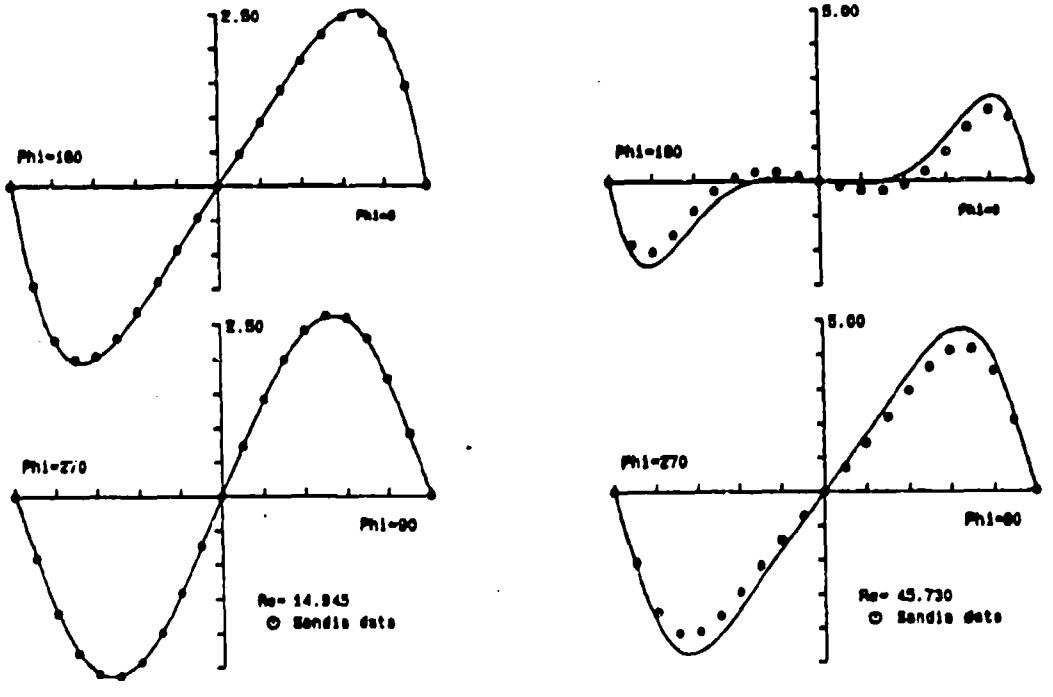

Figure 3. Radial distribution of the axial velocity (in fps) at z=0 for Re=14.9 and Re=45.7. The symbols show the solution to the full Navier-Stokes equations.

Fig. 3 compares the dimensional velocity distributions obtained from (5), (10) with computational results for the center cross-section (z=0) of the cylinder.* The agreement for Re=14.9 is considered representative for the range of lower Reynolds numbers. The numerical simulation provides very small components v_r, v_θ and hence verifies our estimates. At the higher value Re=45.7, a systematic deviation between the two results seems to be due to a superposed cellular motion that is not yet incorporated into our analysis. It is encouraging, however, that the simple theory of the basic flow yields results in essential agreement with the computational solution of the full Navier Stokes equations for a finite-length cylinder.

4. MOMENTS. With the deviation velocity $\underset{\sim}{V}_d = (0,0,\omega a v_z)$ and v_z given, the moments on a finite-length section of the cylinder can be calculated. We consider a control volume R (surface S) formed by the solid cylindrical wall and liquid surfaces at both ends. Conservation of angular momentum requires

$$\underset{\sim}{M} + \Sigma\,(\underset{\sim}{r} \times \underset{\sim}{F}_d) = \frac{\partial}{\partial t}\iiint_R (\underset{\sim}{r} \times \underset{\sim}{V}_d)\rho dR + \iiint_R [\underset{\sim}{r} \times (2\underset{\sim}{\Omega} \times \underset{\sim}{V}_d)]\rho dR$$
$$+ \iint_S (\underset{\sim}{r} \times \underset{\sim}{V}_d)\rho(\underset{\sim}{V}_d \cdot \underset{\sim}{n})dS + \iint_S (\underset{\sim}{r} \times \underset{\sim}{V}_s)\rho(\underset{\sim}{V}_d \cdot \underset{\sim}{n})dS \qquad (13)$$

where $\underset{\sim}{n}$ is the outer unit normal. On the left-hand side, M is the resultant torque on the control volume. The second term accounts for the moments due to the shear force $\underset{\sim}{F}_d$ and vanishes owing to the solid sidewall and cancellation of the contributions from both ends**. On the right-hand side, the first term vanishes for steady $\underset{\sim}{V}_d$. The second term originates from Coriolis forces in the nutating system. The third term vanishes since $\underset{\sim}{V}_d$ has only an axial component. The last term then provides the net rate of angular momentum flux through the control surface.

Substitution of $\underset{\sim}{V}_d$ leads to the following expressions for the cartesian components of $\underset{\sim}{M}$:

$$M_x = m_\ell(2\Omega a\sin\theta)(\omega a)\, m_x,\quad m_x = -\int_0^1 r^2 f dr \qquad (14a)$$

$$M_y = m_\ell(2\Omega a\sin\theta)(\omega a)\, m_y,\quad m_y = -\int_0^1 r^2 g dr \qquad (14b)$$

$$M_z = m_\ell(2\Omega a\sin\theta)^2\, m_z,\quad m_z = \int_0^1 r^2 f dr = -m_x \qquad (14c)$$

where m_ℓ is the liquid mass in the cylinder. In this form, the components M_x, M_y represent the net rate of angular momentum flux through the liquid endwalls, whereas the roll moment M_z is solely due to Coriolis forces. A close

*The data were kindly provided by Dr. H. Vaughn, Sandia National Laboratories.

**Improper account of the sidewall conditions introduced an incorrect factor of two in earlier results for M_x, M_y [10].

relation between roll moment M_z and yaw moment M_x has also been found by Murphy [11] for the range of high Reynolds numbers.

A different interpretation can be derived using the differential equation (9a), integrating by parts, applying (9b), and separating real and imaginary part:

$$m_z = -m_x = \int_0^1 r^2 f dr = -\frac{g'(1)}{Re} \tag{15a}$$

$$m_y = -\int_0^1 r^2 g dr = -\frac{f'(1)}{Re} - \frac{1}{4}. \tag{15b}$$

In this form, the moments are directly related to the shear forces at the cylindrical sidewall, r=1. Since $f'(1)<0$, $g'(1)<0$, the roll moment M_z is always positive (even for $\Omega<0$), while M_x is negative for $\Omega<0$ and changes sign with Ω. For small Re, the series (7) provide the approximations

$$m_z = \frac{Re}{96}, \quad m_y = -\frac{Re^2}{1536} \tag{16}$$

that can be used for quick estimates up to Re≤10. The linear increase of m_z and M_z with Re is consistent with the experimental data. From the analytical solution (10), we obtain

$$F'(1) = g'(1) + if'(1) = 2 - qI_0(q)/I_1(q). \tag{17}$$

Substitution into (15) provides the variation of m_z, m_y with the Reynolds number shown in Fig. 4. The coefficient m_z assumes a pronounced maximum at

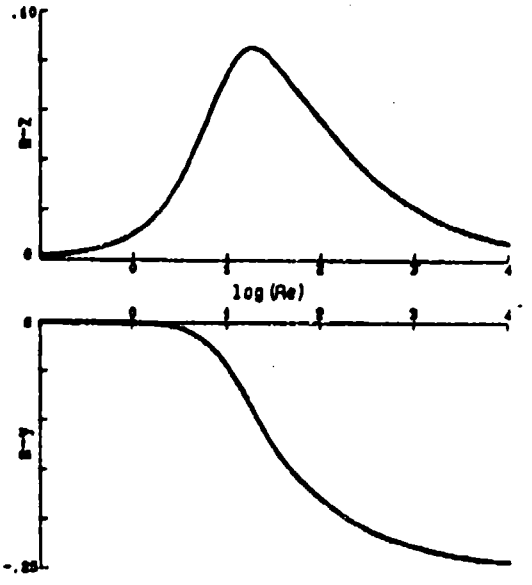

Fig. 4. The nondimensional coefficients m_z, m_y in eq. (14) versus the Reynolds number, Re.

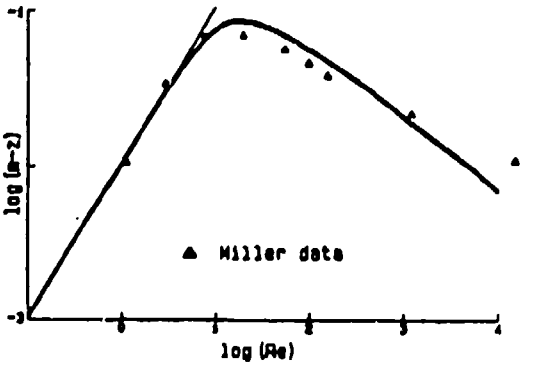

Fig. 5. Comparison of the theoretical result for m_z with experimental data [5]. The straight line shows the asymptotic law $m_z = Re/96$.

Re≈19. The coefficient m_y is negative and reaches an asymptotic value of $m_y \to -1/4$ as $Re \to \infty$. Hence, for $\Omega>0$, M_y reduces the pitch moment due to the solid body rotation. This result is consistent with computations [9]. A comparison of theoretical and experimental [5] results for m_z is given in Fig. 5 on a double logarithmic scale. The initial spin rate ω=4000 rpm was used for reducing the experimental data. For Re<10, the experimental points match the analytical result as well as the asymptotic law $m_z = Re/96$. The occurrence of a maximum of m_z is found to be a property of the basic flow. Only the systematic deviation for higher Reynolds numbers Re<200 may be attributed to a cellular motion. The two data points for $Re>10^3$ probably indicate turbulent flow.

The basic flow, hence, can be considered a first but essential step toward understanding and predicting the gross features of the fluid motion in a spinning and nutating cylinder. Some observations, however, such as the virtual independence of the despin moment on the spin rate require further analysis, especially of the end effects. The occurrence of a cellular motion may be due to hydrodynamic instability of the basic flow.

5. STABILITY ANALYSIS. The stability analysis is currently conducted and only a brief outline is given here. We superpose to the steady flow $v_n=(o,r,v_z)$, p_n disturbances $v'=(u,v,w)$, p sufficiently small for linearization. Substitution into eqs. (2) and neglect of products between disturbances and terms of order $O(\epsilon^2)$ provides the following stability equations:

$$\left(\frac{\partial u}{\partial t} + \frac{\partial u}{\partial \phi} - 2(1+\tau_z)v + \frac{\partial p}{\partial r}\right) - \frac{1}{Re}\left(D''u - \frac{u}{r^2} - \frac{2}{r^2}\frac{\partial v}{\partial \phi}\right) + \left(v_z \frac{\partial u}{\partial z} + 2\tau_\phi w\right) = 0 \tag{18a}$$

$$\left(\frac{\partial v}{\partial t} + \frac{\partial v}{\partial \phi} + 2(1+\tau_z)u + \frac{1}{r}\frac{\partial p}{\partial \phi}\right) - \frac{1}{Re}\left(D''v - \frac{v}{r^2} + \frac{2}{r^2}\frac{\partial u}{\partial \phi}\right) + \left(v_z \frac{\partial v}{\partial z} - 2\tau_r w\right) = 0 \tag{18b}$$

$$\left(\frac{\partial w}{\partial t} + \frac{\partial w}{\partial \phi} + \frac{\partial p}{\partial z}\right) - \frac{1}{Re}(D''w) + \left(\left(\frac{\partial v_z}{\partial r} - 2\tau_\phi\right)u + \left(\frac{1}{r}\frac{\partial v_z}{\partial \phi} + 2\tau_r\right)v + v_z \frac{\partial w}{\partial z}\right) = 0 \tag{18c}$$

$$\frac{1}{r}\frac{\partial}{\partial r}(ru) + \frac{1}{r}\frac{\partial v}{\partial \phi} + \frac{\partial w}{\partial z} = 0 \tag{18d}$$

Three groups of terms have been separated by braces in eqs. (18a-c). The first group, if set to zero, represents the equations for inviscid inertial modes $\sim \exp(im\phi + i\alpha z + st)$, where m is the (integer) azimuthal, α the axial wavenumber, and $s = s_r + is_i$ provides the amplification rate s_r (=0) and frequency s_i. Usually, an equation for the pressure is used for obtaining the analytical solution. We have derived an alternative system in terms of u,v and applied the spectral method to be used for more general cases in order to check the numerical results against the exact values.

The second group of terms multiplied with 1/Re represents the viscous correction to the inertial modes. By eliminating w and p, a system of ordinary differential equations for u and v has been derived. Due to the higher order of this system, all boundary conditions can be satisfied. Programs have been developed for calculating spectra of (complex) eigenvalues, for tracing single eigenvalues as function of Re, α, and for obtaining the eigenfunctions. At high Re, the results follow the trends predicted by asymptotic theories. Our analysis, however, also covers the range of low Reynolds numbers, where the inertial modes suffer rapid decay ($s_r<0$).

The most interesting aspect of the stability equations (18) is the third group of terms. The coefficients in this group, v_z, τ_r, and τ_ϕ, are (1) of order $O(\varepsilon)$ and (2) periodic in ϕ. The periodicity in ϕ leads to a coupling of the mode equations for m and m±1, and may cause primary resonance between inertial modes. In view of viscous damping, this resonance is likely to occur as ε exceeds a critical value that decreases as Re increases. The analysis of this parametric instability is currently in preparation.

ACKNOWLEDGMENT

The open cooperation and sharing of data with Miles C. Miller (CRDC) and Harold R. Vaughn (Sandia Laboratories) are greatly appreciated. This work is supported by the Army Research Office under Contract DAAG29-82-K-0129 and by the Army AMCCOM under Contract DAAK11-83-K-0011.

REFERENCES

[1] Stewartson, K. 1959 "On the Stability of a Spinning Top Containing Liquid," Journal of Fluid Mechanics, Vol. 5, Part 4, pp. 577-592.

[2] Wedemeyer, E. H. 1966 "Viscous Corrections to Stewartson's Stability Criterion," Ballistic Research Laboratory, Report 1325.

[3] D'Amico, W. P. 1977 "Field Tests of the XM761: First Diagnostic Test," Ballistic Research Laboratory, Memorandum Report 2792.

[4] D'Amico, W. P. 1978 "Field Tests of the XM761: Second Diagnostic Test," Ballistic Research Laboratory, Memorandum Report ARBRL-MR-02806.

[5] Miller, M. C. 1982 "Flight Instabilities of Spinning Projectiles Having Nonrigid Payloads," Journal of Guidance, Control, and Dynamics, Vol. 5, pp. 151-157.

[6] D'Amico, W. P. & Miller, M. C. 1979 "Flight Instability Produced by a Rapidly Spinning, Highly Viscous Liquid," Journal of Spacecraft and Rockets, Vol. 16, pp. 62-64.

[7] Herbert, Th. 1982 "Fluid Motion in a Rotating and Nutating Cylinder - Part I," Report prepared under the Scientific Services Program.

[8] Miller, M. C. 1981 "Void Characteristics of a Liquid Filled Cylinder Undergoing Spinning and Coning Motion," Journal of Spacecraft and Rockets, Vol. 18, 286-288.

[9] Vaughn, H. R., Oberkampf, W. L. & Wolfe, W. P. 1983 "Numerical Solution for a Spinning Nutating Fluid-Filled Cylinder," Sandia Report SAND 83-1789.

[10] Herbert, Th. 1983 "The Flow of Highly Viscous Fluid in a Spinning and Nutating Cylinder," Proceedings of the 1983 Scientific Conference on Chemical Defense Research, Aberdeen Proving Ground, Md.

[11] Murphy, C. M. 1984 "A Relationship between Liquid Roll Moment and Liquid Side Moment," Ballistic Research Laboratory Memorandum Report ARBRL-MR-03347.

Appendix A.3

ON THE VISCOUS ROLL MOMENT IN A SPINNING AND NUTATING CYLINDER

by

Thorwald Herbert

Department of Engineering Science and Mechanics
Virginia Polytechnic Institute and State University
Blacksburg, Virginia 24061

Proceedings of the
1984 Scientific Conference on Chemical Defense Research
November 13-16, 1984
Aberdeen Proving Ground, Maryland

APPENDIX A

On the Viscous Roll Moment in a Spinning and Nutating Cylinder

Thorwald Herbert

Department of Engineering Science and Mechanics
Virginia Polytechnic Institute and State University
Blacksburg, Virginia 24061

Abstract

Spin-stabilized projectiles with liquid payloads can experience a severe flight instability characterized by a rapid yaw angle growth and a simultaneous loss in spin rate. Laboratory experiments and field tests have shown that this instability originates from the internal fluid motion in the range of high viscosity. We have developed a simple model of this internal motion that provides the flow field and the liquid moments in analytical form. A detailed comparison of the roll moment with data from spin-down equipments is given. New experimental procedures are suggested.

1. Introduction

It is well-known that spin-stabilized shells carrying liquid payloads can suffer dynamical instability. For cylindrical cavities and low viscosity of the liquid, the instability due to basically inviscid inertial waves can be predicted by the Stewartson-Wedemeyer theory. The instability of certain shells like the XM761, however, escapes such a prediction and is also distinguished in character by the rapid loss in spin rate. Experiments with a full-scale liquid-filled cylinder [1] and subsequent field tests [2] establish that this new flight instability is most pronounced for liquid fills of very high viscosity.

We have conducted a theoretical analysis of the problem with special attention to the range of high viscosity. Two observations have permitted the development of a simple model of the internal fluid motion. First, the nutation rate and angle appear as a small parameter in the nondimensional equations for the deviation from solid-body rotation [3]. Therefore, the forcing term due to nutation can be considered sufficiently small for linearization in the situation of practical interest. Second, in a sufficiently long cylinder, the velocity field consists of primarily an axial component that is independent of the axial position [4]. The other components are of the same order only in the neighborhood of the end walls. Therefore, essential features of the internal fluid motion can be obtained by studying the flow in a finite segment of an infinitely long cylinder.

Although the agreement of the theoretical and experimental results on the roll moment is surprisingly good, there seems to be an essential discrepancy: while the theoretical result depends (via the Reynolds number) on the spin rate, Miller [1] found that "the despin moment was not a function of the canister spin rate, provided a sufficient spin rate is present. With more detailed data available in a wide range of Reynolds numbers, we shed some light on this virtual disagreement. The experimental data follow in fact the theoretically predicted trends. A systematic deviation persists in the range of extremely high viscosities. This deviation is likely to originate from changes in temperatures and consequently in viscosity. It also turns out that a survey of the roll-moment versus Reynolds number curve can be obtained in very few experimental runs at different viscosity.

2. Analysis of the Flow Field

We consider the motion of a fluid of density ρ and viscosity μ in a cylinder of radius a and length $2c$ that rotates with the spin rate ω about its axis of symmetry, the z-axis. We consider the motion with respect to the nutating coordinate system x,y,z. This system is obtained from the inertial system X,Y,Z, by a rotation with the nutation angle θ about the axis $Y=y$. Therefore, x is in the Z,z-plane, and this plane rotates about the Z-axis with the nutation rate Ω. The two axes of rotation intersect in the center of mass of the cylinder, as shown in Fig. 1. In contrast to the experimental procedures [1], we consider $\omega>0$, Ω, and $0\leq\theta\leq\pi/2$ as constant.

It is convenient [3] to split the velocity and pressure fields according to

$$\mathbf{V}_n = \mathbf{V}_s + \mathbf{V}_d, \quad P_n = P_s + P_d \tag{1}$$

where $\mathbf{V}_s,P_s$ describe the state of pure solid body rotation, whereas $\mathbf{V}_d,P_d$ represent the deviation from solid body rotation. The advantage of this isolated view on the deviation is obvious: $\mathbf{V}_d$ and the reduced pressure P_d are responsible for the observed flight instability. A glance at the equations [3] shows that $\mathbf{V}_d \equiv 0$ and $P_d \equiv 0$ if either $\omega=0$, $\Omega=0$, $\theta=0$, or $\mu\to\infty$ (solid fill).

The effect of nutation and hence the deviation velocity is of order $0(\epsilon)$ where $\epsilon = (\Omega/\omega)\sin\theta$. In the situations of practical interest, ϵ turns out to be rather small: a conservative estimate provides values of $\epsilon\leq 0.054$. Consequently, it seems well justified to linearize the equations in ϵ. This linearization imposes no restriction on the Reynolds number $Re = \rho\omega a^2/\mu$. Recalling that the flow in a relatively long cylinder (aspect ratio $\lambda = 4.3$) at low Re exhibits little axial variation over much of the cylinder length [3], we have relaxed the boundary conditions at the end walls.

In cylindrical coordinates r,θ,z, we obtain [3] in an infinitely long cylinder

$$\mathbf{V}_d = (0,0,\omega a v_z), \quad P_d = 0 \tag{2}$$

where

$$v_z = v_z(r,\phi) = 2\epsilon[f(r)\cos\phi + g(r)\sin\phi]. \tag{3}$$

and g and f are the real and imaginary parts, respectively, of

$$F(r) = g + if = r - I_1(qr)/I_1(q). \tag{4}$$

where I_1 is the modified Bessel function, and $q = (1+i)(Re/2)^{1/2}$. This solution is valid for arbitrary Re but may be unstable as Re exceeds some critical value. Comparison of the velocity distribution with computational results [5] for $Re = 14.9$ has shown excellent agreement in the center section of the cylinder. At the higher Reynolds number $Re = 45.7$, the agreement is still satisfactory, with systematic deviations due to a weak cellular motion not yet incorporated in our analysis.

3. Moments

With given deviation velocity $\mathbf{V}_d$, the moments on a finite-length section of the cylinder can be calculated. We consider a control volume R (surface S) formed by the solid cylindrical wall and liquid surfaces at both ends. Conservation of angular momentum requires

$$\mathbf{M} + \sum(\mathbf{r}\times\mathbf{F}_d) = \frac{\partial}{\partial t}\int\int_R\int(\mathbf{r}\times\mathbf{V}_d)\rho\,dR + \int\int_R\int[\mathbf{r}\times(2\Omega\times\mathbf{V}_d)]\rho\,dR \tag{5}$$
$$+\int\int_S(\mathbf{r}\times\mathbf{V}_d)(\mathbf{V}_d\cdot\mathbf{n})\rho\,dS + \int\int_S(\mathbf{r}\times\mathbf{V}_s)(\mathbf{V}_d\cdot\mathbf{n})\rho\,dS$$

where n is the outer unit normal. On the left-hand side, M is the resultant torque on the control volume. The second term accounts for the moments due to the shear force $\mathbf{F}_d$. This term vanishes along the solid sidewall and the contributions from both ends cancel. On the right-hand side, the first term vanishes for steady $\mathbf{V}_d$. The second term originates from Coriolis forces in the nutating system. The third term vanishes since $\mathbf{V}_d$ has only an axial component. The last term then provides the net rate of angular momentum flux through the control surface.

Substitution of $\mathbf{V}_d$ leads to the following expressions for the components of M:

$$M_x = m_l(2\Omega\, a\sin\theta)(\omega a)\; m_x,\; m_x = -\int_0^1 r^2 f\,dr \tag{6a}$$

$$M_y = m_l(2\Omega\, a\sin\theta)(\omega a)\; m_y,\; m_y = -\int_0^1 r^2 g\,dr \tag{6b}$$

$$M_z = m_l(2\Omega\, a\sin\theta)^2\, r_*,\; m_z = \int_0^1 r^2 f\,dr = -m_x \tag{6c}$$

where m_l is the liquid mass in the cylinder. In this form, the components M_x, M_y represent the net rate of angular momentum flux through the liquid endwalls, whereas the roll moment M_z is solely due to Coriolis forces.

A different interpretation can be derived using the differential equation for F [4]:

$$m_z = -m_x = \int_0^1 r^2 f\,dr = -\frac{g'(1)}{Re},\quad m_y = -\int_0^1 r^2 g\,dr = -\frac{f'(1)}{Re}\qquad \frac{1}{4.} \tag{7}$$

In this form, the moments are directly related to the shear forces at the cylindrical sidewall, $r = 1$. Since $f'(1)<0$, $g'(1)<0$, the roll moment M_z is always positive (even for $\Omega<0$). From (4), we obtain

$$F'(1) = g'(1) + i f'(1) = 2 - qI_0(q)/I_1(q). \tag{8}$$

For small Reynolds numbers, use of series expansions for the modified Bessel functions provides the approximations $m_z \approx Re/96$, $m_y \approx -Re^2/1536$, that can be used for quick estimates up to $Re \leq 10$. These results disregard the effect of the solid end walls of the cylinder, where the axial flow reverses direction. We expect that the effect of this flow reversal will be primarily on the pitch moment M_y. We also expect that the result for the roll moment M_z is rather accurate, and slightly overestimates the effect of Coriolis forces. Experimental data for a verification of our results are scarce. Only the roll moment has been reliably measured in spin-down experiments with a full-scale cylinder [1].

4. Comparison of the Roll Moment with Experiments

Figure 2 shows the comparison of theoretical and experimental results for the roll coefficient m_z on a doubly logarithmic scale. The initial spin rate $\omega = 4000$ rpm has been used for reducing the experimental data. For $Re < 10$, the experimental data match the analytical data as well as the asymptotic law $m_z \approx Re/96$. The coefficient m_z assumes a pronounced maximum at $Re \approx 19$. Whereas this maximum was earlier thought to originate from hydrodynamic instability with respect to a cellular motion, we find a simple explanation in the properties of the axial velocity component f in the $z,z-$plane. The systematic deviation for Reynolds numbers $20 < Re < 200$ may be attributed to either the effect of a cellular motion or to the neglect of the end walls. The two data points at $Re > 10^3$ are likely to be for a turbulent internal flow.

REFERENCES

[1] Miller, M. C. 1982 "Flight Instabilities of Spinning Projectiles Having Nonrigid Payloads," *Journal of Guidance, Control, and Dynamics*, Vol. 5, pp. 151-157.

[2] D'Amico, W. P. & Miller, M. C. 1979 "Flight Instability Produced by a Rapidly Spinning, Highly Viscous Liquid," *Journal of Spacecraft and Rockets*, Vol. 16, pp. 62-64.

[3] Herbert, Th. 1982 "Fluid Motion in a Rotating and Nutating Cylinder - Part I," Report prepared under the Scientific Services Program. Published as Report CRDC-CR-84087, 1984

[4] Herbert, Th. 1984 "Highly Viscous Fluid Flow in a Spinning and Nutating Cylinder," Proceedings of the Second Army Conference on Applied Mathematics and Computing, Troy, NY.

[5] Vaughn, H. R., Oberkampf, W. L. & Wolfe, W. P. 1983 "Numerical Solution for a Spinning Nutating Fluid-Filled Cylinder," Sandia Report SAND 83-1789.

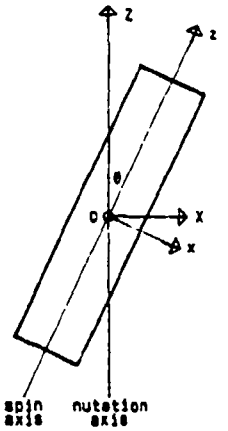

Figure 1. Definition sketch

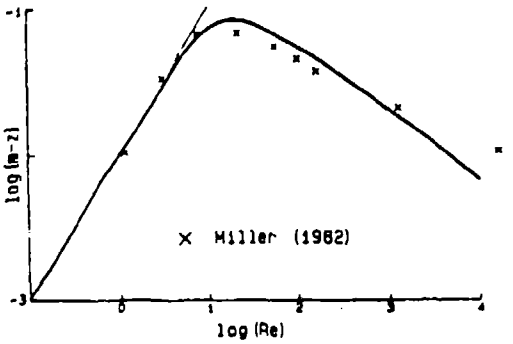

Figure 2. Comparison of the theoretical result for m_s vs. Re with experimental data [1]. The straight line shows the asymptotic law $m_s \approx Re/96$.

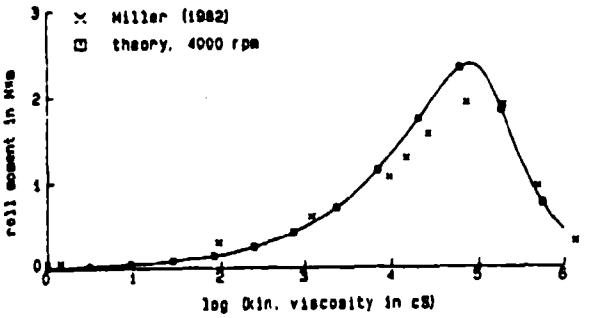

Figure 3. Comparison of the theoretical result for the roll moment M_s vs. kinematic viscosity ν with experimental data [1]. Parameters: $a = 60.3mm$, $c/a = 4.29$, $\theta = 20^0$, $\Omega = 500rpm$.

APPENDIX A

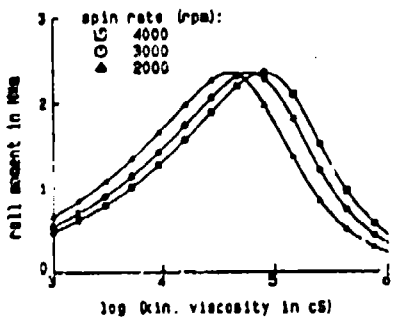

Figure 4. Theoretical results for the roll moment M_s vs. kinematic viscosity ν for different spin rates ω. Parameters as in Fig. 3.

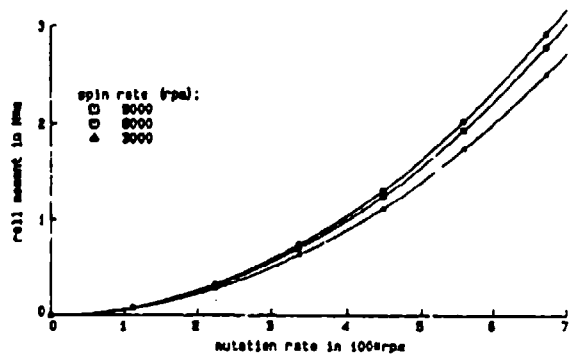

Figure 5. Theoretical results for the roll moment M_s vs. nutation rate Ω for different spin rates ω. Parameters: $a = 50.4mm$, $c/a = 4.5$, $\theta = 20^0$, $\nu = 10^6 cS$.

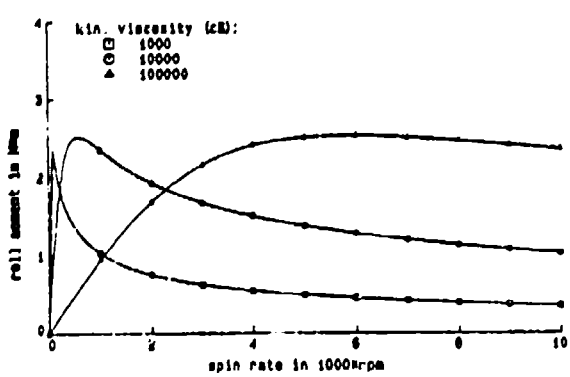

Figure 6. Theoretical results for the roll moment M_s vs. spin rate ω for different kinematic viscosities ν. Parameters: $a = 50.4mm$, $c/a = 4.5$, $\theta = 20^0$, $\Omega = 625rpm$.

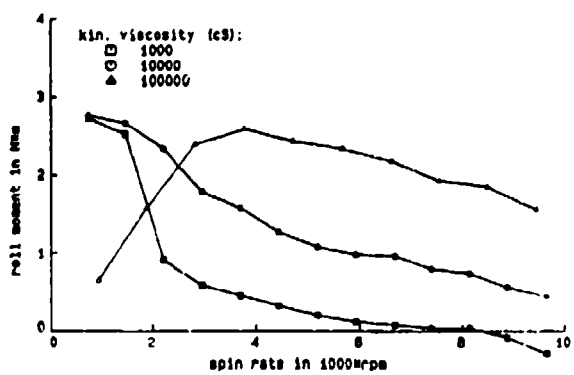

Figure 7. Experimental results for the roll moment M_s vs. spin rate ω for different kinematic viscosities ν. Parameters: $a = 50.4mm$, $c/a = 4.5$, $\theta = 20^0$, $\Omega \approx 600rpm$.

APPENDIX A

Appendix A.4

Viscous Fluid Motion in a Spinning and Nutating Cylinder

by

Thorwald Herbert

Department of Engineering Science and Mechanics
Virginia Polytechnic Institute and State University
Blacksburg, Virginia 24061

July 1985

Submitted to:

Journal of Fluid Mechanics

APPENDIX A

ABSTRACT

Spin-stabilized projectiles with liquid payloads can experience a severe flight instability characterized by a rapid yaw-angle growth and a simultaneous loss in spin rate. Laboratory experiments and field tests have shown that this instability originates from the internal fluid motion in the range of high viscosity. After evaluation of the experimental data and analysis of the equations for the fluid motion in a spinning and nutating cylinder, we have developed a simple model of this flow. Disregarding the finite length of the cylinder, this model provides the flow field and the viscous contribution to the liquid moments in analytical form. At low Reynolds number, the flow field agrees well with computational results for the center section of a cylinder of aspect ratio 4.3. The roll moment caused by this flow largely agrees with experimental data for a wide range of Reynolds numbers. Estimates of the temperature variation indicate that discrepancies at very low Reynolds numbers may originate from associated changes of the viscosity during the experiments.

1. Introduction

It is well-known that spin-stabilized shells carrying liquid payloads can suffer dynamical instability. For cylindrical cavities and low viscosity of the liquid, the instability due to basically inviscid inertial waves can be predicted by the Stewartson-Wedemeyer theory (Stewartson 1959; Wedemeyer 1966). This theory rests on the boundary-layer approach and is, therefore, restricted to the range of sufficiently large Reynolds numbers. The instability of certain shells like the XM761 (D'Amico 1977; 1978), however, escapes such a prediction and is also distinguished in character owing to the rapid loss in spin rate. Experiments with a full-scale liquid-filled cylinder (Miller 1982) and subsequent field tests (D'Amico & Miller 1979) establish that this new flight instability is most pronounced for liquid fills of very high viscosity.

We conduct a theoretical analysis of this problem in order to support the ongoing experiments and to independently obtain insight into the anatomy of the flow phenomena. The initial steps of this analysis are reported elsewhere (Herbert 1982): evaluation of the experimental data base, dimensional analysis, scaling aspects, governing equations, and discussion of various simplifying assumptions. Two observations in this earlier work led to the approach discussed in the following. First, if the despin (negative roll) moments (Miller 1982) and void observations (Miller 1981) are correlated with the Reynolds number Re, at least three regions can be distinguished. At low Re, the despin moment increases proportional to Re, and the void in an incompletely filled cylinder is parallel to the spin axis. This suggests a simple fluid motion that is essentially independent of the axial coordinate, except in the neighborhood of the end walls. In a middle range of Re, the despin moment assumes a maximum, and a wavy distortion of the void seems to indicate a cellular structure of the fluid motion. This cellular motion can, in principle, originate from hydrodynamic instability of the basic flow with respect to axially periodic disturbances. At still higher Reynolds numbers, the despin moment decreases with increasing Re in a manner not clearly defined by the few available data points. The void observations indicate, however, that the motion ultimately becomes turbulent.

The second observation is the appearance of the nutation rate and angle as a small parameter in the equations for the deviation from solid-body rotation. The forcing term due to nutation can be considered small enough for linearization of the equations in the situations of practical interest.

In the following, we describe the development of a simple system of equations for the basic flow. Analytical solutions are given for the flow field, for the liquid moments, and for the

APPENDIX A

rate of change of temperature. A comparison is made with computer simulations of the flow (Vaughn et al. 1983; 1985) and with experimental data for the moments (Miller 1982).

2. Governing Equations

We consider the motion of a fluid of density ρ and viscosity μ in a cylinder of radius a and length $2c$ that rotates with the spin rate ω about its axis of symmetry, the z-axis. We consider the motion with respect to the nutating coordinate system x,y,z. This system is obtained from the inertial system X,Y,Z, by a rotation with the nutation angle θ about the axis $Y=y$. Therefore, z is in the Z,x-plane, and this plane rotates about the Z-axis with the nutation rate Ω. The two axes of rotation intersect in the center of mass of the cylinder, as shown in figure 1. In contrast to the experimental procedures (Miller 1982), we consider $\omega>0$, Ω, and $0\leq\theta\leq\pi/2$ as constant.

The fluid motion is governed by the Navier-Stokes equations written in the nutating coordinate system:

$$\rho\left[\frac{D\mathbf{V}_n}{Dt}+2\boldsymbol{\Omega}\times\mathbf{V}_n+\boldsymbol{\Omega}\times(\boldsymbol{\Omega}\times\mathbf{r})\right]=-\nabla P_n+\mu\nabla^2\mathbf{V}_n\,, \tag{1a}$$

$$\nabla\cdot\mathbf{V}_n=0\,. \tag{1b}$$

$\mathbf{V}_n$ is the velocity measured in the nutating frame, P_n the pressure, and $\mathbf{r}$ the position vector. The body force due to gravity has been disregarded. Equations (1) are subject to the no-slip and no-penetration conditions at the cylinder walls.

It is convenient (Herbert 1982) to split the velocity and pressure fields according to

$$\mathbf{V}_n=\mathbf{V}_s+\mathbf{V}_d\,,\quad P_n=P_s+P_d\,, \tag{2}$$

where $\mathbf{V}_s,P_s$ describe the state of pure solid body rotation, whereas $\mathbf{V}_d,P_d$ represent the deviation from solid body rotation. The advantage of this isolated view on the deviation is obvious: $\mathbf{V}_d$ and the reduced pressure P_d are responsible for the observed flight instability. A glance at the equations shows that $\mathbf{V}_d\equiv 0$ and $P_d\equiv 0$ if either one of the following conditions is

satisfied: $\omega = 0$, $\Omega = 0$, $\theta = 0$ or $\mu \to \infty$ (solid fill).

The equations for $\mathbf{V}_d, P_d$ are written in terms of nondimensional quantities $\mathbf{v}_d, p_d$. We use a, ω, and ρ for scaling length, time and mass. Note that this choice is ambiguous (Herbert 1982) and excludes the case $\omega=0$ which lacks practical interest. The problem then depends on four nondimensional parameters:

$\lambda = c/a$	aspect ratio
θ	nutation angle
$\tau = \Omega/\omega$	frequency
$Re = \rho\omega a^2/\mu$	Reynolds number.

The aspect ratio enters the solution only through the boundary conditions. The boundary conditions on $\mathbf{v}_d$ are homogeneous.

In cylindrical coordinates r, ϕ, z, the equations for the nondimensional deviation velocity $\mathbf{v}_d = (v_r, v_\phi, v_z)$ and pressure p_d take the form

$$\frac{1}{r}\frac{\partial}{\partial r}(rv_r) + \frac{1}{r}\frac{\partial v_\phi}{\partial \phi} + \frac{\partial v_z}{\partial z} = 0 , \tag{3a}$$

$$D'v_r - \frac{v_\phi^2}{r} - 2(1+\tau_z)v_\phi + 2\tau_\phi v_z = \tag{3b}$$

$$-\frac{\partial p_d}{\partial r} + \frac{1}{Re}\left[D''v_r - \frac{v_r}{r^2} - \frac{2}{r^2}\frac{\partial v_\phi}{\partial \phi}\right] ,$$

$$D'v_\phi + \frac{v_r v_\phi}{r} + 2(1+\tau_z)v_r - 2\tau_r v_z = \tag{3c}$$

$$-\frac{1}{r}\frac{\partial p_d}{\partial \phi} + \frac{1}{Re}\left[D''v_\phi - \frac{v_\phi}{r^2} + \frac{2}{r^2}\frac{\partial v_r}{\partial \phi}\right] ,$$

$$D'v_z + 2\tau_r v_\phi - 2\tau_\phi v_r = -\frac{\partial p_d}{\partial z} - 2r\tau_r + \frac{1}{Re}D''v_z , \tag{3d}$$

where

$$D' = \frac{\partial}{\partial t} + \frac{\partial}{\partial \phi} + v_r\frac{\partial}{\partial r} + v_z\frac{\partial}{\partial z} ,$$

$$D'' = \frac{\partial^2}{\partial r^2} + \frac{1}{r}\frac{\partial}{\partial r} + \frac{1}{r^2}\frac{\partial^2}{\partial \phi^2} + \frac{\partial^2}{\partial z^2} ,$$

APPENDIX A

and

$$\tau_r = -\epsilon\cos\phi \ , \ \tau_\phi = \epsilon\sin\phi \ , \ \tau_z = r\cos\theta \ , \ \epsilon = r\sin\theta \ . \tag{4}$$

The primary effect of nutation is contained in the ϕ-periodic force term $-2r\tau_r = 2\epsilon r\cos\phi$ in the z-momentum equation (3d). If this term vanishes throughout, $\epsilon = 0$, equations (3) support a trivial solution $v_d = 0$, $p_d = 0$.

The system (3) of equations is similar to the system numerically solved by Vaughn et al. (1983; 1985), but simplified by introducing the reduced pressure p_d. We also note that this system supports certain symmetries. Let v_r, v_ϕ, v_z and p_d be the solution at point r, ϕ, z, then the velocities and pressure at the corresponding point $r, \phi + \pi, -z$ are $v_r, v_\phi, -v_z$ and p_d. These symmetries can be exploited for essential savings in computational work.

2.1 *Linearized equations*

For sufficiently small $\epsilon \neq 0$, it is obvious that the deviation velocity is of order $O(\epsilon)$. In the situations of practical interest, $\epsilon = (\Omega/\omega)\sin\theta$ turns out to be a rather small parameter. Even a conservative estimate with $\Omega \leq 500$ rpm, $\omega \geq 3000$ rpm, and $\theta \leq 20°$ provides values of $\epsilon \leq 0.054$. Consequently, it seems well justified to linearize the equations in ϵ. This linearization imposes no restriction on the Reynolds number.

While the continuity equation remains unaffected, linearization of the momentum equations provides

$$D'v_r - 2(1+\tau_z)v_\phi = -\frac{\partial p_d}{\partial r} + \frac{1}{Re}\left[D''v_r - \frac{v_r}{r^2} - \frac{2}{r^2}\frac{\partial v_\phi}{\partial \phi}\right] , \tag{5a}$$

$$D'v_\phi + 2(1+\tau_z)v_r = -\frac{1}{r}\frac{\partial p_d}{\partial \phi} + \frac{1}{Re}\left[D''v_\phi - \frac{v_\phi}{r^2} + \frac{2}{r^2}\frac{\partial v_r}{\partial \phi}\right] , \tag{5b}$$

$$D'v_z = -\frac{\partial p_d}{\partial z} - 2r\tau_r + \frac{1}{Re}D''v_z \ . \tag{5c}$$

The system (3a), (5a)-(5c) of equations is still quite difficult to solve. Any serious attempt to satisfy all boundary conditions leads directly to a purely computational approach. Use of the

boundary-layer approximation would simplify the task but seems inappropriate in the interesting range of low Reynolds numbers.

APPENDIX A

3. The core flow

We recall that the flow in a relatively long cylinder (aspect ratio $\lambda = 4.3$) at low Reynolds number is expected to have a rather simple structure and to provide a roll moment proportional to Re (Herbert 1982). Closer analysis of the equations suggests that this flow exhibits little axial variation over much of the cylinder length. The effect of the end walls will be essential only over an axial distance of $O(1)$ from the ends. Therefore, we have relaxed the boundary conditions at the end walls. In this way, we seek a steady flow in a finite segment of an infinitely long cylinder.

The z-independent force term in eq. (5c) can be balanced only by a purely axial deviation velocity. It is consistent with the linearized equations to assume a solution in the form

$$\mathbf{v}_d = (0,0,v_z) \ , \quad p_d = 0 \ . \tag{6}$$

Moreover, since v_z is of order $O(\epsilon)$ and periodic in ϕ, we write

$$v_z = v_z(r,\phi) = 2\epsilon[f(r)\cos\phi + g(r)\sin\phi] \ , \tag{7}$$

where f and g are the imaginary and real parts, respectively, of the complex function

$$F(r) = g(r) + i f(r) \tag{8}$$

Substituting (6)-(8) into the linearized equations and the no-slip conditions at the cylinder wall provides

$$r^2F'' + r F' - (1 + i Re\, r^2)F = - i Re\, r^3 \ , \tag{9a}$$

$$F = 0 \ \text{ at } \ r = 1 \ , \tag{9b}$$

$$F \text{ finite at } \ r = 0 \ , \tag{9c}$$

where (9c) is necessary for a physical solution. The primes denote d/dr.

3.1 *Solution for* $Re \to 0$ and $Re \to \infty$

APPENDIX A

For $Re \to 0$, the solution of equations (9) equations can be found in the form of series expansions in Re,

$$f = \frac{Re}{8}(r - r^3) - \frac{Re^3}{9216}(7r - 12^3 + 6r^5 - r^7) + O(Re^5)\,, \tag{10a}$$

$$g = \frac{Re^2}{192}(2r - 3r^3 + r^5) + O(Re^4)\,. \tag{10b}$$

With higher terms included, these series converge for $Re \leq 12$.

In the limit $Re \to \infty$, one obtains

$$f \to 0,\ g \to r \ \text{ as } \ Re \to \infty. \tag{11}$$

Owing to the loss of the highest derivatives, however, this solution cannot satisfy the boundary conditions (9b) and is valid only outside thin boundary layers near the wall at $r = 1$.

Even without any knowledge of the solution in the intermediate range, the different character of the basic flow at low and high Reynolds numbers is evident. At low Re, the component f in the x,z-plane $\phi = 0$ dominates the solution. At high Re, f is negligible except near the wall of the cylinder while g in the y,z-plane $\phi = 90°$ is dominating. One might well expect that the initial linear increase of f with Re and the change in the flow structure is related to the observed properties of the roll moment.

3.2 *Solution for arbitrary values of Re*

In earlier work (Herbert 1983), we have applied a spectral collocation method for numerically solving a real system of equations for f and g equivalent to eqs. (9). Series in odd Chebyshev polynomials for the interval $0 \leq r \leq 1$ provide accurate solutions at rather low truncation. This experience together with the minor effect of harmonics in the azimuthal direction at small ϵ suggests the use of spectral methods for efficiently solving the nonlinear equations (3).

Here, we derive an analytical solution for the core flow in a sufficiently long cylinder. A particular solution of the inhomogeneous equation (9a) is $F_0 = r$, whereas the homogeneous part of (9a) is the equation for the modified Bessel functions $I_1(qr)$ and $K_1(qr)$ of the complex argument qr where $q = (1 + i)(Re/2)^{1/2}$. In order to satisfy (9c), $K_1(qr)$ cannot contribute to the solution. Finally, (9b) provides

APPENDIX A

$$F(r) = g + i f = r - I_1(qr)/I_1(q) \ . \tag{12}$$

This solution is valid for arbitrary Re but may be unstable as Re exceeds some critical value. Although expressible in simple form, the resulting flow field exhibits very interesting properties.

Rewriting the solution in terms of Kelvin functions of real argument is of little advantage for the numerical evaluation. We have used a combination of ascending series and asymptotic expansions for large arguments (Abramowitz & Stegun 1972) for evaluating $F(r)$. With the solution (12) at hand, it is straightforward to derive the approximations (10) from the ascending series for I_1 (and to explain the convergence problem for larger Re). Complementary to (11), the asymptotic expansion for large arguments, i.e. large Reynolds numbers provides the boundary-layer behavior

$$F \approx r - \sqrt{r}\ e^{q(r-1)} \ . \tag{13}$$

This expression agrees to within 1% with (11) provided $r \leq 1-\delta$. The boundary layer thickness δ can be obtained from the transcendental equation

$$\delta = \sqrt{2/Re}\ \left[4.605 - \frac{3}{2}\ln(1-\delta)\right] \ , \tag{14}$$

e.g., $\delta = 0.223$ for $Re = 1000$.

3.3 *The velocity field*

We have chosen three different graphical representations in order to illustrate the characteristic changes of the velocity distribution over the cylindrical cross section with increasing Re. Figure 2 shows the components f (in the x,z-plane) and g (in the y,z-plane) for a wide range of Reynolds numbers. The opposite sign of the velocity at diametral points assures zero net flux of mass through the cross section. The curves represent cuts through the contour plots of these functions of r and Re in figure 3 at the tick marks $Re = 1, 10, 100,$ and 1000. Up to $Re \approx 5$, the velocity distribution is governed by f. This component never exceeds a value of

0.4, assumes a maximum at $Re \approx 20$ and retains significant size only in a shrinking neighborhood of the wall as Re increases. The component ρ rapidly increases from negligible values as $Re > 5$ and approaches the linear increase with r according to (11) except near the wall at $r = 1$. In figure 4, the data of figure 2 are combined into contour plots of the axial velocity $v_z/(2\epsilon)$ over the cylindrical cross section. These plots clearly show the shift of the velocity maximum (marked by +) from $\phi \approx 0$ at $Re = 1$ to $\phi \approx 90°$ at $Re = 1000$. Figure 4d also illustrates the ramp-like velocity distribution over most of the cross section and the boundary layers with $\delta = 0.223$.

Superposition of the deviation velocity $\mathbf{V}_d$ and the solid body rotation $\mathbf{V}_s$ according to eq. (2) leads to an azimuthally periodic velocity field $\mathbf{V}_n$ which is steady in the nutating frame. The paths of fluid elements are circular orbits about axes that are inclined to the z-axis. The inclination depends on radius and Reynolds number.

Figure 5 compares the dimensional velocity distributions obtained from (7), (12) with computational results for the center cross-section ($z = 0$) of a cylinder of aspect ratio 4.3.* The agreement for $Re = 14.9$ is considered representative for the range of lower Reynolds numbers. We have repeated the numerical simulation of the flow at this Reynolds number with a modified version of the Sandia code and obtained very small components $|v_r| < 0.005$ m/s, $|v_\phi| < 0.05$ m/s at $z = 0$. These results verify our estimates and justify the use of linearized equations. Moreover, disregarding the presence of end walls seems to have little effect in the center portion of the cylinder. The radial distribution of V_z in the range $-3.5 \leq z \leq 3.5$ is nearly identical with the data shown in figure 5.

Figure 6 shows a similar comparison for $Re = 45.7$. At this higher Reynolds number, we find a systematic deviation between the theoretical result and numerical results at different axial positions. We attribute this deviation to a superposed cellular motion that is not yet incorporated into our analysis.

*The data were kindly provided by Dr. H. Vaughn, Sandia National Laboratories.

4. Moments

With the deviation velocity $\mathbf{V}_d = (0,0,\omega a v_z)$ and v_z given, the moments on a finite-length section of the cylinder can be calculated. We consider a control volume R (surface S) formed by the solid cylindrical wall and liquid surfaces at both ends. Conservation of angular momentum requires

$$\mathbf{M} + \sum(\mathbf{r}\times\mathbf{F}_d) = \frac{\partial}{\partial t}\int\int_R\int(\mathbf{r}\times\mathbf{V}_d)\rho\,dR + \int\int_R\int[\mathbf{r}\times(2\Omega\times\mathbf{V}_d)]\rho\,dR \qquad (15)$$

$$+\int\int_S(\mathbf{r}\times\mathbf{V}_d)(\mathbf{V}_d\cdot\mathbf{n})\rho\,dS+\int\int_S(\mathbf{r}\times\mathbf{V}_s)(\mathbf{V}_d\cdot\mathbf{n})\rho\,dS\,,$$

where $\mathbf{n}$ is the outer unit normal. On the left-hand side, $\mathbf{M}$ is the resultant torque on the control volume. The second term accounts for the moments due to the shear force $\mathbf{F}_d$ and vanishes owing to the solid sidewall and cancellation of the contributions from both ends. On the right-hand side, the first term vanishes for steady $\mathbf{V}_d$. The second term originates from Coriolis forces in the nutating system. The third term vanishes since $\mathbf{V}_d$ has only an axial component. The last term then provides the net rate of angular momentum flux through the control surface.

Substitution of $\mathbf{V}_d$ leads to the following expressions for the cartesian components of $\mathbf{M}$:

$$M_x = m_l(2\Omega\, a\sin\theta)(\omega a)\, m_x\,,\ m_x = -\int_0^1 r^2 f\,dr\,, \qquad (16a)$$

$$M_y = m_l(2\Omega\, a\sin\theta)(\omega a)\, m_y\,,\ m_y = -\int_0^1 r^2 g\,dr\,, \qquad (16b)$$

$$M_z = m_l(2\Omega\, a\sin\theta)^2\, m_z\,,\ m_z = \int_0^1 r^2 f\,dr = -m_x\,, \qquad (16c)$$

where $m_l = 2\pi\rho a^2 c$ is the liquid mass in the cylinder. In this form, the components M_x, M_y represent the net rate of angular momentum flux through the liquid ends, whereas the roll moment M_z is solely due to Coriolis forces. A close relation between roll moment M_z and yaw moment M_x has also been found by Murphy (1984, 1985).

APPENDIX A

A different interpretation can be derived using the differential equation (9a), integrating by parts, applying (9b), and separating real and imaginary parts:

$$m_z = -\pi_{\cdot\cdot} = \int_0^1 r^2 f\,dr = -\frac{g'(1)}{Re}\,, \tag{17a}$$

$$m_y = -\int_0^1 r^2 g\,dr = -\frac{f'(1)}{Re} - \frac{1}{4}\,. \tag{17b}$$

In this form, the moments are directly related to the shear forces at the cylindrical sidewall, $r = 1$. Since $f'(1) < 0$, $g'(1) < 0$, the roll moment M_z is always positive (even for $\Omega < 0$), while M_z is negative for $\Omega > 0$ and changes sign with Ω. For small Re, the series (10) provide the approximations

$$m_z \approx \frac{Re}{96}\,,\ m_y \approx -\frac{Re^2}{1536}\,, \tag{18}$$

that can be used for quick estimates up to $Re \leq 10$. The linear increase of m_z and M_z with Re is consistent with the experimental data. From the analytical solution (10), we obtain

$$F'(1) = g'(1) + i f'(1) = 2 - qI_0(q)/I_1(q). \tag{19}$$

Substitution into (17) provides the variation of m_z, m_y with the Reynolds number shown in figure 7. The coefficient m_z assumes a pronounced maximum at $Re \approx 19$. The occurrence of this maximum was earlier thought to originate from hydrodynamic instability with respect to a cellular motion. Here, we find a simple explanation in the properties of the axial velocity component f in the r,z- plane and the derivative $g'(1)$. The coefficient m_y is negligible for $Re < 5$, rapidly decreases with increasing Re and reaches an asymptotic value of $m_y \to -1/4$ as $Re \to \infty$. Hence, for $\Omega > 0$, M_y tends to reduce the pitch moment due to the solid body rotation. We note, however, that these moments represent only the effect of viscous shear at the cylindrical side wall. Shear at the end walls and the contribution of the pressure are

neglected.

The data base for the yaw and pitch moments is scarce. Computations by Vaughn et al. (1985) indicate, however, that the pressure contributions to these moments are larger (and opposite in sign) than the viscous components. Only the viscous component can be estimated from our solution. Therefore, we concentrate in the following on a detailed comparison for the roll moment.

In figure 8 we compare the asymptotic law (18) and the theoretical result (17) with experimental data (Miller 1982) and computational results (Vaughn et al. 1985) for the roll coefficient m_s on a doubly logarithmic scale. The initial spin rate $\omega = 4000$ rpm has been used for obtaining the nondimensional values from the experiment. For $Re < 10$, the experimental data match the analytical result as well as the asymptotic law $m_s \approx Re/96$. The deviation between theoretical and computational results is probably due to a larger axial extend of the end effects at very low Reynolds numbers. Good agreement with the computational results is obtained near the maximum of m_s. The point at $Re = 113$ is close to the Reynolds number where the numerical simulation fails to converge to a steady solution, and may not be very accurate. The experiments find the maximum roll moment at slightly lower Reynolds numbers than the theoretical value. In fact, this discrepancy will increase as lower spin rates ω are used for data reduction. In view of the agreement between theoretical and computational results, the discrepancy can not arise from the approximations employed in our analysis. A first possible source may be the effect of unsteadiness in the spin-down experiments. More likely, however, the shift is caused by changes of temperature and viscosity during the experiments. A moderate increase in temperature would reduce the viscosity of the working fluids (silicone oil, corn syrup) and hence shift the maximum to higher Reynolds numbers. Miller (personal communication) observed a temperature increase by $\approx 2.5°$C per run up to $\approx 10°$C above ambient temperature after repeated runs. Vaughn et al. (1985) used these values for correcting the results, with some improved agreement. We waive such a correction but discuss the temperature increase in more detail in the next chapter.

As a final observation in figure 8, we note the change in tendency for the two experimental data points at $Re > 10^3$. It is likely that the internal flow becomes unsteady and ultimately turbulent as the Reynolds number increases. Preliminary results from flow visualization in a small-scale experiment (Pierpont 1985) indicate that these two points are for a turbulent internal flow.

In figure 9 we recast experimental, computational and theoretical results for the dimensional roll moment M_z in different form. Whereas the asymptotic properties are concealed, the linear scale for M_z reveals the pronounced maximum of the roll moment for viscosities near $\nu = 10^5$ cSt and more clearly indicates that theory and computation yield larger maximum values than the despin experiments with the old test fixture (Miller 1982). More recent measurements with a new test fixture at higher spin rates (Miller, personal communication) provide larger maximum values slightly in excess of the theoretical result.

For the roll moment as a function of nutation angle and rate, Herbert (1983) derived from Miller's data (1982, fig. 12) the empirical relation $M_z = 0.00814\,(\Omega \sin\theta)^2$ Nm. The theory provides M_z in the same form but with a somewhat larger factor of 0.0111. This comparison for a fluid of kinematic viscosity $\nu = 2{\cdot}10^5$ cSt is likely to be biased by temperature effects. A notable feature of the roll moment as a function of nutation rate at different spin rates is shown in figure 10. For these parameters in the range of the maximum roll moment, the dependence of M_z on ω is non-monotonic, e.g. the data for $\omega = 9000$ rpm are in between those for $\omega = 3000$ and 9000 rpm. This puzzling behavior has been observed by Miller in experiments with the new test fixture. From the theoretical result it is obvious that M_z decreases (increases) with ω for sufficiently small (large) viscosities to the left (right) of the maximum in figure 9.

The interpretation of the experimental results has been hampered by the observation of Miller (1982) that "the despin moment was not a function of the canister spin rate, provided a sufficient spin rate is present". In contrast, the theoretical result (14c),(15a),(19) depends on the spin rate since $q \sim Re^{1/2}$ and $Re \sim \omega$ for fixed a and ν. Figure 11 shows the theoretical results for M_z as a function of the spin rate ω for viscosities $\nu = 10^3$, 10^4, and 10^5 cSt on linear scales. Note that in some range of ω, M_z appears indeed nearly independent of the spin rate, especially for $\nu = 10^5$ cSt where the maximum of M_z stretches out over most of the observed range ($3000 < \omega < 9000$ rpm) of spin rates. Figure 11 also shows different prototypes of behavior that are distinguished by the position of the maximum roll moment along the ω axis. Experimental data for similar conditions are shown in figure 12 and verify the theoretically predicted behavior. Moreover, these data suggest major simplifications in the experimental procedures. Whereas the experimental data in figure 9 were obtained by using numerous working fluids of different viscosities, a more complete set of data can be generated by carefully monitoring the spin-down for a few runs with fluids in the range of low, medium, and high viscosities as in figure 12.

5. Temperature effect

The comparison of theoretical and computational results with experimental data seems to be biased by the effect of increasing temperature on the viscosity of the working fluid. These effects appear more pronounced at high viscosities and high spin rates. For an estimate of the rate of change of the average temperature T, we consider a control volume R (surface S) formed by liquid surfaces along the cylinder's side and end walls. The material properties are assumed to be constant and heat transfer through the surface is disregarded. Balancing the rate of change of energy with the work done on the control volume, we obtain after some simplifications

$$m_l c_v \frac{dT}{dt} = \int_S \int \tau \cdot \mathbf{V}_i \, dS, \tag{20}$$

where c_v is the specific heat, τ the vector of tangential stresses, and $\mathbf{V}_i$ the velocity measured in an inertial frame. Since $\mathbf{V}_i$ is independent of z, the contributions from the cylinder ends cancel. The only contribution is due to the shear stress

$$\tau_m = \mu \frac{\partial(\omega a v_z)}{\partial r}|_{r=1} = 2\mu\Omega \, a \sin\theta \{ f'(1)\cos\phi + g'(1)\sin\phi \} \tag{21}$$

in the axial direction. The relevant axial component of the velocity $(\Omega + \omega) \times \mathbf{r}$ of some point on the surface S is given by $-\Omega \, a \sin\theta \sin\phi$. Integration over the cylindrical surface yields

$$m_l c_v \frac{dT}{dt} = -\mu (2\Omega \, a \sin\theta)^2 \pi \, ac \, g'(1) \, . \tag{22}$$

After substituting for m_l and introducing the Reynolds number, this result can be written as

$$\frac{dT}{dt} = \frac{\omega}{2c_v} (2\Omega \, a \sin\theta)^2 \left(- \frac{g'(1)}{Re} \right) . \tag{23}$$

Comparison with eq. (15a) shows that the rate of change of temperature can be directly expressed in terms of the roll moment,

$$\frac{dT}{dt} = \frac{\omega}{2c_v} (2\Omega \, a \sin\theta)^2 m_l = \frac{\omega}{2 m_l c_v} M_z \, . \tag{24}$$

This result immediately shows that the temperature rise per run cannot be specified as a single number, nor should a uniform correction be applied to the experimental data. Moreover, the temperature changes increase with the spin rate, and consequently are quite different for the

experiments with the old (Miller 1982) and the new test fixture. Using the maximum value $m_z \approx 0.0854$, we obtain for the 1982 experiments ($a = 60.3$ mm, $\omega = 4000$ rpm, $\Omega = 500$ rpm, $\theta = 20°$) with silicone oil ($c_v \approx 1600$J/(kg°C) a temperature rise of $dT/dt = 0.055$°C/s. Using the same fluid in the new test fixture ($a = 55.4$ mm, $\omega = 10^4$ rpm, $\Omega = 600$ rpm, $\theta = 20°$) leads to a temperature increase of $dT/dt = 0.158$°C/s.

A single run consists of three phases (Miller, personal communication). The spin-up period of ≈ 30 s is followed by a sudden start of the nutation and a period of ≈ 30 s in order to reach steady conditions. Finally, the shutdown of the spin drive is followed by a spin-down period of ≈ 15 s. The second period at nearly steady conditions and maximum spin rate appears most relevant to the modification of the viscosity. At the start of the third phase, the average temperature may have increased by ≈ 1.56°C in the 1982 experiments, and by ≈ 4.75°C in the more recent experiments at higher spin and nutation rates. These values are for conditions of maximum roll moment, and may be considerably lower in other cases. The value of 2.5°C measured in the new fixture is well within the estimated range. Our result (24) indicates, however, that a single measurement is insufficient for evaluating the temperature effects, especially those in a different experimental setup.

APPENDIX A

6. Concluding remarks

We have developed a simple model of the viscous fluid motion in a spinning and nutating cylinder. The disregard of the end walls has some obvious consequences: the turning flow near the ends and the associated contributions of pressure and shear stresses to the moments cannot be obtained from this model. Nevertheless, we gather understanding as well as quantitative information. The velocity field of the core flow agrees well with computational results for low Reynolds numbers. The analytical result is an evident example for the formation of boundary layers. The core flow can be utilized as a basic flow in studies of hydrodynamic instability with respect to cellular motions. The parametric excitation of such cells by the azimuthally periodic deviation has been discussed by Herbert (1984). The core flow also represents the lowest-order approximation to the solution of the nonlinear equations (3) and can be extended by higher-order terms in ϵ.

The roll moment agrees well with measured and computed values, and can also be found at Reynolds numbers too large for successful numerical simulations. The roll moment originates from Coriolis forces. While the direct calculation of the yaw moment suffers from neglecting the pressure contribution, the yaw moment can be found from the roll moment using the relations given by Murphy (1984, 1985). The pitch moment remains an open issue. The estimates for the change in average temperature need further verification once more detailed data become available.

The simple form and scaling relations of our results provide guidance for sorting and evaluating the experimental data base. The results also suggest various improvements in the experimental procedures. First, the changes in temperature and viscosity should be carefully monitored. With the effective viscosity known, a closer agreement between theory and observation is to be expected. Second, the yet neglected variation of the roll moment with the spin rate is considered relevant and in fact provides the roll moment in some range of Reynolds numbers. Instead of producing the data for figure 9 by using numerous viscosities at fixed spin rate, very similar data can be generated by varying the spin rate for a few fluids.

ACKNOWLEDGMENT

The open cooperation and sharing of data with Miles C. Miller (CRDC) and Harold R. Vaughn (Sandia Laboratories) are greatly appreciated. Ri-Hua Li deserves credit for his assistance in developing the analytical solution. This work is supported by the Army Research Office under Contract DAAG29-82-K-0129 and by the Army AMCCOM under Contract DAAK11-83-K-0011.

APPENDIX A

REFERENCES

Abramowitz, M. & Stegun, I. A. 1972 " Handbook of Mathematical Functions," New York: Dover Publications, Inc.

D'Amico, W. P. 1977 "Field Tests of the XM761: First Diagnostic Test," Ballistic Research Laboratory, Memorandum Report 1325.

D'Amico, W. P. 1978 "Field Tests of the XM761: Second Diagnostic Test," Ballistic Research Laboratory, Memorandum Report ARBRL-MR-02806.

D'Amico, W. P. & Miller, M. C. 1979 "Flight Instability Produced by a Rapidly Spinning, Highly Viscous Liquid," *J. of Spacecraft and Rockets*, Vol. 16, pp. 62-64.

Herbert, Th. 1982 "Fluid Motion in a Rotating and Nutating Cylinder - Part I," Report prepared under the Scientific Services Program. Published as Report CRDC-CR-84087 (1984).

Herbert, Th. 1983 "The Flow of Highly Viscous Fluid in a Spinning and Nutating Cylinder," Proc. of the 1983 Scientific Conference on Chemical Defense Research, Aberdeen Proving Ground, MD.

Herbert, Th. 1984 "Highly Viscous Fluid Flow in a Spinning and Nutating Cylinder," Proc. of the Second Army Conference on Applied Mathematics and Computing, Troy, NY.

Miller, M. C. 1981 "Void Characteristics of a Liquid Filled Cylinder Undergoing Spinning and Coning Motion," *J. of Spacecraft and Rockets*, Vol. 18, pp. 286-288.

Miller, M. C. 1982 "Flight Instabilities of Spinning Projectiles Having Nonrigid Payloads," *J. of Guidance, Control, and Dynamics*, Vol. 5, pp. 151-157.

Murphy, C. M. 1984 "A Relationship between Liquid Roll Moment and Liquid Side Moment," Ballistic Research Laboratory Memorandum Report ARBRL-MR-03347.

Murphy, C. M. 1985 "A Relation between Liquid Roll Moment and Liquid Side Moment," *J. of Guidance, Control, and Dynamics*, Vol. 8, pp. 287-288.

Pierpond, D. 1985 "Design of an Experiment for Visualization of the Flow in a Spinning and Nutating Cylinder," Senior Project Report, VPI & SU.

Stewartson, K. 1959 "On the Stability of a Spinning Top Containing Liquid," *J. of Fluid Mech.*, Vol. 5, Part 4, pp. 577-592.

Vaughn, H. R., Oberkampf, W. L & Wolfe, W. P. 1983 "Numerical Solution for a Spinning Nutating Fluid-Filled Cylinder," Sandia Report SAND 83-1789.

APPENDIX A

Vaughn, H. R., Oberkampf, W. L. & Wolfe, W. P. 1985 "Fluid Motion Inside a Spinning Nutating Cylinder," *J. of Fluid Mech.*, Vol. 150, pp. 121-138.

Wedemeyer, E. H. 1966 "Viscous Corrections to Stewartson's Stability Criterion," Ballistic Research Laboratory, Report 1325.

APPENDIX A

FIGURE CAPTIONS

Figure 1. Definition sketch

Figure 2. Components f and g of the axial velocity $v_z/(2\epsilon)$ for various Reynolds numbers: □, $Re = 1$; ○, 10; Δ, 10^2; +, 10^3.

Figure 3. Contour lines of the components f and g of the axial velocity $v_z/(2\epsilon)$ as a function of radius r and Reynolds number Re. Intervals are 0.05; the zero level is given by the heavy line.

Figure 4. Contour lines of equal axial velocity, $v_z/(2\epsilon) = \text{const.}$, for (a) $Re = 1$; (b) 10; (c) 10^2; (d) 10^3. Intervals are 0.01, 0.1, 0.2, 0.2, respectively. The zero level is given by the heavy line, the velocity maximum is marked by +.

Figure 5. Radial distribution of the dimensional velocity V_z at $z = 0$ for $Re = 14.9$. The symbols show the numerical solution to the Navier-Stokes equations (Vaughn 1983, personal communication). Parameters: $a = 60.3$ mm, $c/a = 4.3$, $\theta = 20^0$, $\omega = 3000$ rpm, $\Omega = 500$ rpm, $\rho = 1400$ kg/m^3.

Figure 6. Radial distribution of the dimensional velocity V_z at $z = 0$ for $Re = 45.7$. The symbols show the numerical solution to the Navier-Stokes equations (Vaughn 1983, personal communication). Parameters: $a = 60.3$ mm, $c/a = 4.3$, $\theta = 20^0$, $\omega = 3000$ rpm, $\Omega = 500$ rpm, $\rho = 1400$ kg/m^3.

Figure 7. The nondimensional coefficients m_z, m_y in eq. (17) vs. the Reynolds number Re.

Figure 8. Comparison of the theoretical result for m_z with: ×, experimental data (Miller 1982); ○, computational results (Vaughn et al. 1985). The straight line shows the asymptotic law $m_z \approx Re/96$.

APPENDIX A

Figure 9. Comparison of the theoretical result for the roll moment M_z at $\omega = 3000$ rpm vs. kinematic viscosity ν with: $\times$, experimental data (Miller 1982) for $\omega = 2000 - 4000$ rpm; $\bigcirc$, computational results (Vaughn et al. 1985) for $\omega = 3000$ rpm. Parameters: $a = 60.3$ mm, $c/a = 4.29$, $\theta = 20^0$, $\Omega = 500$ rpm, $\rho = 1000$ kg/m^3.

Figure 10. Theoretical results for the roll moment M_z vs. nutation rate Ω for different spin rates: Δ, $\omega = 3000$; $\bigcirc$, 6000; $\square$, 9000 rpm. Parameters: $a = 50.4$ mm, $c/a = 4.5$, $\theta = 20^0$, $\nu = 10^5$ cSt, $\rho = 1000$ kg/m^3.

Figure 11. Theoretical results for the roll moment M_z vs. spin rate ω for different kinematic viscosities: $\square$, $\nu = 10^3$; $\bigcirc$, 10^4, Δ, 10^5 cSt. Parameters: $a = 50.4$ mm, $c/a = 4.5$, $\theta = 20^0$, $\Omega = 625$ rpm, $\rho = 1400$ kg/m^3.

Figure 12. Experimental results for the roll moment M_z vs. spin rate ω for different kinematic viscosities: $\square$, $\nu = 10^3$; $\bigcirc$, 10^4, Δ, 10^5 cSt. Parameters: $a = 50.4$ mm, $c/a = 4.5$, $\theta = 20^0$, $\Omega \approx 600$ rpm, $\rho = 1400$ kg/m^3.

APPENDIX A

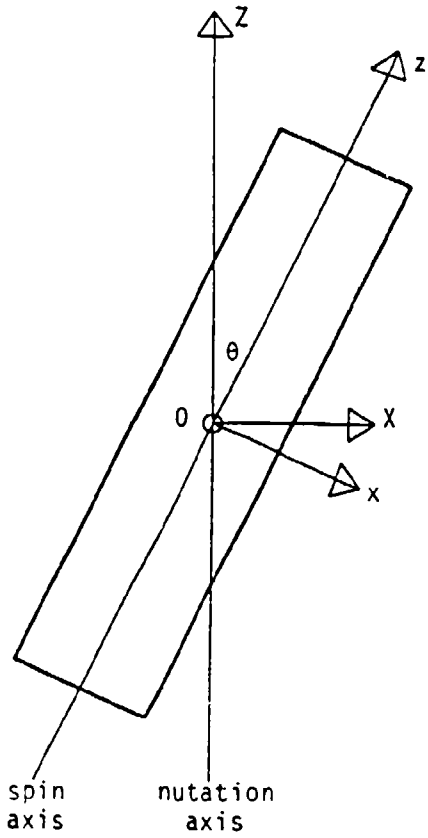

Figure 1.

APPENDIX A

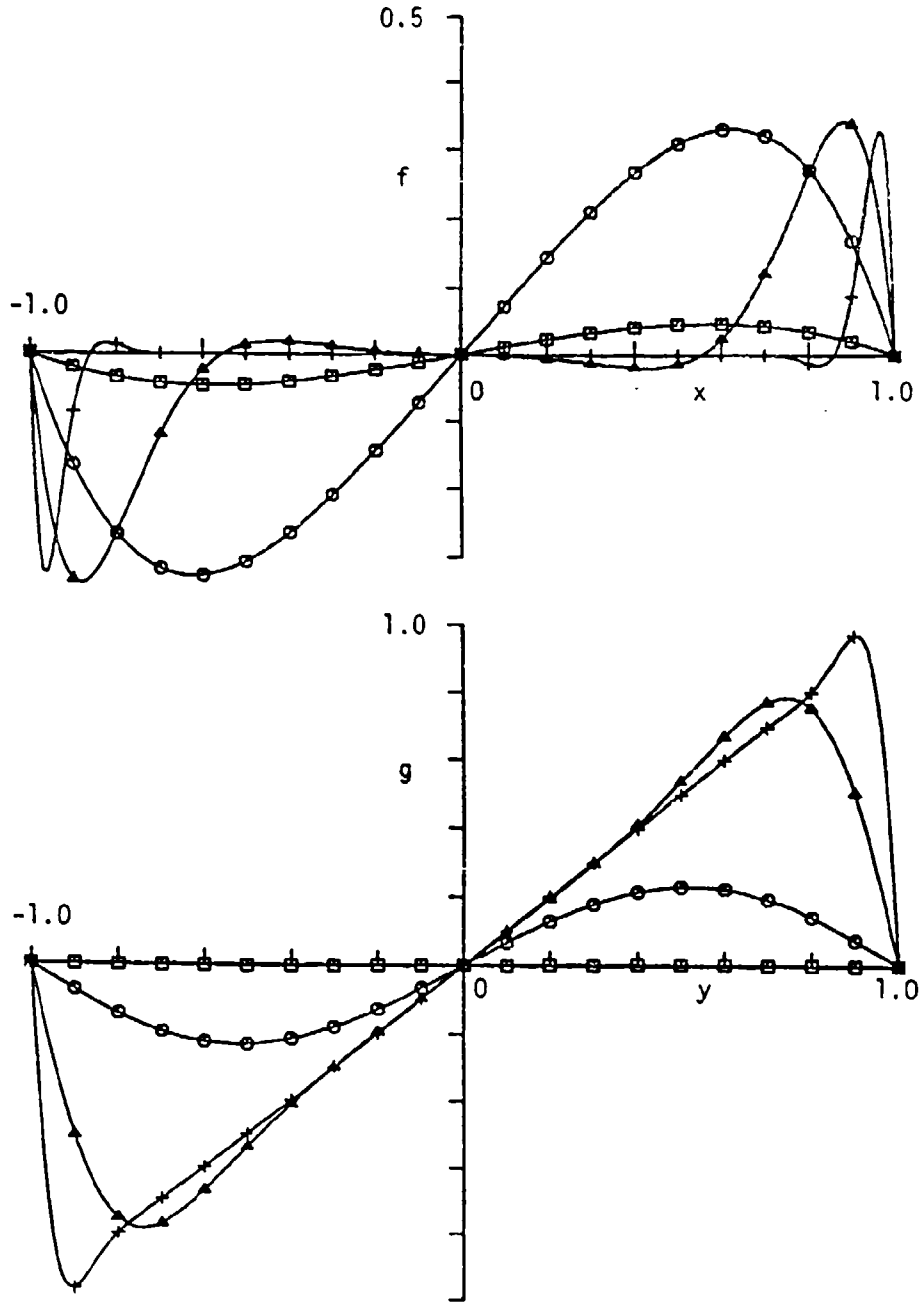

Figure 2.

APPENDIX A

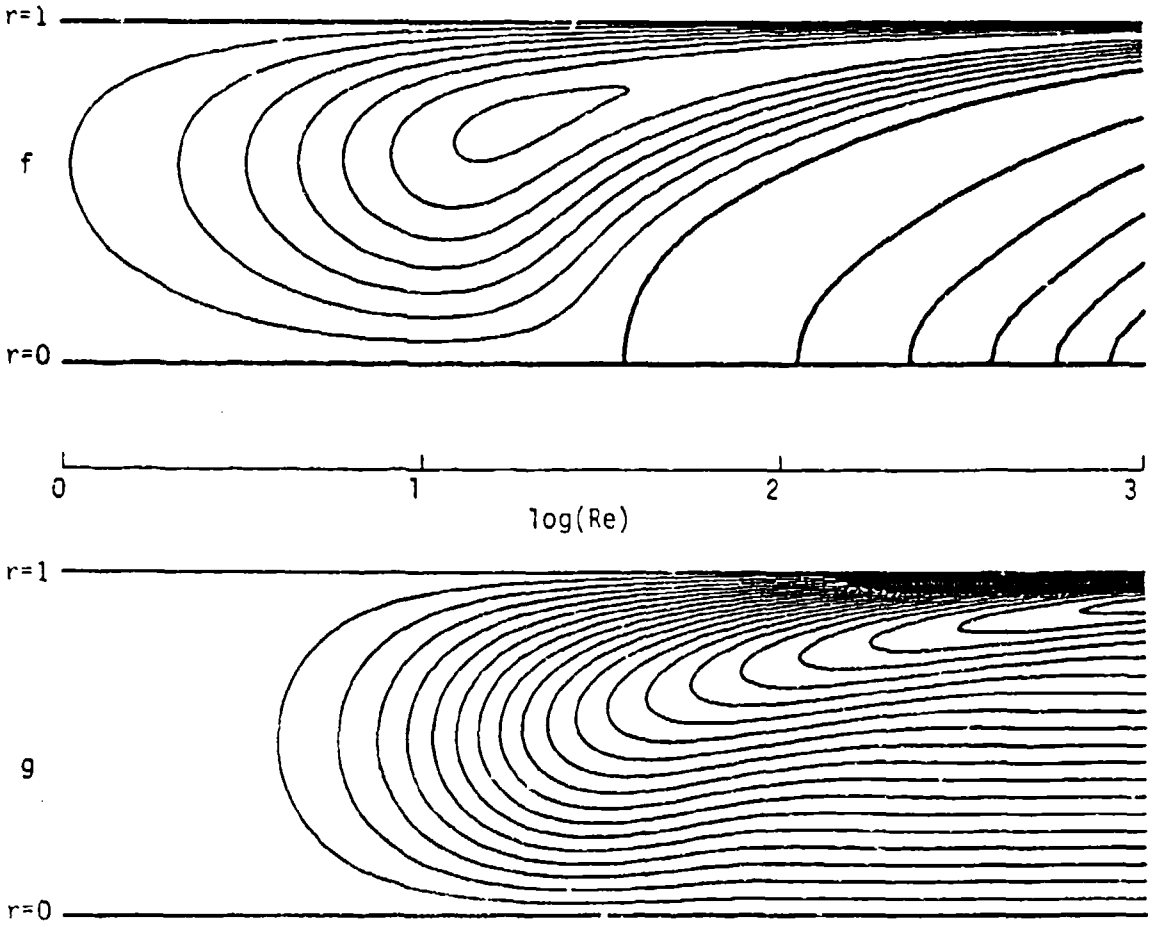

Figure 3

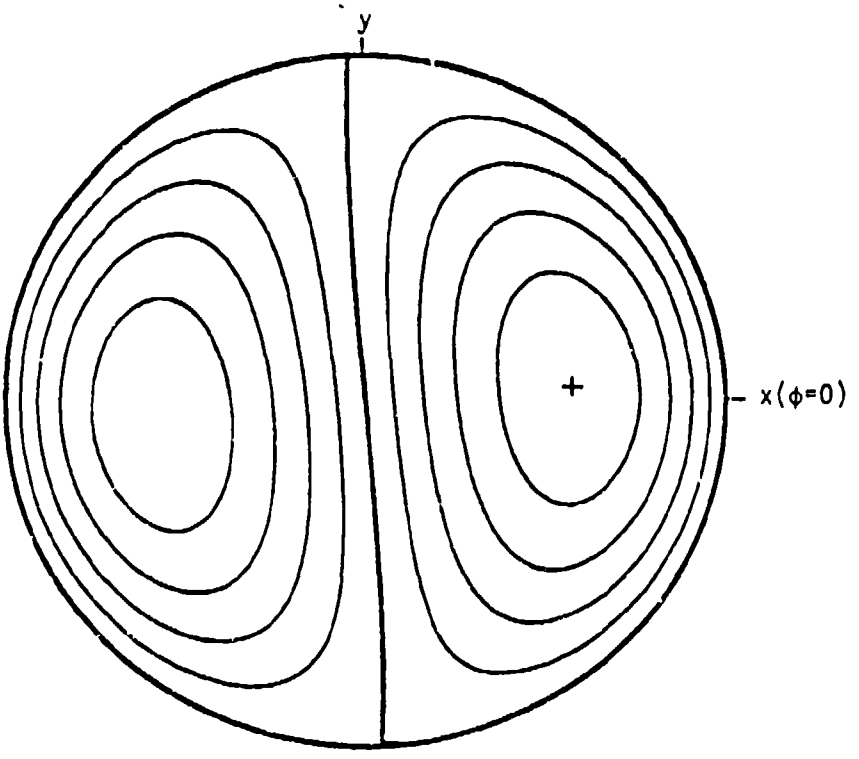

Figure 4a

APPENDIX A

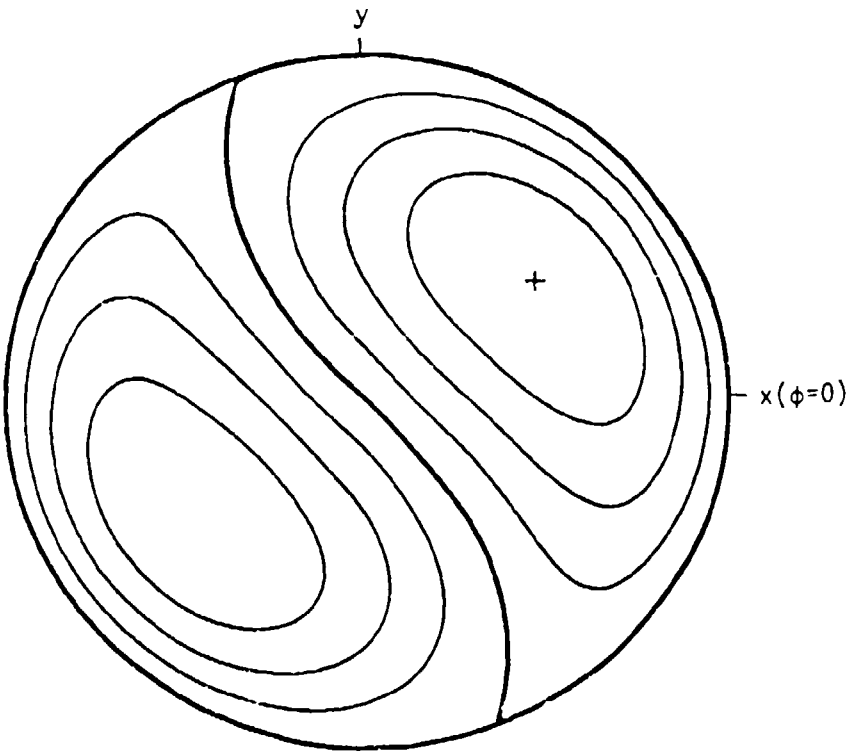

Figure 4b

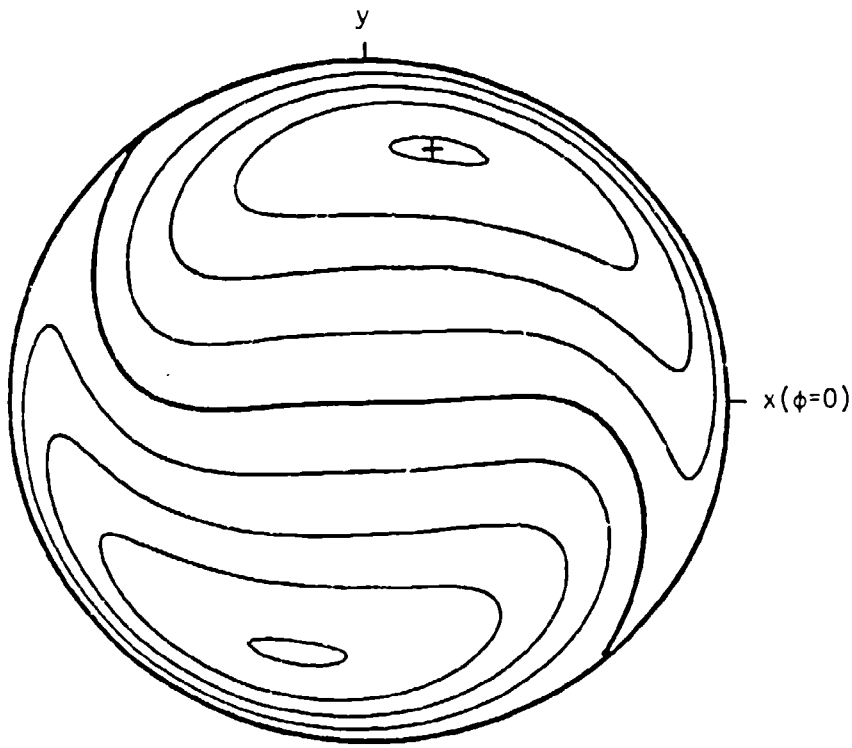

Figure 4c

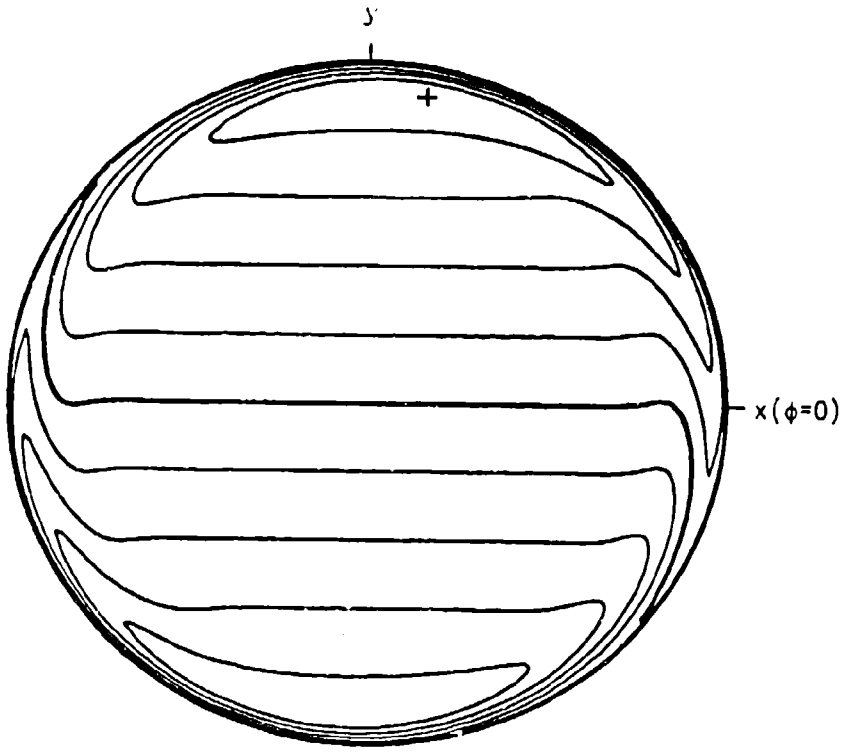

Figure 4d

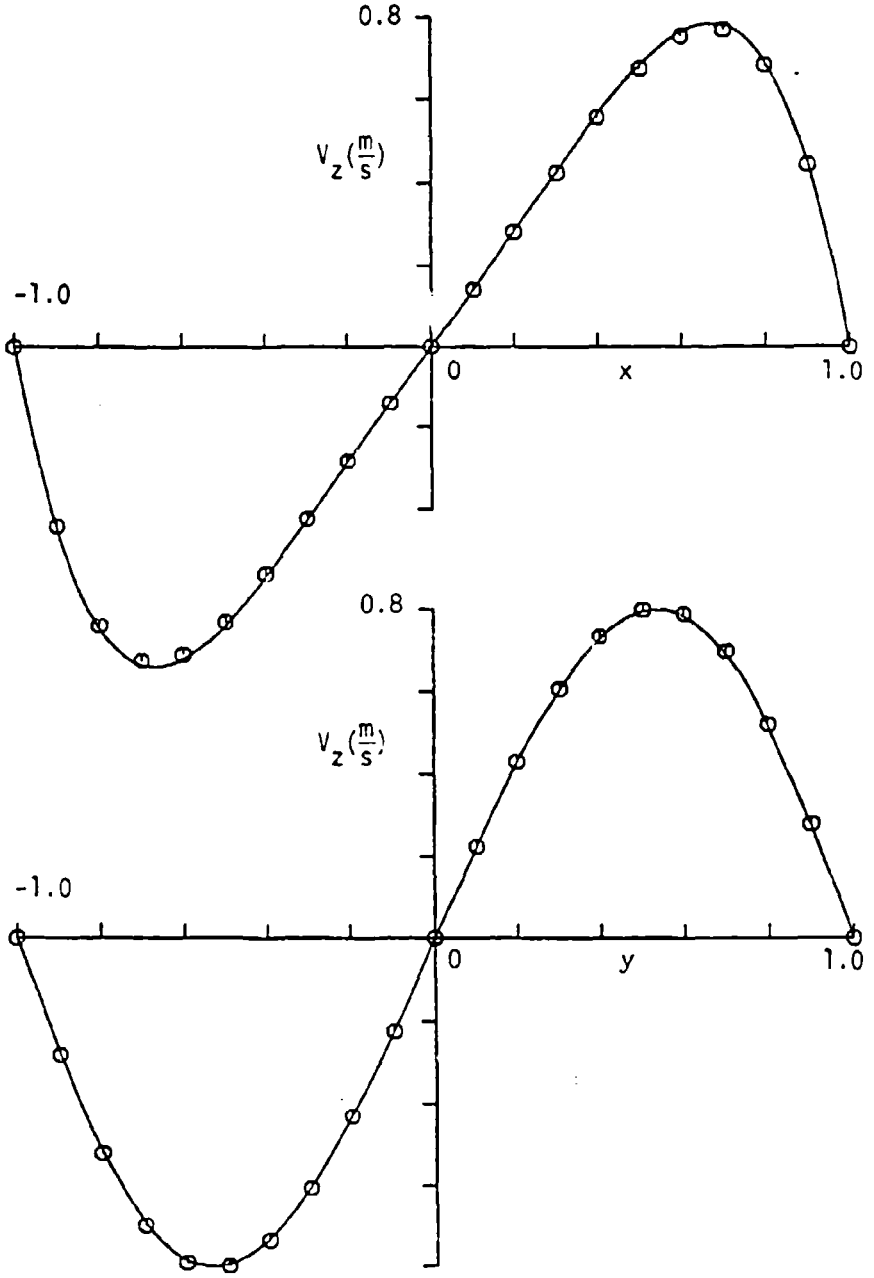

Figure 5

APPENDIX A

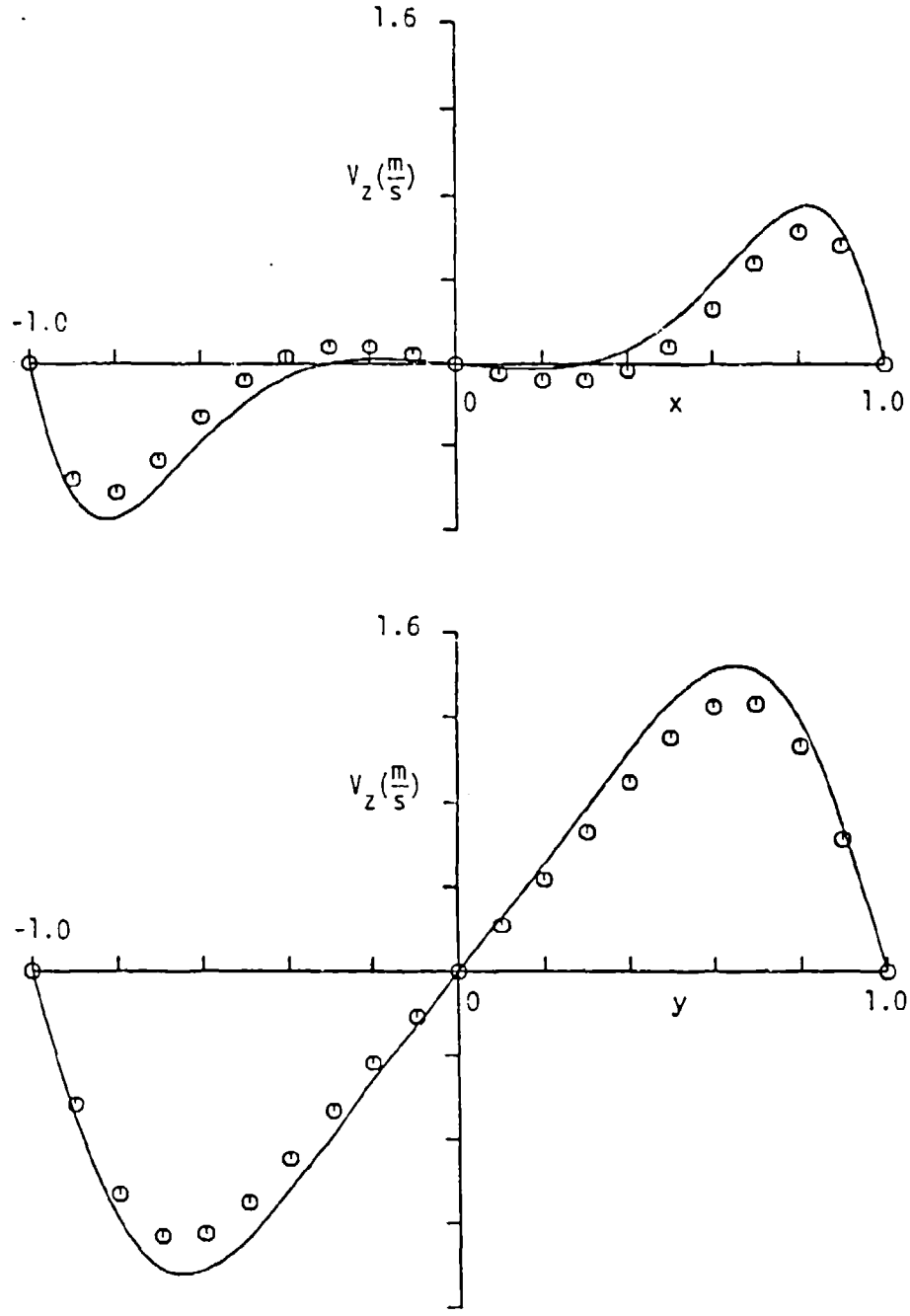

Figure 6

APPENDIX A

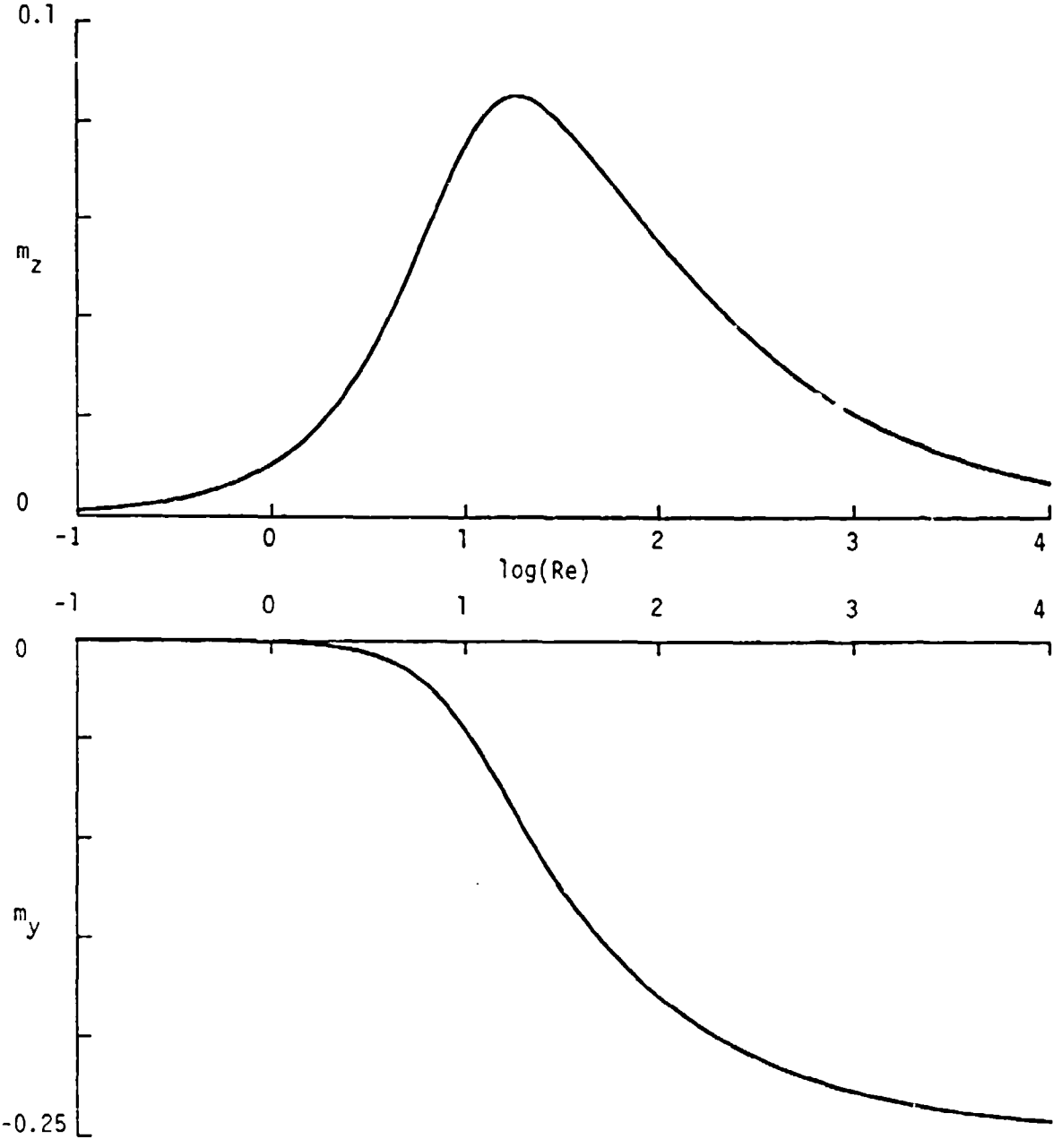

Figure 7

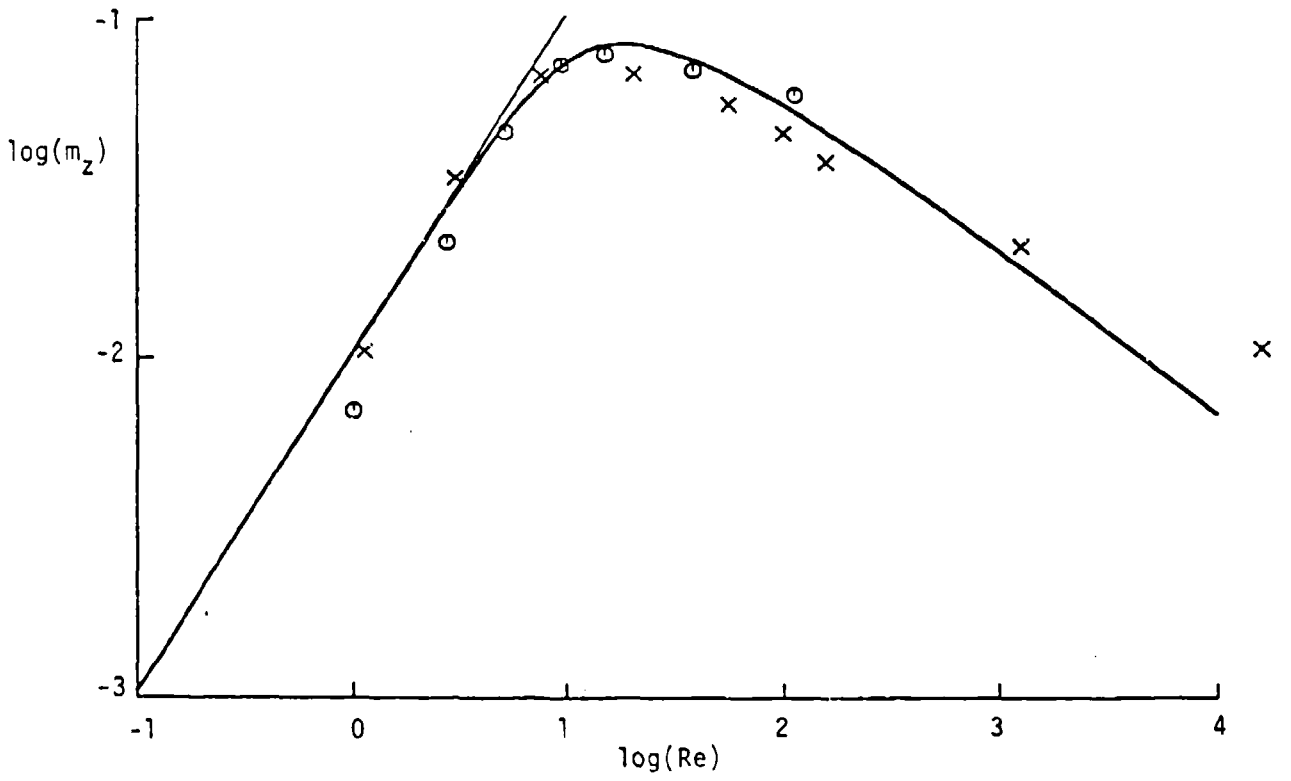

Figure 8.

APPENDIX A

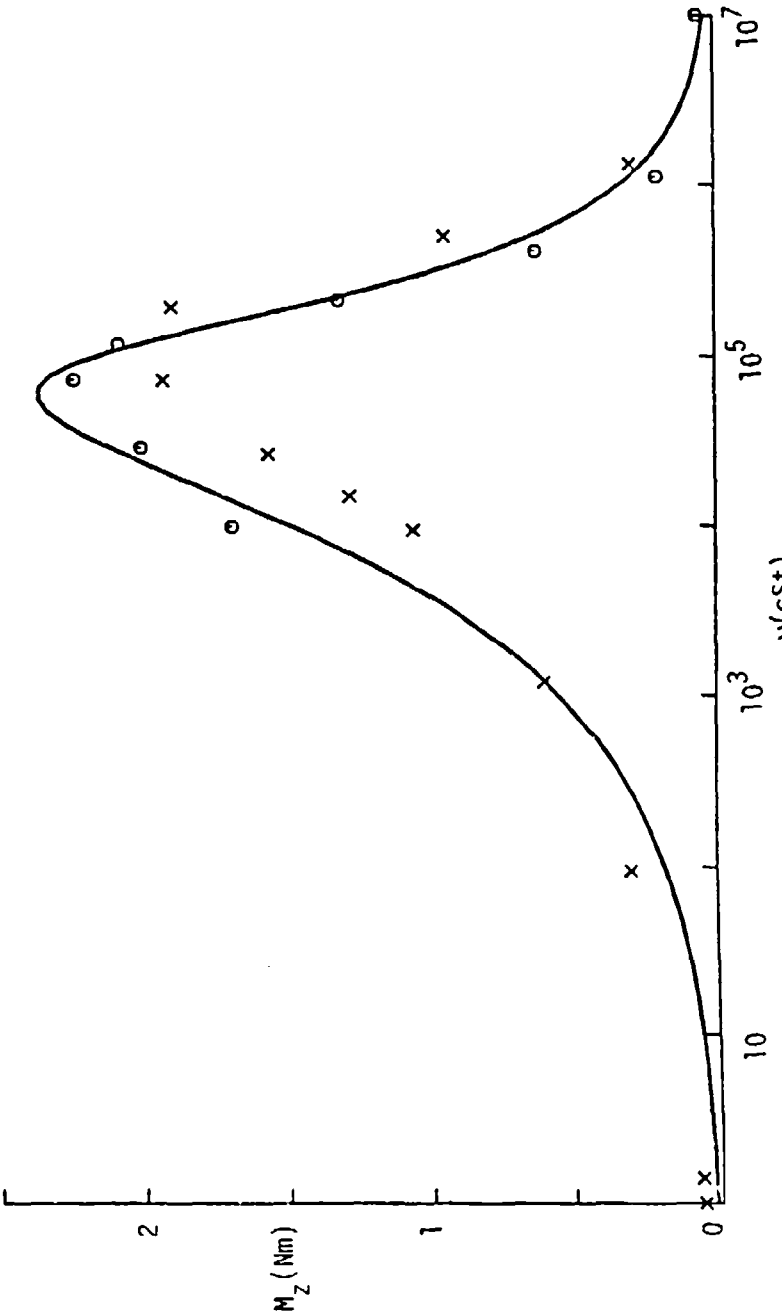

Figure 9.

APPENDIX A

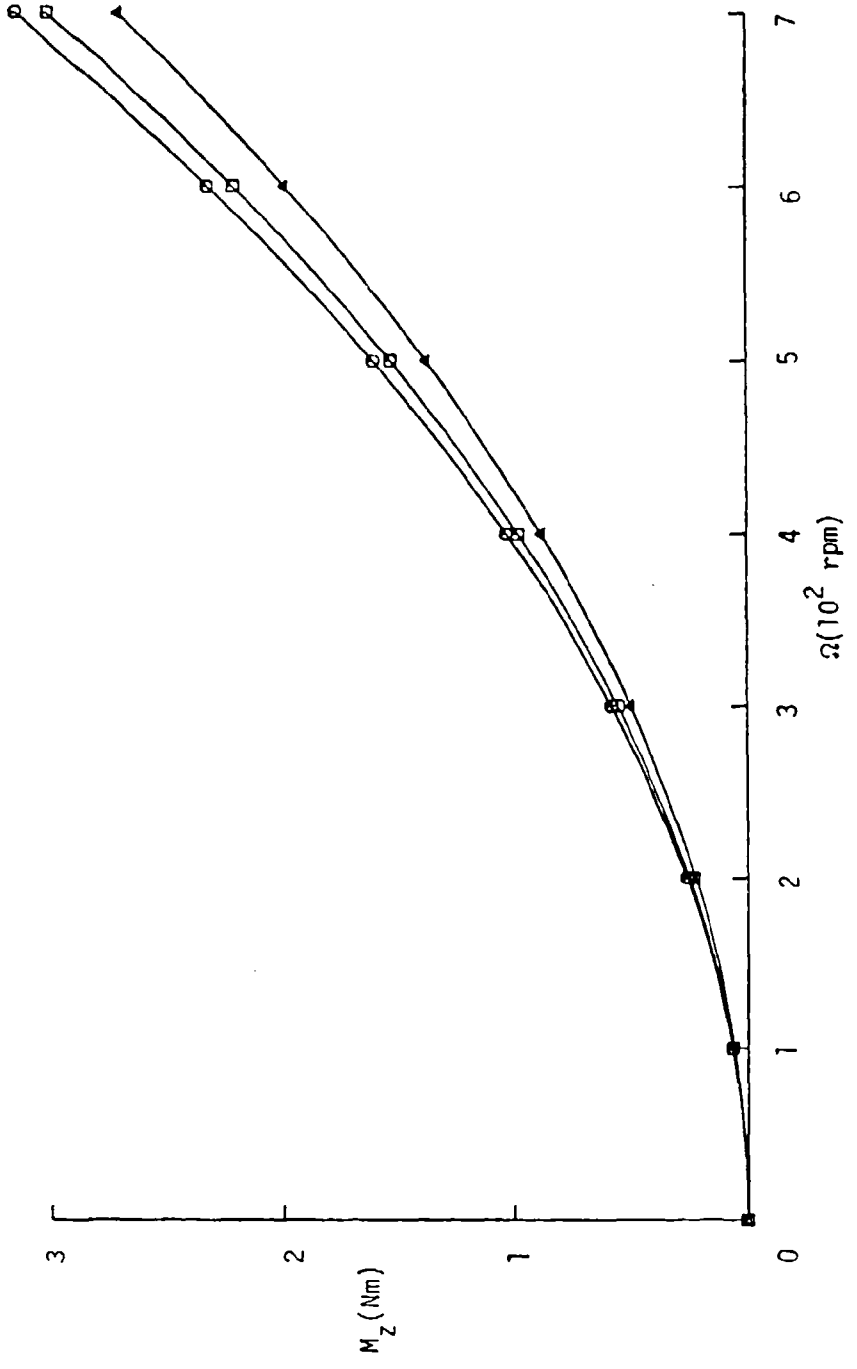

Figure 10.

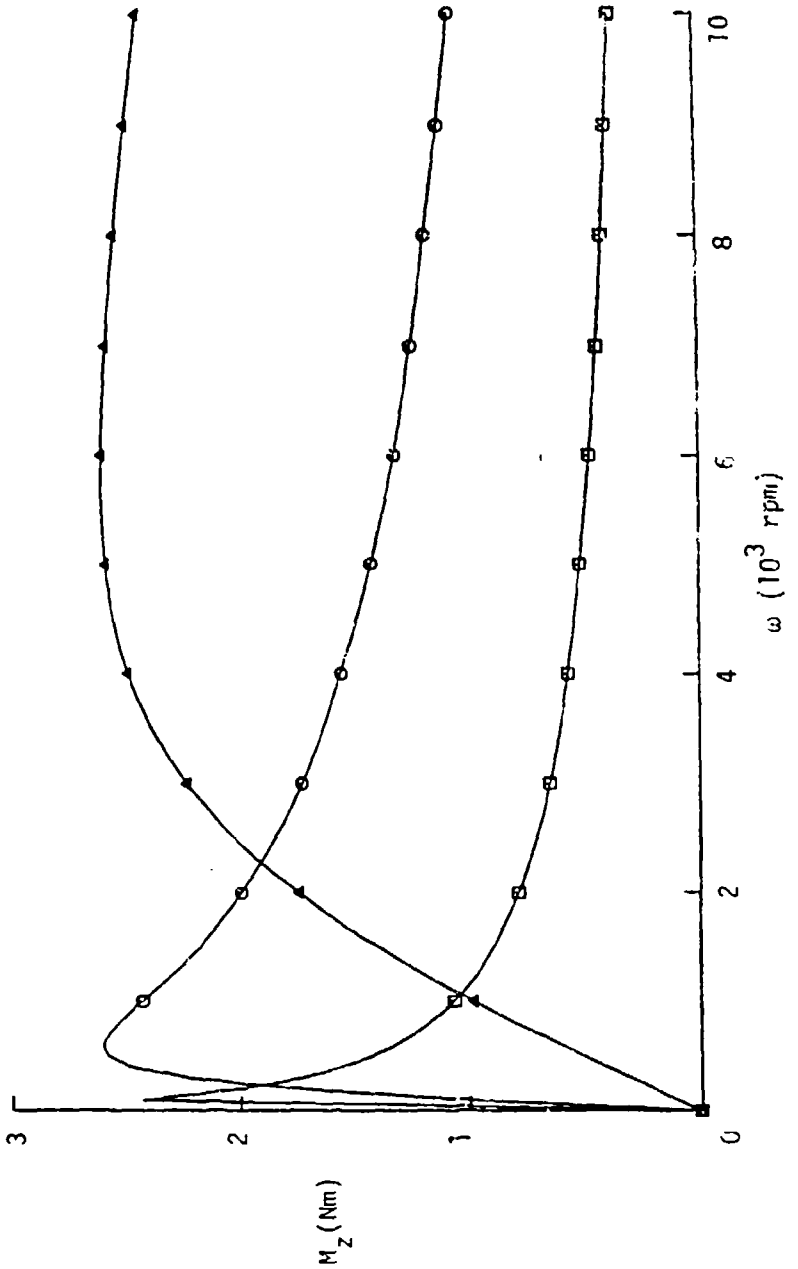

Figure 11.

APPENDIX A

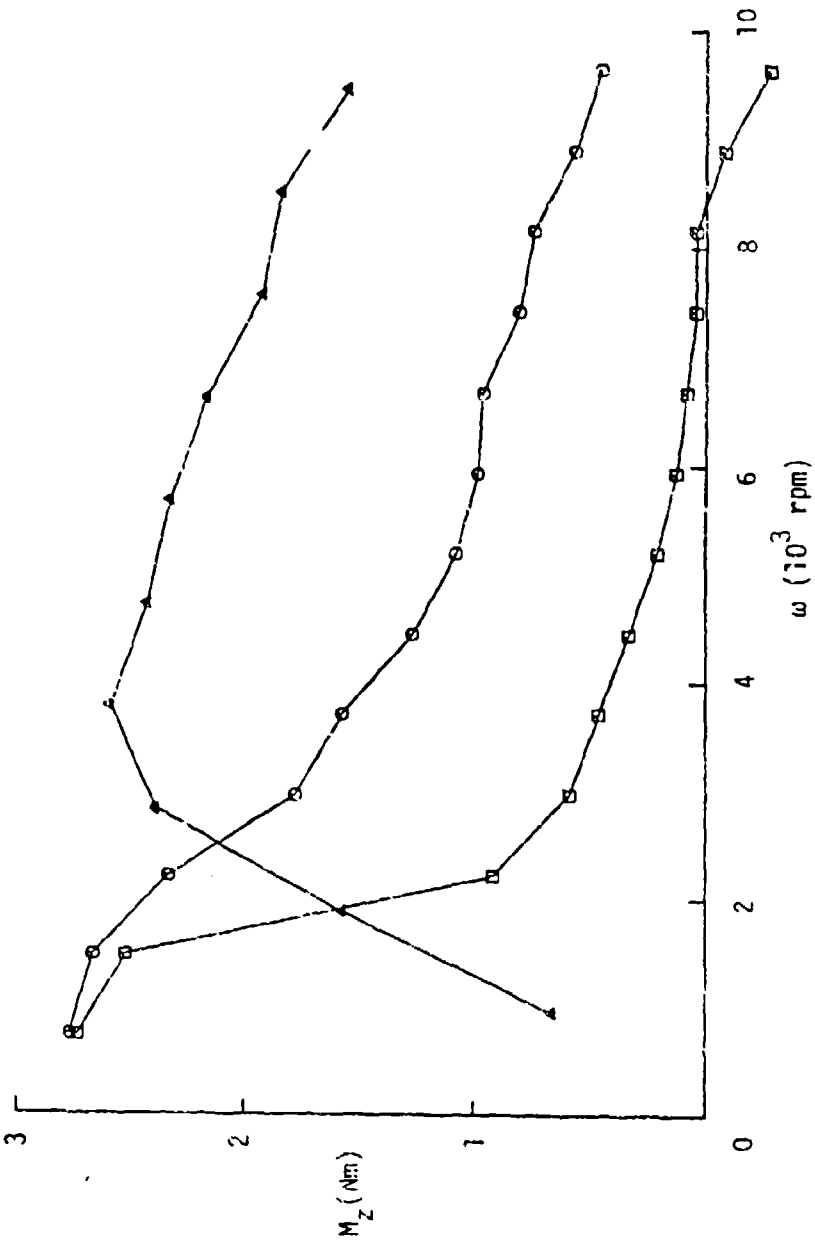

Figure 12.

APPENDIX A

Appendix B

Blank

Appendix B

This appendix gives listings of a sample program, subroutines, and input/output. Subroutine PARAM converts dimensional quantities as prompted into English and SI units and into nondimensional parameters. If the input line starts with a slash (/), the displayed default value is used. If a value of zero is given for the viscosity, the program prompts for the value of the kinematic viscosity. Subroutine EVALA calculates the functions f and g in Appendix A.4, eq. (12) at $r = k/K$, $k = 0, \ldots K$ if $K > 0$, as well as $f'(1)/Re$ and $g'(1)/Re$ used in Appendix A.4, eq. (19) for calculating the moments. Subroutine EVALA uses subroutines BESI1 and BESI0 in order to calculate the ratios of Bessel functions in Appendix A.4, eqs. (12), (19). Additional information is given by comments within the programs.

The sample run provides results for the run of the Sandia code at $Re = 14.95$ used in the comparison Appendix A.4, figure 5.

```
C ********** FLUID FILLED CYLINDER * SAMPLE PROGRAM *************
C *          LINEARIZED EQUATIONS, Z-INDEPENDENT FLOW           *
C *          WRITTEN BY THORWALD HERBERT,  VPI & SU             *
C *                                                             *
C * SHOWS THE USE OF THE SUBROUTINES FOR OBTAINING A LIST OF    *
C *      (1) PARAMETERS                                         *
C *      (2) VALUES OF F(R), G(R), F'(1)/RE, G'(1)/RE           *
C *      (3) DIMENSIONAL VELOCITIES AND MOMENTS                 *
C *************************************************************
C
      COMMON /FLOW/ REY,KK,R(101),F(101),G(101),FS1,GS1
      COMMON /ENGL/ RIN,ZIN,OSR,ONR,THD,SG,DENO,VISO,VIKO,VFT
     *             ,MLO,UMOO
      COMMON /METR/ RMM,ZMM,OS,ON,TH,OX,OY,OZ,OP,DEN,VIS,VIK,VMS
     *             ,ML,UMO
      COMMON /PARM/ AR,TAU,EPS,RE
      REAL ML,MLO
      CHARACTER*1 FF
      FF=CHAR(12)
C
C***  READ AND PRINT PARAMETERS
C
      PRINT 2000, FF
2000  FORMAT (A1,'LIN_S 07/25/85 *** SAMPLE PROGRAM')
      CALL PARAM (1)
      REY=RE
C
C***  SPECIFY NUMBER OF RADIAL STEPS KK (<101)
C
      KK=20
C
C***  EVALUATE AND PRINT F,G AT RADIAL POSITIONS
C
      PRINT 2001, FF
2001  FORMAT (A1)
      KK=MIN(KK,100)
      CALL EVALA(1)

C***  CONVERT F,G INTO DIMENSIONAL VELOCITY (M/S)
C
      PRINT 2002, FF
2002  FORMAT (A1,8X,'r, m',7X,'VELOCITY, m/s'/
     * 15X,'x,z-plane y,z-plane'/)
      DO 1 K=0,KK
      DR=RMM*R(K+1)/1E3
      DVX=VMS*2*EPS*F(K+1)
      DVY=VMS*2*EPS*G(K+1)
1     PRINT 2003, K,DR,DVX,DVY
2003  FORMAT (I4,3F10.6)
C
C***  CONVERT M SUB Z, M SUB Y INTO DIMENSIONAL FORM
C
      DMZ=-UMO*4*EPS**2*GS1
      DMY=-UMO*2*EPS*(FS1+.25)
      PRINT 2004, DMZ,DMY
2004  FORMAT (/2X,'VISCOUS ROLL  MOMENT:',F11.6,' N*m'/
     *         2X,'VISCOUS PITCH MOMENT:',F11.6,' N*m'/)
      PRINT 2001, FF
      STOP
      END
```

```
C ********** FLUID FILLED CYLINDER **** PARAMETERS **************
C *          WRITTEN BY THORWALD HERBERT,  VPI & SU              *
C *                                                              *
C * SUBROUTINE FOR READING AND CONVERTING DIMENSIONAL VALUES     *
C * INTO METRIC UNITS AND DIMENSIONLESS PARAMETERS.              *
C * PRINT VALUES IF IO>0                                         *
C ****************************************************************
C
      SUBROUTINE PARAM (IO)
      COMMON /ENGL/ RIN,ZIN,OSR,ONR,THD,SG,DENO,VISO,VIKO,VFT
     *             ,MLO,UMOO
      COMMON /METR/ RMM,ZMM,OS,ON,TH,OX,OY,OZ,OP,DEN,VIS,VIK,VMS
     *             ,ML,UMO
      COMMON /PARM/ AR,TAU,EPS,RE
      REAL ML,MLO
      CHARACTER*4 ID(18)
      DATA PI,RAD1,RAD2/3.14159,57.2958,9.54930/,IFIRST/1/
C
C***  SET PHYSICAL PARAMETERS TO DEFAULT VALUES
C
      IF (IFIRST.EQ.0) GO TO 1
      RIN= 2.375
      ZIN=10.375
      OSR=3000
      ONR=500
      THD=20
      SG=1.4
      DEN=SG*999.84
      VIS=1.07E05
      VIK=1000*VIS/DEN
C
C***  READ ACTUAL PARAMETERS
C
1     PRINT 2000
2000  FORMAT (/'PARAM 09/25/84 *** PARAMETER CONVERSION'//'ID:')
      READ 1000, ID
1000  FORMAT (18A4)
      PRINT 2001, RIN
2001  FORMAT (/'RIN = radius (inch) :       /',F6.3)
      READ *, RIN
      PRINT 2002, ZIN
2002  FORMAT (/'ZIN = half-length (inch) :  /',F6.3)
      READ *, ZIN
      PRINT 2003, OSR
2003  FORMAT (/'OSR = spin rate (rpm) :     /',F6.0)
      READ *, OSR
      PRINT 2004, ONR
2004  FORMAT (/'ONR = nutation rate (rpm):  /',F6.0)
      READ *, ONR
      PRINT 2005, THD
2005  FORMAT (/'THD = nutation angle (deg): /',F6.1)
      READ *, THD
      PRINT 2006, SG
2006  FORMAT (/'SG = specific gravity (-):  /',F6.3)
      READ *, SG
      DEN=SG*999.84
      PRINT 2007, VIS
2007  FORMAT (/'VIS = viscosity/zero (cp):  /',F8.0)
      READ *, VIS
      VIK=VIS*1000/DEN
```

```
      IF (VIS.GT.0) GO TO 2
      PRINT 2008, VIK
2008  FORMAT (/'VIK = kin. viscosity (cs):  /',F8.0)
      READ *, VIK
      VIS=VIK*DEN/1000
C
C***  CONVERT PHYSICAL PARAMETERS
C
2     RFT=RIN/12
      RMM=RIN*25.4
      ZFT=ZIN/12
      ZMM=ZIN*25.4
      AR=ZIN/RIN
      OS=OSR/RAD2
      ON=ONR/RAD2
      TAU=ONR/OSR
      TH=THD/RAD1
      OZ= ON*COS(TH)
      OY= ON*SIN(TH)
      OX=-OY
      OP=OS+OZ
      EPS=OY/OS
      VFT=RFT*OS
      VMS=VFT*0.3048
      VEL=VFT*2*EPS
      DENO=1.94*SG
      VISO=VIS*2.089E-05
      VIKO=VISO/DENO
      ML=2*PI*RMM**3*AR*DEN*1E-9
      MLO=2*PI*RFT**3*AR*DENO
      RE=VFT*RFT/VIKO
      UMO=ML*(RMM*OS)**2*1E-6
      UMOO=MLO*(RFT*OS)**2
      IF (IO.LE.0) RETURN
C
C***  OUTPUT SECTION: LIST OF PARAMETERS
C
      PRINT 2010
2010  FORMAT (/18('----')/)
      PRINT 2011,ID,RIN,RMM,ZIN,ZMM,AR
2011  FORMAT (/'ID: ',18A4/
     *        /10X,'A =',F10.3,' IN',F16.3,' MM'
     *        /10X,'C =',F10.3,' IN',F16.3,' MM',8X,'C/A =',F10.4)
      PRINT 2012,OSR,OS,ONR,ON,TAU
2012  FORMAT (/9X,'OS =',F10.1,' RPM',F15.2,' /S'
     *        /9X,'ON =',F10.1,' RPM',F15.2,' /S',8X,'TAU =',F10.4)
      PRINT 2013,VFT,VMS,THD,TH,EPS
2013  FORMAT (/8X,'VEL =',F10.3,' FPS',F15.3,' M/S'//6X,'THETA =',F10.2,
     *   ' DEG',F15.4,' RAD',7X,'EPS =',F10.4)
      PRINT 2014,DENO,DEN,SG,MLO,ML
2014  FORMAT (/8X,'DEN =',0PF10.3,' SLUG/FT3',F10.1,' KG/M3',6X,
     *       'SG =',F10.3/9X,'ML =',0PF10.4,' SLUG',F14.3,' KG')
      PRINT 2015,VISO,VIS,VIKO,VIK,RE
2015  FORMAT (/8X,'VIS =',1PE10.3,' LBS/FT2',E11.3,' CP',/
     *    /7X,'VISK =',1PE10.3,' FT2/S',E13.3,' CS',8X,' RE =',E10.3)
      PRINT 2016,UMOO,UMO
2016  FORMAT (/6X,'U-MOM =',1PE10.3,' FT-LBS',E12.3,' N*M')
      PRINT 2010
      RETURN
      END
```

```
C ********** FLUID FILLED CYLINDER * F,G AND DERIVATIVES ********
C *          WRITTEN BY THORWALD HERBERT,  VPI & SU             *
C *                                                             *
C * SUBROUTINE FOR CALCULATING:                                 *
C *          F AND G AT KK EQUIDISTANT POINTS IF KK>0,          *
C *          FS1= F'(1)/RE, GS1= G'(1)/RE                       *
C *          THE VALUES ARE PRINTED IF IO>0                     *
C *************************************************************
C
      SUBROUTINE EVALA(IO)
      COMMON /FLOW/ RE,KK,RR(101),FF(101),GG(101),FS1,GS1
      COMPLEX Z,Z0,S,S0
      DIMENSION SS(2)
      EQUIVALENCE (S,SS(1))
C
      IF (IO.GT.0) PRINT 2000
2000  FORMAT (/'EVALA 09/25/84 *** FUNCTIONS F,G AND DERIVATIVES')
C
C CALCULATE F AND G
      X0=SQRT(RE/2)
      CALL BESI1(X0,Z0,S0)
      IF (KK.LE.0) GO TO 2
      IF (IO.GT.0) PRINT 2001
2001  FORMAT (/3X,'k',5X,'r',9X,'f',9X,'g'/)
      K=0
      RR(1)=0
      FF(1)=0
      GG(1)=0
      IF (IO.GT.0) PRINT 2002, K,RR(K+1),FF(K+1),GG(K+1)
2002  FORMAT (I4,3F10.6)
      DR=1./KK
C
      DO 3 K=1,KK
      R=K*DR
      RR(K+1)=R
      CALL BESI1(R*X0,Z,S)
      S=S*EXP(Z-Z0)/S0
      FF(K+1)= -SS(2)
      GG(K+1)=R-SS(1)
      IF (IO.GT.0) PRINT 2002, K,RR(K+1),FF(K+1),GG(K+1)
3     CONTINUE
C
C EVALUATE F',G' AT R=1
C
2     CALL BESI0(X0,Z,S)
      S=(Z-S/S0)/RE
      FS1=SS(2)
      GS1=SS(1)
      IF (IO.GT.0) PRINT 2003, FS1,GS1
2003  FORMAT (/5X,9Hf'(1)/Re=,F10.6/5X,9Hg'(1)/Re=,F10.6/)
      RETURN
      END
```

```
C ********** FLUID FILLED CYLINDER * BESSEL FUNCTIONS **********
C *          WRITTEN BY THORWALD HERBERT,  VPI & SU             *
C *                                                             *
C * SUBROUTINE FOR CALCULATING THE MODIFIED BESSEL FUNCTION     *
C *          I1(Z)/EXP(Z), Z=X*(1+I)                            *
C *                                                             *
C *************************************************************
C
      SUBROUTINE BESI1(X,Z,S)
      COMPLEX Z,ZZ,S
      DATA PI/3.14159265/
      Z=CMPLX(X,X)
      S=1
      IF (X.GE.10.) GO TO 1
C
C ASCENDING SERIES
C
      ZZ=Z*Z/4
      DO 2 L=1,25
      K=26-L
2     S=S*ZZ/(K*(K+1))+1
      S=S*Z*EXP(-Z)/2
      RETURN
C
C ASYMPTOTIC SERIES
C
1     ZZ=8*Z
      DO 3 L=1,18
      K=19-L
3     S=S*((2*K-1)**2-4)/(K*ZZ)+1
      S=S/SQRT(2*PI*Z)
      RETURN
      END
```

```
C ********** FLUID FILLED CYLINDER * BESSEL FUNCTIONS ***********
C *          WRITTEN BY THORWALD HERBERT,  VPI & SU             *
C *                                                             *
C * SUBROUTINE FOR CALCULATING THE MODIFIED BESSEL FUNCTION     *
C *          Z*I0(Z)/EXP(Z), Z=X*(1+I)                          *
C *                                                             *
C *************************************************************
C
      SUBROUTINE BESI0(X,Z,S)
      COMPLEX Z,ZZ,S
      DATA PI/3.14159265/
      Z=CMPLX(X,X)
      S=1
      IF (X.GE.10.) GO TO 1
C
C ASCENDING SERIES
C
      ZZ=Z*Z/4
      DO 2 L=1,25
      K=26-L
2     S=S*ZZ/(K*K)+1
      S=S*Z*EXP(-Z)
      RETURN
C
C ASYMPTOTIC SERIES
C
1     ZZ=8*Z
      DO 3 L=1,18
      K=19-L
3     S=S*(2*K-1)**2/(K*ZZ)+1
      S=S*SQRT(Z/(2*PI))
      RETURN
      END
```

```
LIN_S 07/25/85 *** SAMPLE PROGRAM

PARAM 09/25/84 *** PARAMETER CONVERSION

ID:
Sandia run at Re=14.95

RIN = radius (inch) :        / 2.375
/

ZIN = half-length (inch) :   /10.375
/

OSR = spin rate (rpm) :      / 3000.
/

ONR = nutation rate (rpm):   /  500.
/

THD = nutation angle (deg): /  20.0
/

SG = specific gravity (-):   / 1.400
/

VIS = viscosity/zero (cp):   / 107000.
/
```

ID: Sandia run at Re=14.95

A =	2.375	IN	60.325	MM	
C =	10.375	IN	263.525	MM	C/A = 4.3684
OS =	3000.0	RPM	314.16	/S	
ON =	500.0	RPM	52.36	/S	TAU = 0.1667
VEL =	62.177	FPS	18.952	M/S	
THETA =	20.00	DEG	0.3491	RAD	EPS = 0.0570
DEN =	2.716	SLUG/FT3	1399.8	KG/M3	SG = 1.400
ML =	0.5779	SLUG	8.434	KG	
VIS =	2.235E+00	LBS/FT2	1.070E+05	CP	
VISK =	8.230E-01	FT2/S	7.644E+04	CS	RE = 1.495E+01
U-MOM =	2.234E+03	FT-LBS	3.029E+03	N*M	

EVALA 09/25/84 *** FUNCTIONS F,G AND DERIVATIVES

k	r	f	g
0	0.000000	0.000000	0.000000
1	0.050000	0.032883	0.051961
2	0.100000	0.065817	0.103001
3	0.150000	0.098828	0.152194
4	0.200000	0.131880	0.198616
5	0.250000	0.164852	0.241340
6	0.300000	0.197510	0.279443
7	0.350000	0.229474	0.312012
8	0.400000	0.260191	0.338160
9	0.450000	0.288910	0.357039
10	0.500000	0.314655	0.367869
11	0.550000	0.336197	0.369971
12	0.600000	0.352040	0.362801
13	0.650000	0.360400	0.346007
14	0.700000	0.359201	0.319480
15	0.750000	0.346067	0.283427
16	0.800000	0.318339	0.238448
17	0.850000	0.273092	0.185618
18	0.900000	0.207178	0.126587
19	0.950000	0.117281	0.063679
20	1.000000	0.000000	0.000000

f'(1)/Re= -0.176700
g'(1)/Re= -0.084015

	r, m	VELOCITY, m/s x,z-plane	y,z-plane
0	0.000000	0.000000	0.000000
1	0.003016	0.071047	0.112268
2	0.006033	0.142206	0.222545
3	0.009049	0.213529	0.328833
4	0.012065	0.284941	0.429133
5	0.015081	0.356182	0.521444
6	0.018098	0.426743	0.603769
7	0.021114	0.495804	0.674139
8	0.024130	0.562172	0.730633
9	0.027146	0.624224	0.771423
10	0.030163	0.679848	0.794824
11	0.033179	0.726392	0.799364
12	0.036195	0.760622	0.783873
13	0.039211	0.778686	0.747587
14	0.042227	0.776094	0.690272
15	0.045244	0.747718	0.612377
16	0.048260	0.687808	0.515194
17	0.051276	0.590047	0.401049
18	0.054293	0.447632	0.273506
19	0.057309	0.253399	0.137586
20	0.060325	0.000000	0.000000

VISCOUS ROLL MOMENT: 3.307994 N*m
VISCOUS PITCH MOMENT: -25.315350 N*m